Specific and programmable release of target molecules via DNA strand displacement reaction

by

Hamid Ramezani

A thesis submitted in partial fulfillment of the requirements for the degree of

Doctor of Philosophy

Department of Chemistry
University of Alberta

ABSTRACT

DNA strand displacement reaction (SDR) is a fast, isothermal, and sequence specific reaction. In SDR, an invading DNA single strand, also known as the “fuel” strand, unzips a partial duplex to form a more thermodynamically stable duplex. The complementary strand to the fuel strand is referred to as the template. SDR releases the initial complement to the template upon formation of the fuel-template duplex. In DNA computation, the initial complement is called the “output” strand. In this work, we demonstrated how the output strand could be programmed to execute different functions such as specific release of biomolecules or interrogating the presence of a particular target molecule in the chemical system.

The capture and subsequent release of molecules from a solid phase has far-reaching applications in separation science and chemical analyses. Different molecular properties have been exploited to capture molecules on the solid phase offering a big repertoire of mechanisms for capture. The spectrum of capture mechanisms ranges from very general hydrophobicity-based partitioning of molecules in gas or liquid chromatography to the highly specific molecular recognition between ligands and analytes in the affinity chromatography techniques. The release mechanisms, while very diverse on the generic extreme of the spectrum, are very limited in terms of specificity. Here, we proposed SDR as a specific release mechanism for solid phase extraction that could be triggered only by the presence of a proper DNA fuel strand. We demonstrated that integration of SDR to a fluoroimmunoassay on silica microparticles for a thyroid

cancer biomarker, thyroglobulin, offers a very effective *in situ* cleanup method, especially in the presence of a complex biological fluid such as whole serum.

The unique ability of DNA to carry information in its sequence compelled us to further extend the application of SDR to characterization and purification of transcription factors (TFs). TFs are DNA-binding proteins regulating the gene expression levels in cells by binding to the specific regions of genome. The non-specific methods of release for elution of captured TFs from the DNA affinity solid phase result in losing information about the DNA sequences acting as the binding sites for the TFs of interest. It is also very difficult to multiplex purification of TFs for the mentioned reason. We propose an SDR-based strategy called IDCAPT (for Integrative Discovery, Characterization, Assay, and Purification of TFs) that uses multiple sequential SDRs to characterize the potential binding sites for TFs, quantify, and purify them. We first proved the concept of SDR-mediated multiplexing on beads for three different sets of fluorescently labeled DNA capture strands. We then showed that IDCAPT could successfully interrogate the presence of a model TF, NFκβ, in the solution using its simple sequential SDR-based reasoning module.

In summary, SDR provides us with an efficient, specific, and sequence-encoded release tool opening up the avenue for many applications requiring multiplexation, sample cleanup, and logical gate-based sensing.

PREFACE

This thesis is an original work by Hamid Ramezani. No part of this thesis has been previously published.

DEDICATION

I would like to dedicate this dissertation to my beloved sister, Atefeh, who passed away in November 2012, at the age of 32, after a short battle with cancer. My heart, thoughts, and love are always with her and I pledge that I will continue her battle against cancer by means of science as long as I am alive.

ACKNOWLEDGEMENTS

I would like to express my gratitude to my supervisor, Prof. Jed Harrison, for his supports over the course of my PhD. I would also like to thank Dr. Abebaw Jemere and all Harrison's group members. Special thanks go to Prof. Robert Campbell and Prof. Juli Gibbs-Davis for serving on my supervisory committee over the last five years. I am also very grateful to Prof. Glen Loppnow for attending both my candidacy and PhD defense exams as an examiner. I thank Prof. Robert Corn of University of Irvine, my external examiner, who kindly agreed to travel over from California for my final oral exam.

I need to thank Dr. Tony Cornish, Troy Locke, Sophie Dang, and Cheryl Nargang from the molecular biology service lab (MBSU) for providing me with excellent service and technical supports. I would also like to extend my thanks to Wayne Moffat, the director of analytical and instrumentation lab. The helps and supports from Dr. Randy Whittal, Jing Zheng, and Bela Reiz of the mass spectrometry lab, Gareth Lambkin of biological services lab, Allan Chilton and Kim Do of the electronic shop, and Anita Weiler of the graduate student services are greatly appreciated. I am also very thankful to my friends, Reza Rezaei Darestani, Marjan Barazandeh, Nazanin Assempour, and Amin Morteza Najarian for their assistance with both experimental works and preparation of this manuscript.

I thank financial supports from University of Alberta, National Institute for Nanotechnology (NINT), the NSERC grants to Prof. Jed Harrison, and the National Research Council (NRC) grants to Dr. Abebaw Jemere.

Last but not least, I very much appreciate the supports and sacrifices from my family members; my father, who taught me persistence is the key to achieving my dreams, my mother, who helped me realize kindness matters the most, my late sister, whom I grew up with and learned from how to stand up for what I believe in, and my brother, who always reminded me that giving love and support is more enjoyable than receiving them.

TABLE OF CONTENTS

LIST OF TABLES

LIST OF FIGURES

LIST OF SCHEMES

CHAPTER 1

INTRODUCTION

DNA Strand displacement reaction (SDR)

It has been more than six decades since Watson and Crick proposed a double helical model for the DNA duplex structure. The fascinating simplicity of DNA base pairing between the purine (adenine and guanine) and pyrimidine (thymine and cytosine) nucleobases manifests itself in an incredibly sophisticated manner through the cooperative binding of the two complementary DNA strands. For many years, the four-letter DNA language was thought to be merely the secret code of life in virtue of its role in the central dogma of living cells. In 1982, Nadrian C. Seeman was the first to suggest that DNA could be exploited for engineering a macromolecular lattice well defined for the crystallography of proteins. He laid out the design principles needed to make a class of naturally occurring DNA four-way junctions, also known as Holliday junctions, immobile [1]. Different variations of such immobile Holliday junctions later constituted the building blocks for DNA nanostructure assembly in DNA nanotechnology [2,3]. The DNA motifs or so to speak, monomers, were designed so that they had sticky ends to associate to one another. A sticky end is nothing but two complementary DNA single strands with unequal length forming a duplex. The single stranded portion of the longer strand after duplex formation is called an overhang. It may act as the recognition site for another motif bearing the complementary "overhang" sequence to glue together the two motifs. The second application of the overhang sequence is its ability to be used as a nucleation site for a second duplex formation in a reaction known as strand displacement.

The strand displacement reaction (SDR) takes place when two DNA single strands both complementary to a template strand compete to form a duplex with the template [4]. Starting with a partial duplex between a template and an initial complement, a second single strand capable of forming a larger number of base pairs,

also known as the “fuel” strand, is added. The fuel will replace the initial complement in order to form a more stable duplex with the template strand (Figure 1-1). The whole process is enthalpy-driven as the free energy of hybridization is larger for a longer duplex and there is no big change in entropy. SDR starts with attachment of the invading fuel strand to the overhang of the initial duplex. This overhang has recently been referred to as the “toehold”. After hybridization of the fuel strand to the toehold on the template, it starts unzipping the old duplex through “branch migration”, to the point that the initial complement is fully replaced by the fuel strand on the template (Figure 1-1). Such a reaction was known to occur during cell division in a phenomenon called genetic recombination long before it was put into application in DNA nanotechnology [5]. In fact, Robin Holliday put it forward in 1964 as the underlying mechanism of recombination after formation of Holliday junctions in the mitotic cells [6,7].

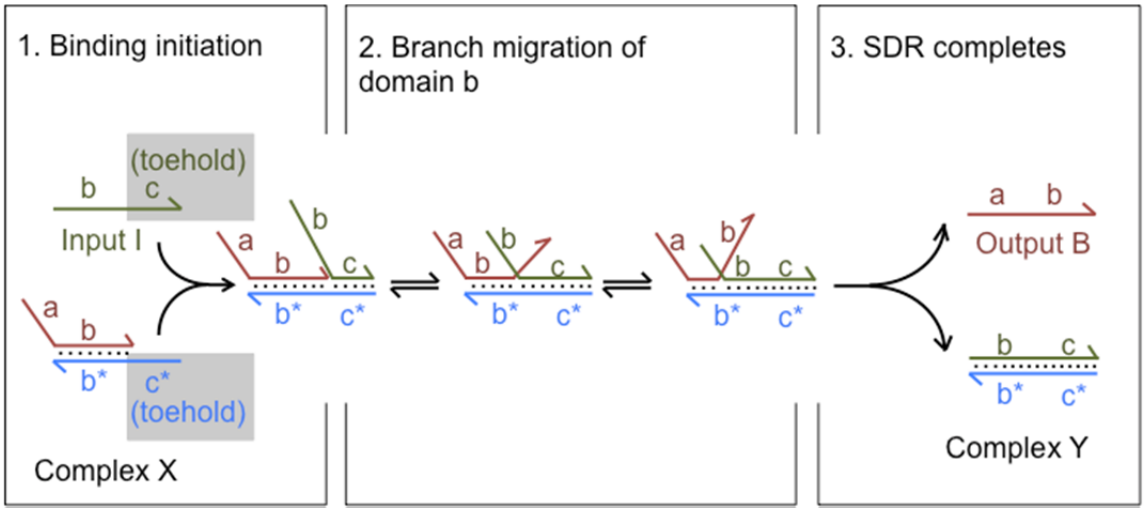

Figure 1-1: Strand displacement reaction starts with hybridization of the fuel strand (green) to the toehold of the template (blue) and progresses via branch migration (middle). The outcome is release of the initial complement (red) and a new, more stable duplex, Y. Reproduced from [4] with permission.

Kinetics of the branch migration in strand displacement was studied in 1981 [8] in its genetic context. The first SDR-based assays for DNA analytes employing quantification of the released radioactive or non-radioactive initial strands from a solid support were reported in 1986-88 [9-11]. The non-radioactive assay format took advantage of the luciferase reporter system [9,12]. The homogenous version of the same assay was also reported in which an RNA reporter strand was released upon SDR and

processed by a phosphorylase, making distinction between single and double stranded RNAs [12]. The SDR-based double stranded DNA probes [13,14] or hairpin molecular beacons [14,15] using the Förster resonance energy transfer (FRET) signal readouts were introduced a decade later. Since then, there has been a diverse range of FRET-based assays using SDR [16-29]. The more recent SDR-based assays utilize the same principle, but use different reporter systems such as osmium tetroxide [30], horseradish peroxidase [31], methylene blue [32], and other detection methods [33-37].

The kinetics, thermodynamics, and mechanism of the strand displacement reaction have been studied in detail [14,38-41]. It was found that the length of the toehold and its composition influence the kinetics of SDR [38]. For toeholds made of only G/C nucleobases, a length of five nucleotides is enough to reach the maximum rate constant, whereas a toehold length of eight is needed when using only A/T nucleotides [38]. On average, increasing the toehold length beyond six nucleotides would have very minimal effect on improving the rate constant of release [38]. It has also been proven that the position of a toehold with respect to the partial duplex matters, so it can be used as a tool to control the kinetics of SDR [41]. For example, leaving a mismatched spacer domain between the toehold and the partial duplex will considerably slow down the SDR [41].

There is a long list of applications based on SDR: it was exploited in DNA computation [42-56], switching on and off nanoparticle aggregation [57-60], molecular imaging [61,62], signal amplification [63-73], DNA cloning through a technique called strand displacement amplification [74-78], single nucleotide polymorphism (SNP) detection [79-87], genotyping [88-90], DNA-templated synthesis [91,92], self-replicating systems [93,94], assembly [95-98] and reconfiguration of DNA nanostructures [99-102], actuation of nanodevices [103-108], molecular switches [109-111], DNA tweezers [112] and walkers [108,113,114]. SDR has also been used in controlling biological functions such as enzyme activity [114-116], gene expression [108,117,118], and characterization of cell surface receptors [119]. Among these applications, DNA computation is of pivotal importance, because it formulates the SDR such that many other applications could be described by the formalisms it defines.

SDR in DNA computation

The concept of DNA logic gates [4,120,121] in DNA computation is relevant to the main theme of this thesis and therefore, is explained here. A logic gate is simply an element of a digital circuit (for instance a diode or transistor) that implements the Boolean functions by performing a logical operation on an input to generate an output. A Boolean function is a mathematical function whose output is either "true" or "false". The main logical gates are "AND", "OR", and "NOT". In an "AND" gate, two inputs must be present to generate an output and for the "OR" gate, either of two inputs will generate the same output. Figure 1-2 shows how SDR could be used to make an "AND" logical gate [4].

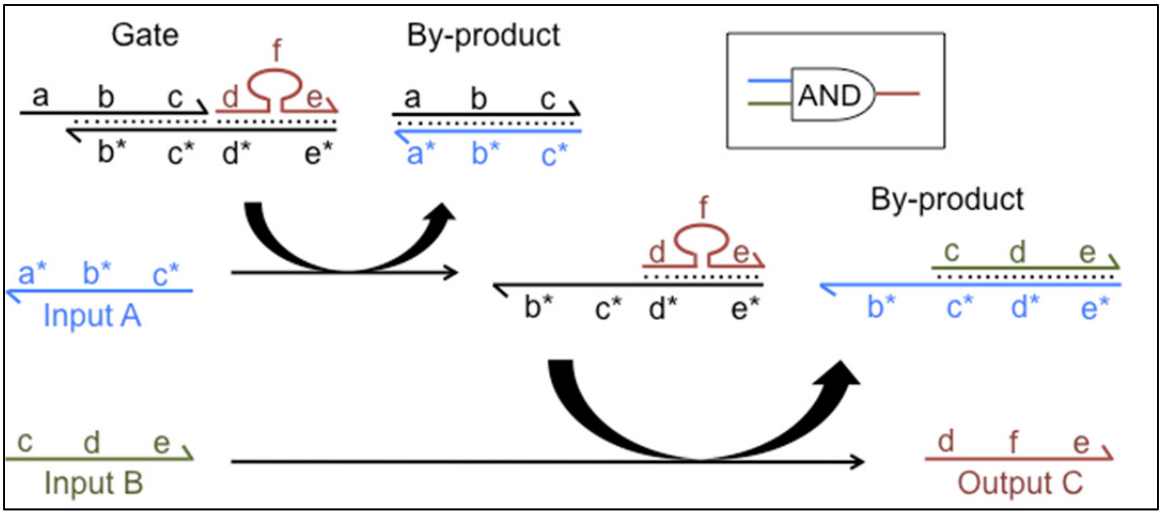

Figure 1-2: A logical "AND" gate made of two SDRs. Product of the first SDR acts as a substrate for the second one. The first SDR exposes the hidden toehold of the gate. Reproduced from [4] with permission.

The simple symbolism described above could be integrated and scaled up into complex digital circuits [120,122]. While the output and input molecules shown in Figure 1-2 are all made of DNA, it is possible to use aptamer targets for inputs as well. Targets for aptamers could elicit a configuration change upon binding to the aptamers and thus, expose a hidden toehold [123-125]. Such gates could accomplish interesting tasks that need reasoning to trigger a response. For instance, the aptamer-based and combined DNA-aptamer-based "AND" logical gates in designs of drug delivery DNA

nanorobots could provide full control of on-demand release of their molecular payloads [126,127]. Transcription factors (TFs) are DNA binding proteins and the DNA sequence they bind to could be used like an aptamer. In Chapter 4, we proposed a new strategy for analysis of transcription factors called IDCAPT (for Integrated Discovery, Characterization, Assay, and Purification of TFs). IDCAPT functions through an "AND" logical gate in which the presence of both transcription factor and DNA inputs is necessary to release a signal strand.

DNA dehybridization via SDR

Niemeyer et al demonstrated that SDR could be used to release the yellow fluorescent protein conjugated to a DNA strand from gold nanoparticles [128]. The goal of that study was to take advantage of gold nanoparticle-induced quenching of yellow fluorescent protein, to show that proteins could maintain their biological activity when conjugated to DNA and assembled on gold nanoparticles. Chapters 2 and 3 explore and optimize a similar release method with the purpose of developing a sample cleanup technique based on SDR. The main premise of these chapters is that SDR could be utilized, to release from a solid phase, an antibody conjugated to a DNA capture strand in a programmable fashion.

The SDR-mediated dehybridization and release is expected to be superior to conventional methods such as thermal and chemical denaturation of the DNA duplex, especially for the applications demonstrated in Chapters 2-4. The generic release through non-specific mechanisms greatly complicates the possibility of multiplexing, as well as giving side release of unwanted matrix molecules. Generic release mechanisms may use drastic changes in pH, solvent type, ionic strength, temperature, chaotropic agents (urea, guanidinium chloride, etc.), and surfactants, to name a few. The fluorescent signal is also sensitive to many of the factors enumerated above. The SDR-facilitated release, on the other hand, is a programmable, sequence-encoded, specific release approach that does not require any change in buffer or solvent properties.

Chapter 2 examines an analytical scheme that uses SDR to release a DNA-antibody conjugate on chip for downstream recapture and quantification by surface plasmon resonance (SPR). The purpose is to integrate an upstream sample cleanup on

chip with a label-free assay for any antigen of interest. Surface plasmon resonance works by sensing the change in refractive index of the environment immediately adjacent to the surface of a thin layer of an inert metal such as gold [129,130]. A beam of light is shone upon the gold layer with nanometer to submicron thickness to excite the plasmon of the gold and generate an evanescent wave (Figure 1-3) [131]. The latter will penetrate into the volume right above the gold surface and therefore, will sense a few hundred nanometers above the surface. Coupling of incident light to the plasmon occurs at a particular angle for each wavelength and any binding events on the surface can be detected by the response of SPR to the change in refractive index [130,132]. The response is quantified in one of three ways; change in the angle of incident beam, intensity, or wavelength [132,133].

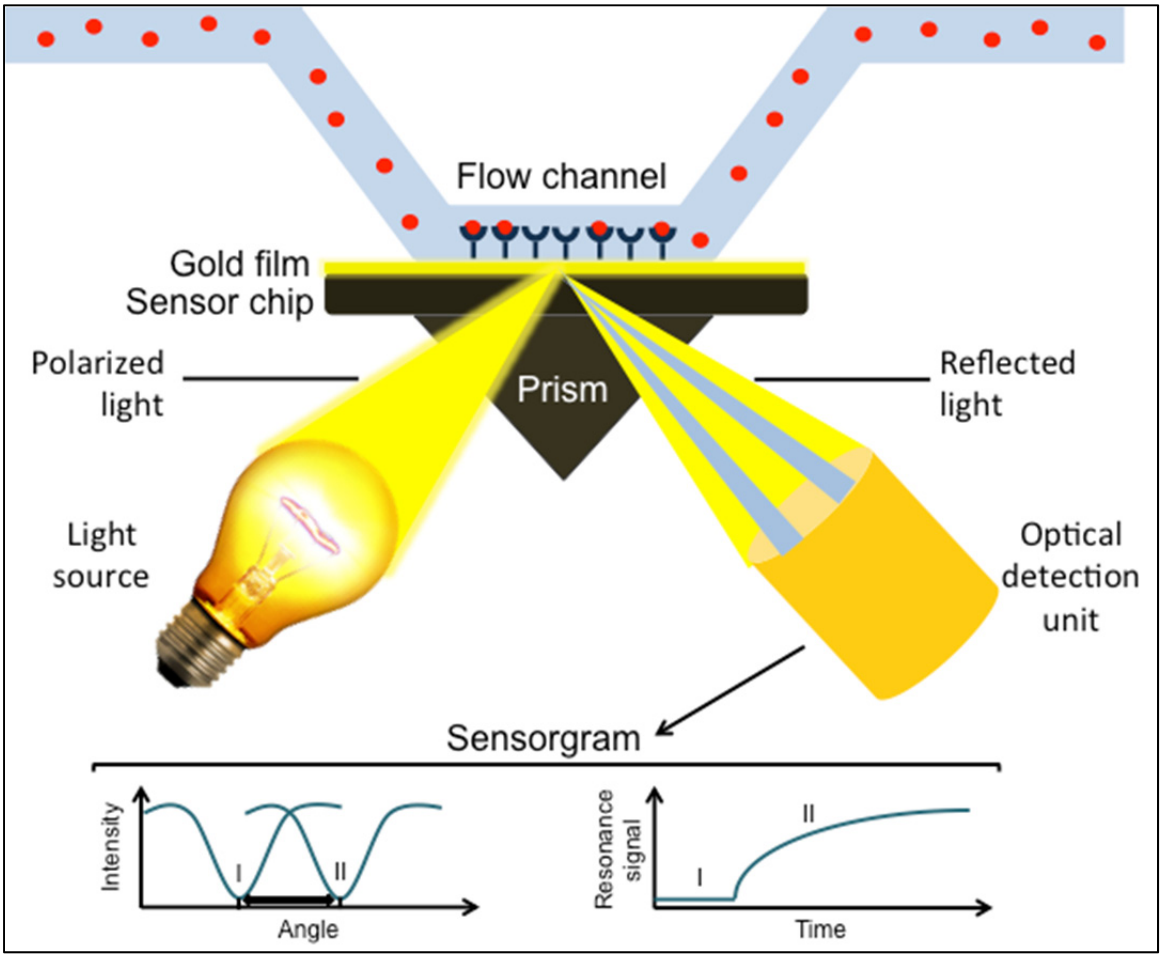

Figure 1-3: Principles of surface plasmon resonance (SPR). Reproduced from [131] with permission.

Chapter 3 investigates how SDR can be utilized as a component of an immunoassay that provides a sample cleanup technique with quantitative performance. Although fluorescence is intrinsically much more sensitive than UV-visible spectroscopy, the enzyme-linked immunosorbent assay (ELISA) is far more common than fluoroimmunoassays (FIA). Part of the reason is, of course, that the catalytic nature of ELISA leads to a huge signal amplification and simpler instrumental setups for UV-Vis spectrometers. However, another challenge for FIA is reading the fluorescent signal from a solid support [134] and dealing with the background correction for a non-uniform surface; a problem that has already contributed to DNA microarray technology's failure to fully deliver its promise in the quantitative realm after two decades. Homogenous FIA techniques are mostly competitive assays, with more limited sensitivity and a susceptibility to interference from the matrix molecules in real samples [134]. Embedding a specific release mechanism such as SDR would benefit FIA on beads in two ways. SDR could allow sample cleanup and also make it possible to measure the fluorescent signal in solution.

In this thesis, we are examining methods to multiplex while using fluorescence detection. There is a signal acquisition method known as the "synchronous scan", which aids in multiplexed fluorescent detection. The method sweeps across two defined wavelength ranges, one for excitation and the other for emission, while keeping a fixed wavelength difference between the excitation and emission wavelengths (a 20.0 nm window in this work). This method allows for detection of multiple fluorophores in the same solution and in one scan, provided that their spectra do not overlap significantly (Figure 1-4).

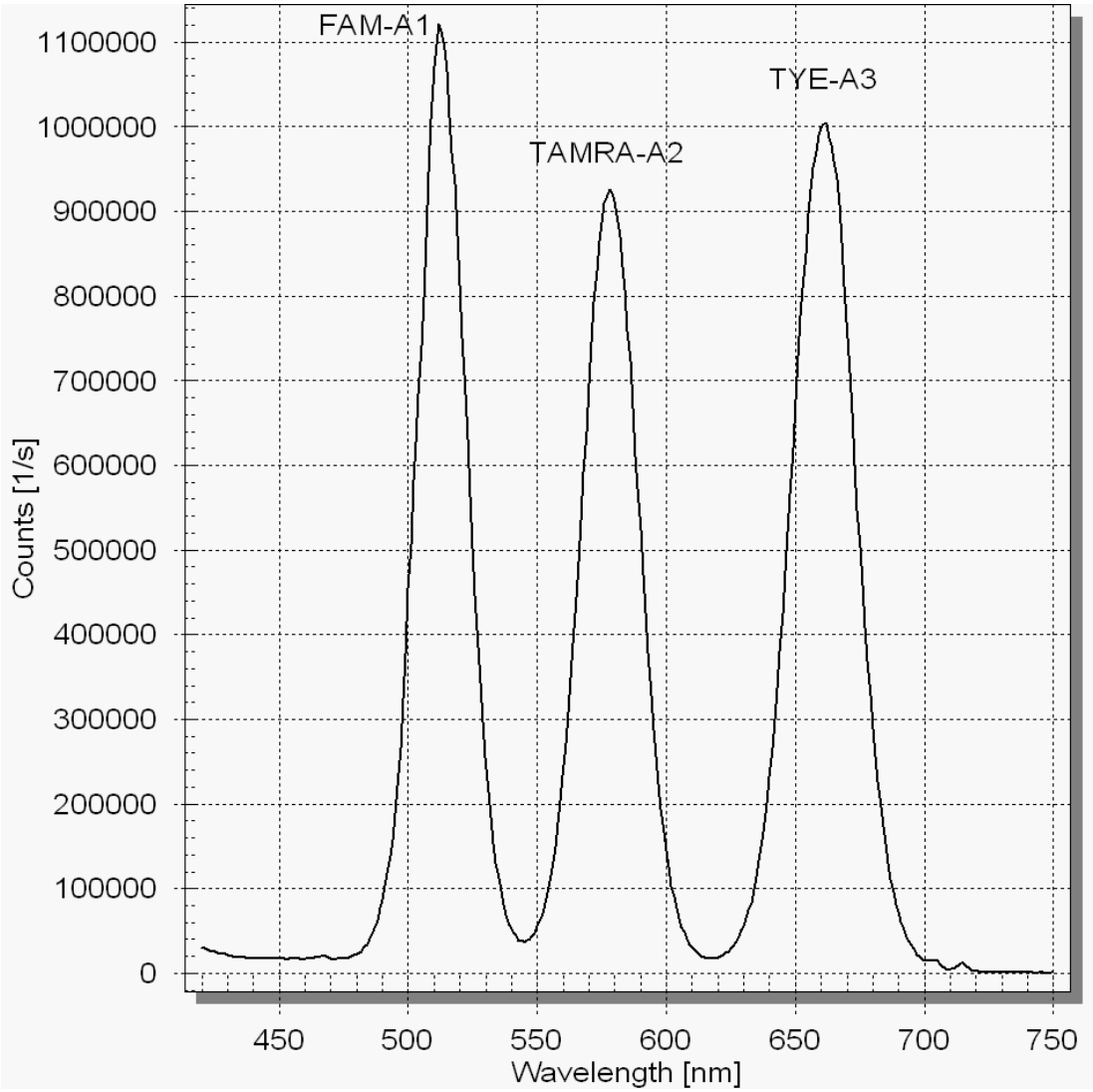

Figure 1-4: Example of a spectrum acquired in the synchronous scan mode of the fluorimeter.

Challenges in multiplexed purification of transcription factors

Chapter 4 looks into inventing a new methodology to study transcription factors (TFs) by harnessing the powerful sequence encoding capability of DNA for multiplexing. We chose the acronym IDCAPT for our strategy standing for “Integrated Discovery, Characterization, Assay, and Purification of Transcription factors”. IDCAPT demonstrates that encrypting information in the four-letter syntax of DNA could be put into use for both operating parallel, programmed releases and retrieving information

about the interactions of transcription factors with DNA. As pointed out earlier, the method makes use of an "AND" logical gate to release a signal strand in the presence of a transcription factor and an "interrogator" DNA strand. The cornerstone of IDCAPT is a series of multiple sequential SDR steps, enabling it to execute a radar-like propensity to interrogate the binding status of a transcription factor. Detailed discussion of the IDCAPT method will be presented in chapter 4.

TFs comprise several superfamilies of DNA-binding proteins that regulate the gene expression levels by binding to a sequence of DNA. Some TFs have binding sites in the genome that are very simple and only mildly specific, such as the GA-binding protein family. However, there are many others with much more sequence-specific TF binding sites (TFBS) with around eight or more nucleotides [135]. There are numerous methods developed to exclusively focus on one area of TF studies, for instance characterization or purification. A vast majority of techniques can be classified in two main categories; the ones that approach the study of TF-DNA binding from the genomic perspective (starting with putative TFBSs) and those adopting a proteomic approach (starting with a purified TF). IDCAPT takes an integrative strategy in which both TF and TFBS could be recovered. Protein binding microarrays (PBMs) [136,137] and PICh (proteomics of isolated chromatin segments) [138] are two well-established techniques that are compared here to IDCAPT, in terms of principles.

PICh is an evolved chromatin immunoprecipitation (ChIP) technique with many advantages over traditional ChIP. It does not need any antibody against TFs to pull down the crosslinked TF-TFBS adducts. The workflow of PICh is shown in Figure 1-5. The goal is to isolate proteins as they are bound to DNA in a cell. The DNA-proteins are crosslinked by formaldehyde in the fixation step, the cells are disrupted and the protein-DNA adducts are pulled down using long DNA probes functionalized with desthiobiotin (the hybridization step in Figure 1-5). After capturing the protein-DNA adduct on avidin-functionalized magnetic beads, the beads are washed, then biotin is added to release the protein-DNA adduct from the beads via stronger affinity of biotin for avidin compared to desthiobiotin. The protein-DNA adduct could be characterized by either SDS-PAGE or mass spectrometry. The main reason for using the biotin/desthiobiotin exchange reaction is to reduce the non-specific release of the matrix molecules [138]. Multiplexing is a major challenge with PICh, since there are many TFs bound to DNA all

the time. The formaldehyde crosslinking takes a snapshot of the protein-protein and DNA-protein interactions within the cell. While the method captures multiple DNA-protein adducts at the same time, the PICh approach does not retain the TF-TFBS information due to its non-specific release mechanism. The sequence-encoded multiplexing in IDCAPT is supposed to offer a great control over the release process, in contrast to the non-specific biotin-desthiobiotin release mechanism.

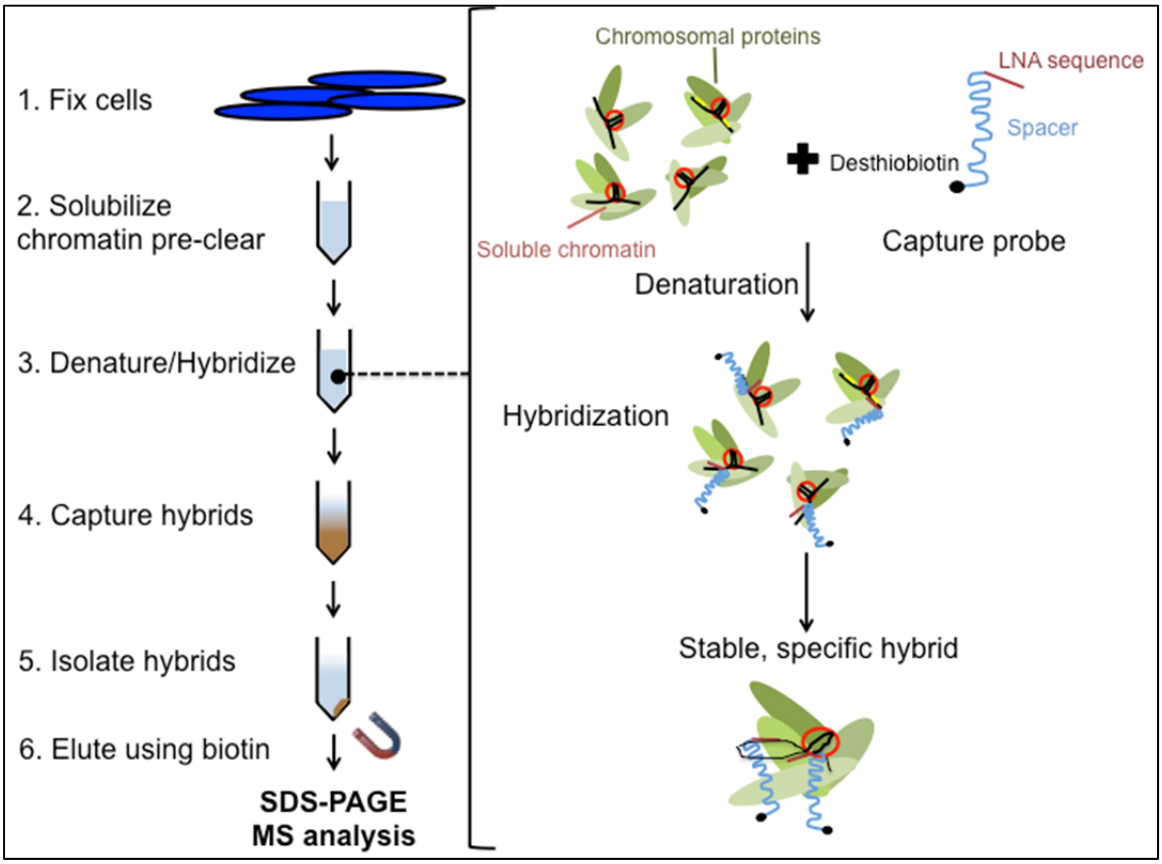

Figure 1-5: Workflow of PICh. Elution from avidin magnetic beads occurs via biotin-desthiobiotin exchange. Utilization of locked nucleic acid (LNA) probes leads to the much higher melting points and stability of the chromatin-probe hybrids. Reproduced from [138] with permission.

The second TF characterization technique described here is the protein binding microarray (PBM) [136,137]. PBM aims at characterizing all possible TFBSs for a purified TF *in vitro*. All possible 10-mer DNA binding sites are spotted on microarray slides. The TF of interest is expressed as a fusion protein with glutathione S-transferase (GST), which is added to the microarrays. To detect the DNA-bound GST-tagged TFs, a

labeled antibody against GST is added. The plus side of PBM is that it does not need any prior knowledge of TFBSs, but it faces several challenges. It needs expression of an epitope-tagged TF in each case, which might change the binding affinity of the TF. It tries to use DNA microarray technology for a quantitative analysis to extract the binding constants and therefore, it requires multiple fluorescent labeling for background correction and improving reproducibility. IDCAPT, on the other hand, is set up to measure the fluorescent signals in solution and would make use of a single universal fluorescent label. It is consequently expected to show a better reproducibility and demand less high throughput data analyses.

This thesis attempts to demonstrate how SDR could be applied to solving a number of practical challenges in separation science and bioanalytical chemistry. Chapter 2 tackles the problem of non-specific adsorption of matrix molecules in SPR assays by devising an upstream sample cleanup flow cell using SDR. It also inspects the role of limited mass transport on a chip and the consequences for an assay based on recapture of a released target analyte. Chapter 3 probes coupling of SDR to a fluoroimmunoassay (FIA) on beads and optimizes a number of parameters influencing performance of the assay. Chapter 4 puts forth a combined purification and assay scheme named IDCAPT operating based on sequential SDRs to facilitate isolation and characterization of TFs and their binding sites. IDCAPT attempts to offer a solution for the multiplexing issues of PICh and PBM.

CHAPTER 2

DNA TOEHOLD-MEDIATED RELEASE ON CHIP

In this study, the DNA strand displacement reaction (SDR) on the solid phase is used to temporarily retain an antigen on the chip. As a proof of feasibility of SDR for such a cleanup application on chip, the Surface Plasmon Resonance (SPR) technique was adopted, enabling us to monitor the association and dissociation processes in real time. An analytical scheme for an on-chip assay of a thyroid cancer marker, thyroglobulin, was designed based on the recapture of the antigen on a surface plasmon resonance chip. The SDR could release a significant portion of the captured material, 72- 84%. The yield dependence of SDR on parameters such as concentrations of the capture and releasing strands, flow rates, and hybridization times was studied. The recapture efficiency on chip for the released strand is moderate and does not exceed 30 %. It was found that the highly restricted mass transport to the chip surface strongly hampers the recapture process, especially for the huge antibody-antigen complex.

Introduction

Microfluidic technology holds promise for a diverse range of applications from chemical synthesis of nanomaterials to purification, quantification, and separation of biomolecules, cell sorting, and cell culture [139-143]. In the context of quantification, a detection method should be interfaced with the microfluidic chips and while fluorescence has been probably the most commonly used technique, it suffers from reliance on the molecular labeling. The label-free methodologies, such as surface plasmon resonance (SPR) [144-146] and quartz crystal microbalance (QCM) [147-151], still need to address the issue of poor selectivity resulting from their non-discriminative

modes of action. The interference by sample matrix molecules is often a serious problem. Non-specific adsorption particularly becomes a major obstacle when label-free sensors are utilized for assays in real samples of biological sources such as blood, plasma, and other body fluids. It is possible to alter surface chemistry to make it more resistant to fouling [152,153]. However, this approach may prove insufficient in many cases. The alternative is to devise a sample cleanup unit upstream of the sensor area to eliminate a significant portion of the matrix molecules and also dilute the remaining portion with a buffer exchange.

We hypothesized that DNA-directed immobilization could be exploited in the cleanup chamber of the chip. Molecular recognition capability is then added to the immobilized DNA by conjugation of an antibody. After enriching the surface of the chamber with the analyte of interest and a buffer exchange, the whole antibody-analyte complex is released from the surface via a methodology known as the DNA strand displacement reaction (SDR) [4]. The SDR is a DNA strand exchange on a template DNA wherein two competing strands are both complementary to the same template. The exchange reaction thermodynamically favors formation of the duplex with the larger number of base pairs as the final product. Starting with the less energetically stable duplex, the template strand will release its initial complement for a competing strand, also called the "fuel" strand. If the template strand is immobilized on the surface of a chip, this process could be exploited as a reversible capture system. The solid phase SDR can release the captured α strand single- or double- stranded depending on the fuel strand used (Scheme 2-1). The β probes are immobilized on the surface and the α strand is partially complementary to β probes. If the α' fuel strand fully complementary to α is added after capture of α on the surface, α is released as a duplex (reaction 1 in Scheme 2-1). The β' SDR occurs when the β' fuel strand complementary to the probes on the surface is used resulting in the release of α in its single-stranded form (reaction 2 in Scheme 2-1).

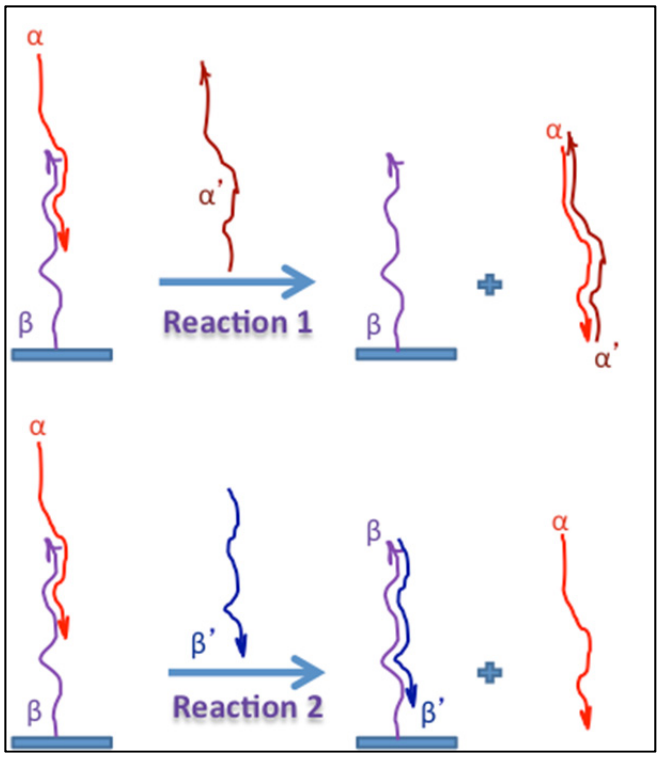

Scheme 2-1: The β probes are immobilized on the surface and are partially matched to a segment of α. If α' fuel strand is used for release (reaction 1), α will be released as a duplex. Adding β' fuel strand releases α single-stranded (reaction 2).

Scheme 2-2 shows how an SDR-based cleanup unit could be embedded upstream of a sensing unit on a chip. The chip consists of three chambers connected together with valves. The capture DNA-antibody conjugate released from the first chamber, the cleanup unit, would be re-captured and quantified in the third chamber, the sensing unit, via DNA hybridization between the other half of the capture strand and the probes on the surface. However, SDR will release the capture strand-antibody conjugate both unreacted, and as a complex with the antigen (analyte). In order to prevent the unreacted capture strand-antibody conjugate from reaching the sensor, a sorting chamber bearing the immobilized antigen is needed between the cleanup and sensing units. This region must ideally entrap the entire unreacted antibody and allow the signal detected to reflect only the amount of antigen in the sample. This scheme demands a very effective mass transport to the surface of the chip, where the immobilized antigen is bound.

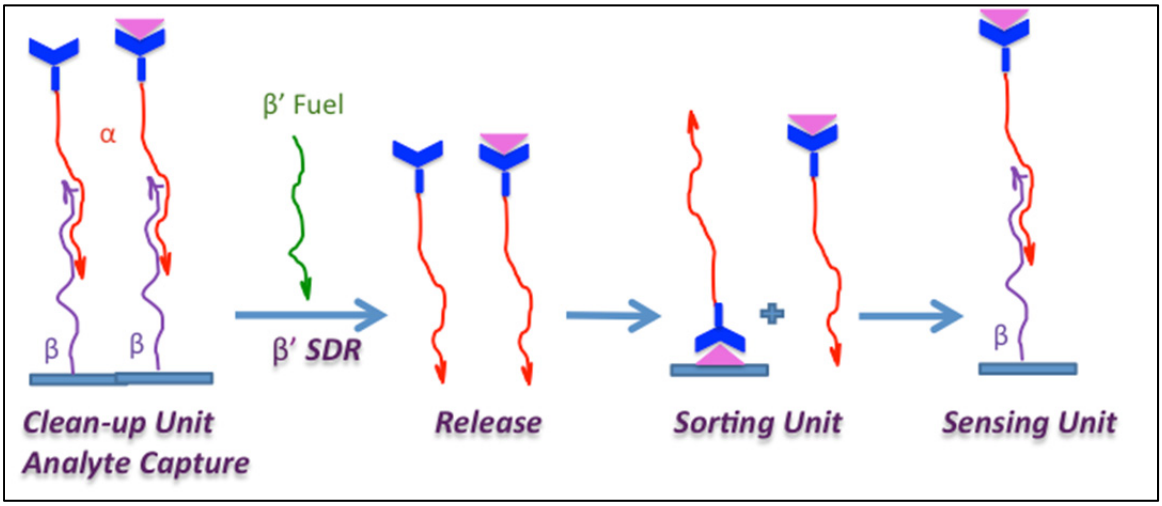

Scheme 2-2: The SDR-based cleanup upstream of the sensing cell: the antibody (in blue) captures the antigen (pink triangle) while immobilized on the chip via its capture DNA, α. Upon release by SDR, the unreacted α-TgAb conjugate is trapped in the sorting cell. Consequently, only the α-TgAb conjugate-antigen complex reaches the sensing cell.

Results and discussion

To evaluate capture and release via SDR, DNA microarray technology was initially used. The capture strand was labeled with Cy5 and the fuel strand with Cy3. After hybridization of the capture strand, the spots on the microarray were detected in the red channel (635 nm). When the fuel strands replaced the capture strands, the red signal was also replaced with the green one (532 nm) (Figure 2-1). While this data provides a qualitative proof of SDR-mediated release, it could not be used to estimate the SDR yield. The signal intensities were dispersed over a wide range and reproducibility was a major issue. The huge variation in signal arises from some combination of the susceptibility of Cy5 to oxidation via ozone [154,155], spot-to-spot printing variations [156], hybridization conditions [157,158] and local heterogeneity in refractive index of the slide and, in turn, its backgrounds, among other factors [159-161].

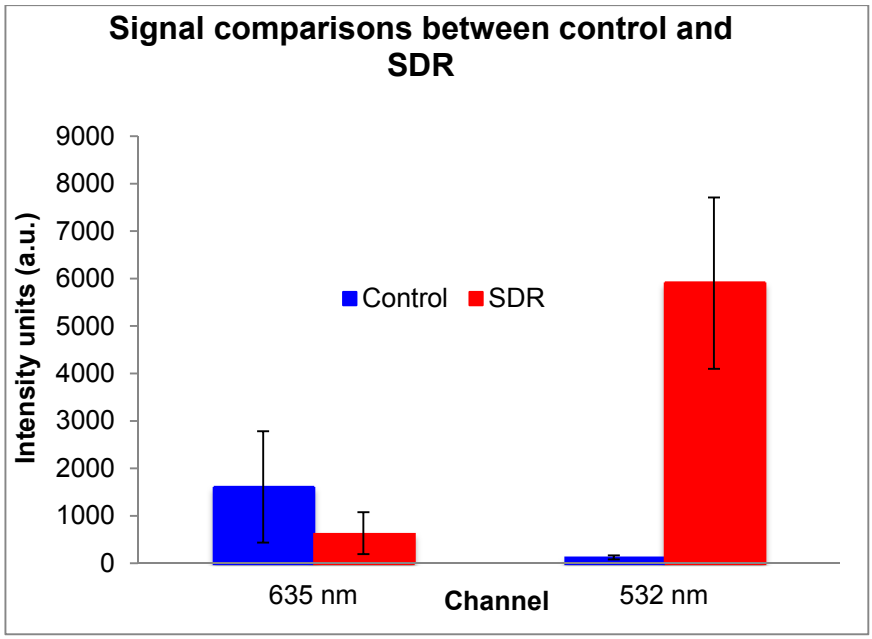

Figure 2-1: DNA microarray experiments provide the qualitative proof of SDR but lack the necessary reproducibility.

An alternative approach to evaluate SDR for an assay is surface plasmon resonance (SPR). Unlike microarray experiments, the reproducibility of DNA hybridization on the BIACORE CM5 chips was very satisfactory (RSD 2.9% over 54 hybridization/ NaOH regeneration cycles). The DNA probes were immobilized on the CM5 chips using the biotin-neutravidin interaction. In each regeneration attempt, the NaOH/NaCl solution was used to dehybridize the DNA duplexed on the chip. Such treatment regenerates the single stranded DNA probes with a very slight loss of probe density. The average signal loss per each regeneration cycle was measured to be 0.14% presumably due to the probe density loss.

When the fuel strand is a full match for the capture strand, α, and orthogonal (no stretch of more than 5 nucleotides can cross-hybridize) to the probes, β, the signal ratio between the signal gain in the capture step and loss in the release step would directly give the α' SDR yield (reaction 1 in Scheme 2-1). However, when the fuel strand, β', is complementary to the probes on the chip the SPR signal will indicate the net mass displaced on the surface as a result of the release of the capture strand and hybridization of the fuel strand to the probes. To deconvolute the signal loss due to the β' SDR (reaction 2 in scheme 2-3) from the gain caused by the simultaneous capture of the β'

fuel strand on the surface, we took advantage of a subsequent α' SDR coupled to the first β' SDR (Scheme 2-3). This makes it possible to estimate the amount of the capture strand still left bound after the β' SDR. Therefore:

β' SDR Yield % = [1 – ((Signal drop due to α' /α' SDR yield)/total signal gained by capturing α))] x 100

The release yields following the α' SDR and the β' SDR of a 30-mer capture strand were 72% and 84%, respectively. The SDR reproducibility was excellent (RSD for α' SDR 0.7% and for β' SDR 1.1%).

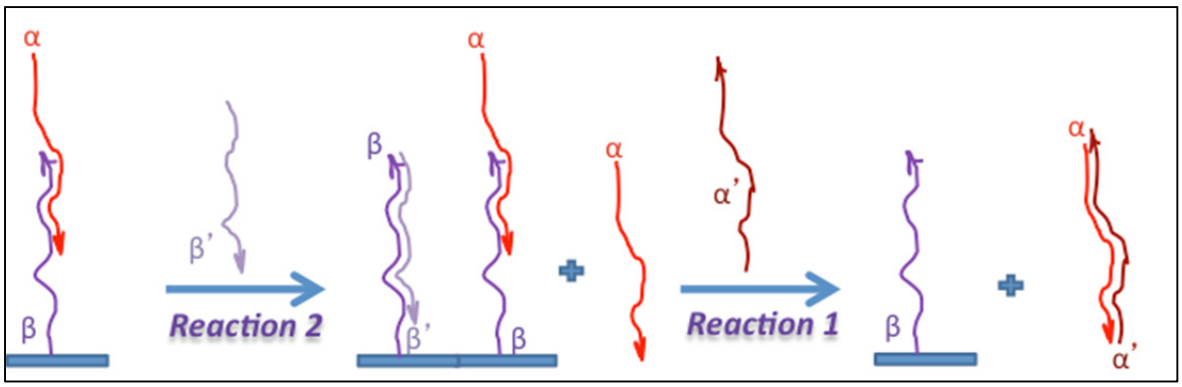

Scheme 2-3: SDR yield measurements on SPR could be performed directly for reaction 1 (α' SDR) but only indirectly for reaction 2 (β' SDR), because β' binding to the surface generates signal and concurrent removal of α leads to the signal loss. To measure the SDR yield of reaction 2, a second step was coupled to it involving reaction 1. The second step measures the amount of α leftover from the first step.

As mentioned earlier, if Scheme 2-2 is to work, there needs to exist a very highly efficient capture of the unreacted DNA-antibody conjugate in the sorting unit. Apart from the equilibrium constant of the antibody-antigen interaction, the mass transfer to the chip surface probably plays the most important role in attaining high capture yields. The laminar flow in a microfluidic channel usually follows a parabolic velocity profile, in which the velocity of the liquid is maximal at the center of the channel and approaches zero at the walls [162]. The reason for the limited mass transport is the existence of a thin layer of the liquid (usually several micrometers thick) called the "stagnant layer" right next to the surface of the chip [163]. The velocity of the stagnant layer is zero, namely, there is no flow of the liquid in it. The molecules within the main stream have to

diffuse across the stagnant layer to reach the surface of the chip and interact with the probes. Higher flow rates and longer injection/ hybridization times should therefore improve the mass transport to the surface of the chip by reducing the thickness of the stagnant layer. Figure 2-2 shows dependence of the signal on the flow rate and the molecular size of the DNA used for the hybridization. The biotinylated β probes were immobilized on the surface of a CM5 chip already functionalized with neutravidin. The hybridization of three different strand sizes (20mer, 30-mer, and 41-mer) partially complementary to β probes at several concentrations was examined. Three calibration curves for each strand were built, each at a fixed flow rate (FR). The semi-log sigmoid dose-response curves for each strand shift toward the left (higher signals for the same concentration) when the flow rate and the mass transport to the chip surface increase. The effect was much less conspicuous for the smallest DNA (β'-20, a 20-mer) where a flow rate change from 10 to 30 μL/min only modestly shifted the curve to the left (Figure 2-2a). The highest concentration at which the curves start to show the same signals for the same concentration shifts to larger values as the molecules become larger (Figure 2-2). This is because the mass transfer is less efficient for the larger molecules, due to their smaller diffusion coefficients.

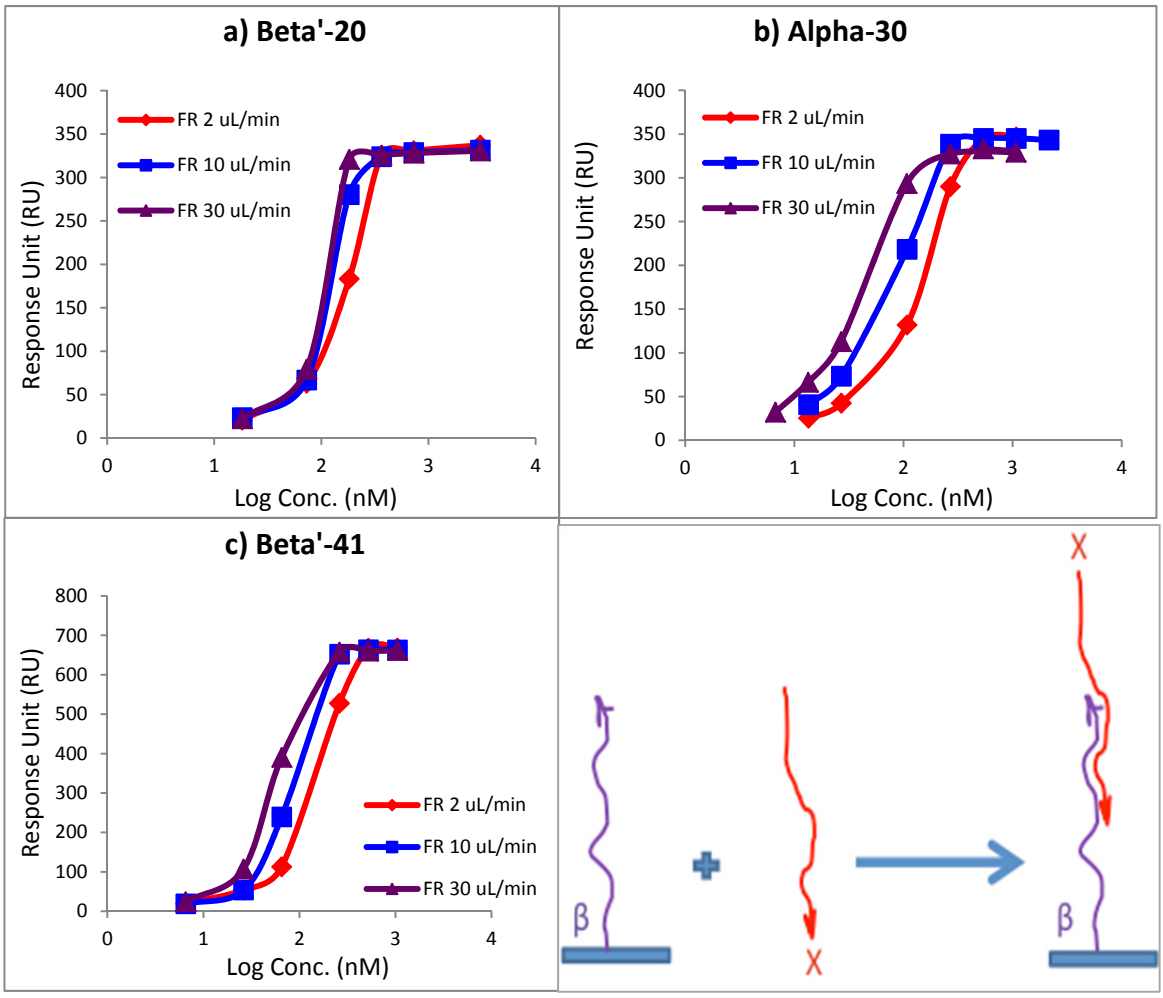

Figure 2-2: Effect of flow rate (FR) on hybridization of surface-bound β to X, where X is a 20-mer in a), a 30-mer in b), and a 41-mer in c). The calibration curves for three different DNA sizes at different flow rates shift toward left with increasing the flow rate and thus the efficiency of the mass transfer.

To further explore the impact of mass transfer limitation on SDR yields, the correlations between the α' SDR yields (reaction 1 in Scheme 2-1) and factors such as flow rates, hybridization times, and concentrations of α and α' were examined. For each data point shown in Figure 2-3, α' SDR was done and its yield was obtained by dividing the signal loss after injection of α'-25 by the signal gained in the capture of α-30. In the blue data series of Figure 2-3a, the flow rate (FR) of α-30 hybridization was changed while all other parameters such as the flow rate for α'-25, hybridization times, and

concentrations were kept constant. For each data point in the blue series of Figure 2-3a the α' SDR was done, but this time, only the flow rate (FR) was changed and all other parameters were the same. To study the effect of hybridization times of α-30 and α'-25 in Figure 2-3b, the flow rates were kept constant, so changing the volume of injection changed the injection time correspondingly. The other parameters such as concentrations of α-30 and α'-25 plus their flow rates were constant throughout the experiments for Figure 2-3b. In panels c) and d) of Figure 2-3 all α' SDR parameters were the same except for concentrations of α-30 and α'-25, respectively. Opposite to the trend observed with the α' hybridization, increasing the concentration, hybridization time or flow rates for α decreases the SDR yield. This is because much higher amounts of α were transferred to the chip surface in the capture step (Figure 2-3). Unexpectedly, there is a drop in the observed yield at very dilute concentrations of α (Figure 2-3c). We believe that it comes from the non-specific adsorption of α to the chip surface, with the small signals falling out of the linear range of the calibration curve.

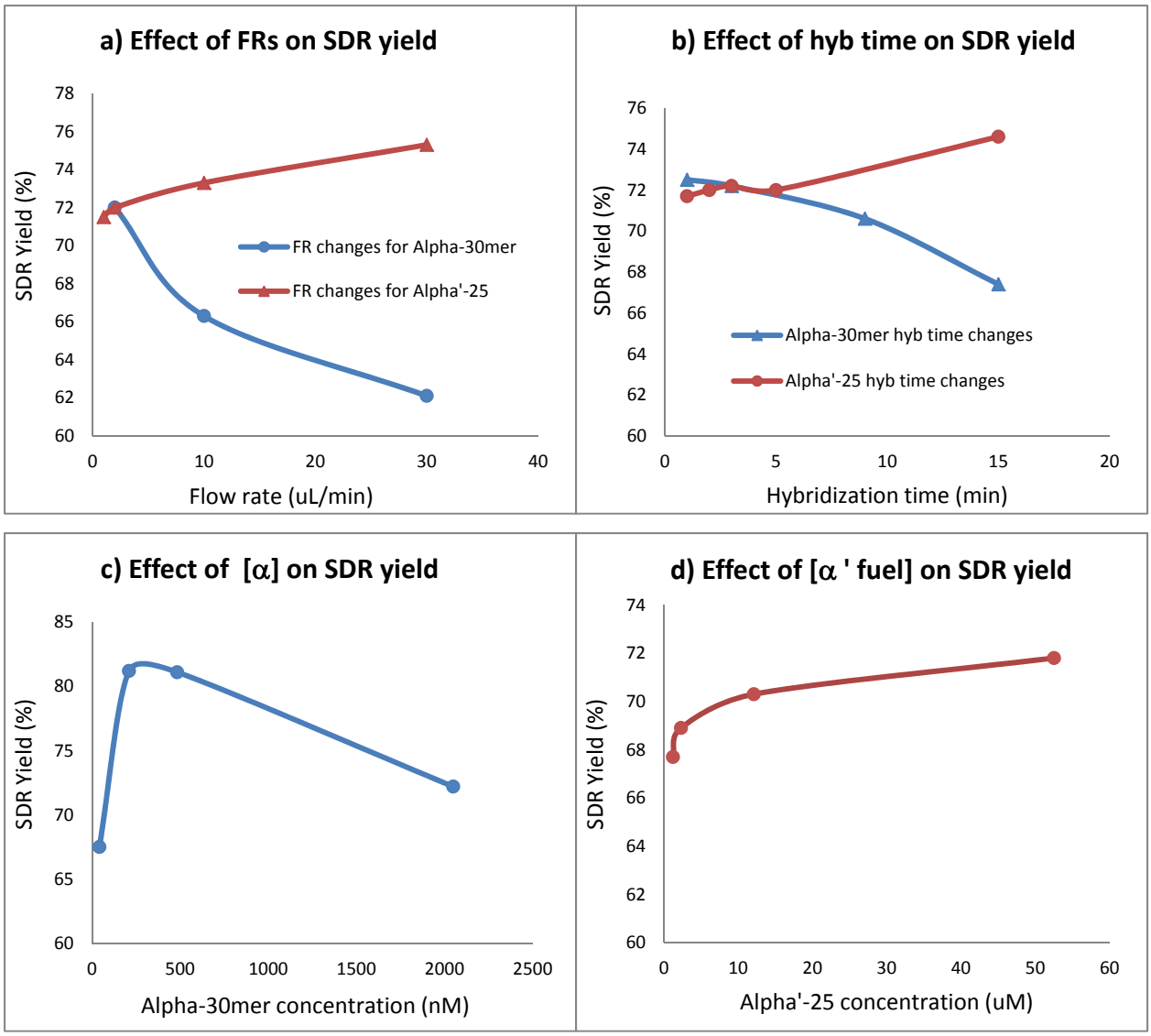

Figure 2-3: Factors changing mass transport to the chip surface affect the α' SDR yields. a) Flow rates (FR) for hybridization of α-30 (blue curve) and α'-25 (red curve) will influence their surface concentrations and hence, the α' SDR yields. b) Hybridization times of α-30 (blue curve) and α'-25 (red curve) were changed by changing their injection volumes at a fixed flow rate. c,d) Concentrations of α-30 and α'-25 affect the α' SDR yields.

There are a number of adsorption isotherms modeling the process of analyte partitioning between solution and solid phases, covering both kinetic and thermodynamic points of view [163,164]. A good number of those models assume the

amount of analyte captured on the solid phase is only a very small fraction of what exists in the solution. Validity of such an assumption, of course, depends on the concentration of the analyte, its actual adsorption isotherm, the capacity of the solid phase to capture and retain the analyte, and how facile the mass transport between the two phases is. If we release the captured fraction into the same volume as the original one, we will observe that the new concentration of the released analyte is much less than its concentration before the capture, unless the capture efficiency is near 100 %. This dilution effect may cause the new concentration to become too dilute to be detectable. Dilution may also lead to a drastic drop in the efficiency of any recapture process, especially if the process suffers from the restricted mass transport. The recapture of the DNA-antibody conjugate released from the cleanup chamber and sorted in the middle chamber is essential to quantifying the analyte in the sensing unit (Scheme 2-2), so dilution is a major concern.

To examine the recapture yield of α following its release by β' SDR, the second flow cell of the BIACORE CM5 chip was functionalized with a new probe called ε-36. The sequence of ε-36 is complementary to the first half of α-30 while the other half is complementary to the other probe, β. The sequence of ε-36 is also orthogonal to all other sequences but to its target, α-30. The α-30 recapture experiment was done in two cycles. In the first cycle α-30 was injected and captured, with the flow path set to pass through only the first flow cell, already functionalized with β probes. In the second cycle, the flow path was directed from the first flow cell to the second one, already functionalized with the ε-36 probes. β'-20 was then injected while the signals in both flow cells were being monitored simultaneously and in real time. The recapture yield was calculated by dividing the amount of signal gained in the second flow cell, after injection of β'-20, by the total signal gained after the α-30 capture in the first cycle. The control experiment, in which the first cycle was skipped, showed no significant signal generation by exposure of the second flow cell to β'-20. The inverse relationship between the flow rate and the recapture yield is indicative of a more serious dilution effect with increased flow rate. Likewise, the volume in which the released DNA strand is carried away increases with flow rate, leading to yet more dilution (Figure 2-4).

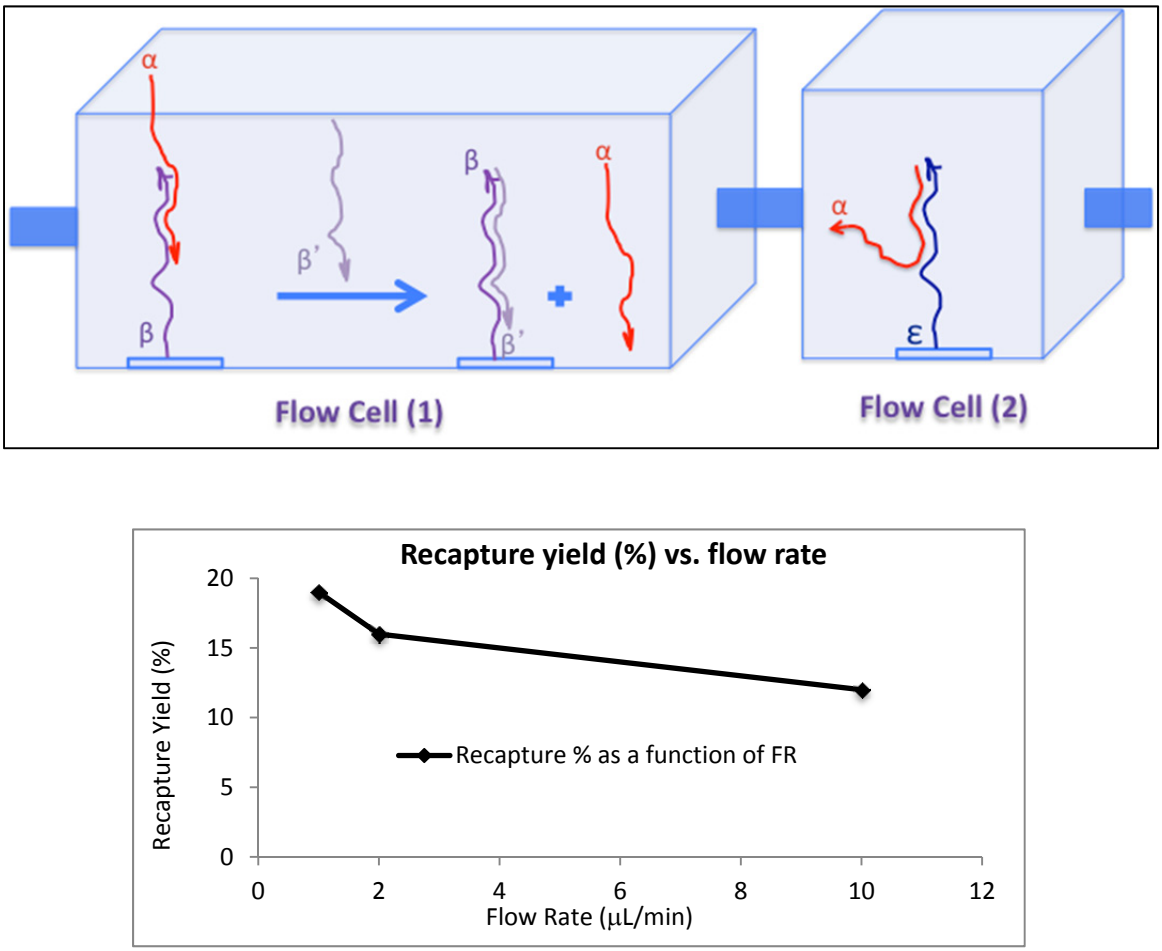

Figure 2-4: The schematic of the recapture experiment is on the top. The percentage of recapture diminishes quickly with the flow rate due to the dilution effect.

As shown in Figure 2-4, the maximum recapture efficiency attainable on the BIACORE chips is less than 20%, due to the dilution effect, the small surface area of the chip, and limited mass transport. This moderate α recapture efficiency will adversely affect the limit of detection of the assay. When two flow cells were functionalized with the ε probes to increase the recapture surface area, 29% recapture efficiency was observed at a flow rate of 2 μL/min. Doubling the relative surface area of recapture enhanced the recaptured amount by about 88% under the same experimental conditions. This indicates the limited mass transport and small surface area play very significant roles.

Thyroglobulin (Tg) is an FDA-approved cancer biomarker for the thyroid cancer [165,166]. Different plasma levels of Tg may be helpful in diagnosing thyroid cancer and

monitoring the progress of the disease and the treatment efficiency [167,168]. The monoclonal antibody against Tg (TgAb) was conjugated to the capture strand, α. The α-TgAb conjugate was then captured on the chip in a BIACORE X instrument and the antigen, Tg, was incubated with it. The whole complex was released via α' SDR with yields in the range of 72-82% depending on the concentrations of the conjugate and Tg.

To test the assay design depicted in Scheme 2-2, the first flow cell of a CM5 BIACORE chip was functionalized with β probes to form the cleanup unit. The second flow cell was functionalized with Tg to construct the sorting unit. The last two flow cells were functionalized with the ε probes to achieve recapture and quantification in the sensing unit. In the capture step, the flow path was set to cover only the cleanup flow cell. As expected, the recapture efficiency of the α-TgAb conjugate alone after a β' SDR is only 17%, compared to 29% for the unconjugated α capture strand under the same conditions due to a more limited mass transfer to the chip surface for the bigger molecule. The severity of the problem manifests itself most in the sorting cell, where only 5% of the α-TgAb conjugate was captured. When Tg was captured through the immobilized α-TgAb conjugate, the recapture yield in the sensing cells dropped even more from 17% (at the flow rate of 2 μL/min) to 5% (at the flow rate of 5 μL/min). These poor recapture efficiencies both in the sorting and sensing cells expose the extent of limited mass transfer and dilution effects. The results call for increasing the surface area functionalized with the capture molecules, in order to achieve less resistance to mass transport and higher capture yields. It seems that the analytical scheme in Scheme 2-2 could not be turned into a high performance sensitive assay unless the capture efficiency, especially in the sorting cell, is quantitative.

Conclusions

We employed DNA strand displacement reaction (SDR) to capture an antigen from the solution on the chip and further released it for detection. Our first efforts with DNA microarrays demonstrated SDR on a surface could be made to work, but the microarrays proved too irreproducible. We then showed the SDR was very reproducible (RSD 0.7-1.1 %) when performed via surface plasmon resonance. While the SDR, itself, proved to be a very efficient means of reversible analyte capture, the small surface area

of the capture and the properties of laminar flow led to inadequate mass transfer. To address this problem, the scheme demonstrated here needs to be refined to function on the beads where the surface to volume ratio is much larger. This approach is explored in the next chapter.

Supplementary information

Table 2-1 shows the reproducibility data for α' SDR yield repeated 12 times on SPR to estimate the RSD value (0.6%).

Cycle	8.7 μM α-30 in 5x SSC (6, 2) Signal	10 μM α'-25 in 5x SSC (4, 2) Signal	α' SDR Yield %
1	401	-290	72.3
2	403	-292	72.5
3	400	-288	72.0
4	397	-286	72.0
5	396	-283	71.5
6	400	-286	71.5
7	395	-282	71.4
8	395	-281	71.1
9	394	-281	71.3
10	394	-280	71.1
11	394	-280	71.1
12	394	-280	71.1
13	392	-279	71.2
Average	396.5	-283.7	71.5
SD	3.4	4.3	0.5
RSD %	0.9	1.5	0.7

Table 2-1: Reproducibility of α' SDR on SPR

Table 2-2 presents the indirect measurement of the β' SDR yield on SPR and its reproducibility over three cycles.

Cycle	8.7 μM α-30 in 5x SSC (6, 2) Signal	3.0 μM β'-20 in 5x SSC (4, 2) Signal	10 μM α'-25 in 5x SSC (4, 2) Signal	α-30 leftover from β' SDR = α'/0.61	β' SDR yield = 1 – (leftover α/ total α) %
1	393	-14	-40	-65.6	83.3
2	388	-12	-40	-65.6	83.1
3	388	-12	-36	-59.0	84.8
Average	389.7	-12.7	-38.7	-63.4	83.7
SD	2.9	1.2	2.3	3.8	0.9
RSD %	0.7	-9.1	-6.0	-6.0	1.1

Table 2-2: Reproducibility of β' SDR on SPR.

Experimental section

Materials and methods

DNA microarray slides were purchased from ArrayIt. Integrated DNA Technologies (IDT) synthesized all DNA strands. Human thyroglobulin (Tg) was purchased from Sigma-Aldrich. The monoclonal anti-thyroglobulin antibody (clone number 2H11) was from GeneTex. NeutrAvidin was obtained from Pierce. 1-Ethyl-3-[3-dimethylaminopropyl]carbodiimide hydrochloride (EDC) and N-hydroxysuccinimide (NHS) were from Sigma-Aldrich. 2-(*N*-morpholino)ethanesulfonic acid (MES) buffer, Phosphate Buffer Saline (PBS), and Saline Sodium Citrate (SSC) buffer were made in the lab and their pH values were adjusted to 6.0, 8.3, and 7.4, respectively. The 10 mM HEPES buffer containing 150 mM NaCl and 0.005% P20 (HBS-P) at pH 7.4 already prepared, degassed, and filtered was from Biacore GE Healthcare. The HPN buffer was

prepared by increasing the NaCl concentration of HBS-P to 500 mM. The NanoDrop ND-1000 UV-Vis spectrometer, Photon Technology International (PTI) Fluorometer, GenePix microarray scanner, OmniGrid DNA microarrayer, Biacore X and Biacore 3000 surface plasmon resonance (SPR) instruments were used. CM5 Chips were from Biacore (now GE Healthcare). The Biacore SPR instruments used in this study work in the fixed angle mode and report the change in intensity in response units (RU). They also take advantage of microfluidic technology that could generate two (in Biacore X model) or four flow cells (in Biacore 3000 model) on each chip. The pneumatic valves allow the flow paths to be chosen. A single flow cell could be isolated from the others by selecting the proper flow path. All DNA hybridizations on SPR were done at 25 °C. GenePix Pro 6.1 was used for the microarray data analysis. The antibody-DNA conjugation was done as described in Chapter 3 between the thyroglobulin antibody and α capture strand.

DNA sequence design

Four DNA sequences were designed using the online packages DINAMelt (http://mfold.rna.albany.edu/?q=DINAMelt/software) and OligoAnalyzer 3.1 (http://www.idtdna.com/analyzer/Applications/OligoAnalyzer/). All sequences were checked for their melting points to make sure they were all above 45 °C. The biotinylated probe strand, β, was made of 46 nucleotides; 13 of which at the 3' end complementary to the first 13 nucleotides of the capture strand, α, at its 3' end. The last 10 nucleotides at the 5' end of β acted as a spacer stretch for the better folding of the duplexes. Two displacing "fuel" strands, β' and α', were also designed to release the captured α strand. β' was composed of 20 nucleotides and a toehold of 7 nucleotides at the 5' end to form a 20 base pair duplex with the probe on the surface. The α' fuel strand had 25 bases complementary to α including a toehold of 12 nucleobases on α and leaving 5 bases as a short spacer between the functional parts of α and the antibody conjugated to it at the 5' end. The recapture biotinylated probe, ε-36, is complementary to a stretch of 16 bases at the 5' end of α-30. β'-41 is fully complementary to β probes. The sequences were optimized to be free of any significant secondary structure at room temperature (on DINAMelt) and cross-hybridization involving a stretch of more than 4 nucleotides

(OligoAnalyzer 3.1). All toeholds were larger than 7 nucleotides to assure a fast SDR kinetics. The sequences are shown below:

α-30: 5- TGA GAG ATA GAA TGA GAG GGA GGT GGC GGA -3

α'-25: 5-TCC GCC ACC TCC CTC TCA TTC TAT C -3

β-46: 5-/Biotin/ TCA CAC ACT ATC ACC ACT TTC TTC CAT CCT CAC TCC GCC ACC TCC C -3

ε-36: 5-/Biotin/ TTT TTT TTT TCC CCC TTT TTT CTC ATT CTA TCT CTC -3

β'-41: 5- GAT TAG GGA GGT GGC GGA GTG AGG ATG GAA GAA AGT GGT GA -3

β'-20: 5-GGG AGG TGG CGG AGT GAG GA -3

DNA microarray experiments

An epoxy-functionalized microarray slide (ArrayIt) was pin-printed in two rows of 8 squares. Each square contained 49 (7x7) individual spots. The β probe solution (10 μM) in 100 mM phosphate buffer was printed on the slides at 55% humidity and was left at 25% humidity for overnight to dry. The slide was then blocked in 5x SSC buffer containing 0.1% SDS and 1% BSA for 2 hour at 62 C in a Coplin jar (pre-hybridization step). After two quick washes in MilliQ water and 0.5x SSC, the slide was dried by centrifugation at 1500 rpm for 9 min. 2.0 μL α-Cy5 (10.0 nM) in 5x SSC containing 0.025% SDS was added to each square of the printed slide and was immediately covered with a coverslip to be protected from drying out. The slide was then put in the hybridization cassette where it was kept under high humidity. After 2 hours, the coverslip was removed and the hybridization solution was gently drained with a piece of Kimwipe. Immediately, to the first six squares was added Ctrl-TYE (2.0 μL/ square, 100 nM) and to the next eight squares β'-Cy3 (2.0 μL/ square, 100 nM) and the SDR was run for 1 hour. The slide was first washed twice with 0.1% SDS in 2x SSC each time for 2 min and then twice with 1x SSC each time 2 min and was finally dried by centrifugation. The slide was scanned in both red and green channels immediately and the images were analyzed using the GenePix Pro 6.1 software package. All DNA hybridizations were done at room temperature (21-24 °C).

SPR reproducibility experiments

The CM5 chips have carboxyl functional groups on their surface. The EDC/NHS standard chemistry was used to immobilize neutravidin on the chips. Equal volumes of 11.5 mg/mL NHS and 75.0 mg/mL EDC both in MilliQ water were mixed immediately upon preparation. For all SPR experiments, the following format is used to report the injection volume and flow rate: **(injection volume, flow rate)**. The hybridization time could simply be calculated by dividing the injection volume in μL by the flow rate in μL/min. The actual injection volume is always 20.0 μL larger than the number reported in the brackets to account for the dead volume of the microfluidic pathways. The mixture of EDC/NHS mentioned above was injected (70, 10). Neutravidin in acetate buffer (1.0 mg/mL, pH= 4.5) was reacted to the activated surface (70, 10). Finally, the chip surface was passivated by injection (70, 10) of 1.0 M ethanolamine hydrochloride in water (pH= 8.5). Three injections (10, 10) of the regeneration solution (50 mM NaOH in 1.0 M NaCl) assured all the non-specifically adsorbed neutravidin was removed. The biotinylated β probe in 5x SSC buffer (1.0 μM) was then immobilized (50, 10) followed by five more regeneration cycles (10, 10) to condition the surface and obtain a reproducible baseline level. The reproducibility experiment involved 54 cycles of NaOH/NaCl injection (2,5) followed by injection (15,5) of β'-20 (3.0 μM in 5x SSC). The drift in the signal level generated by β'-20 hybridization was representative of the relative amount of the probes lost upon exposure to NaOH/NaCl.

SDR proof of concept on SPR

For direct measurement of the α' SDR yield, α-30 (8.7 μM in 5x SSC) was injected (6, 2) first generating 390 RU (response units) signal. α'-25 (10 μM in 5x SSC) was then injected (4, 2) reducing the signal level by 280 RU. The α' SDR yield was calculated to be (280/390) x 100 = 72 %. The same experiment was repeated 12 times to estimate the RSD value (see Table 2-1).

For indirect measurement of the β' SDR yield, the steps shown in Table 2-2 were done. As a control and to calculate the α' SDR yield at a concentration of α-30 that would lead to the same amount of signal loss upon an α' SDR, the surface was first exposed to different dilutions of β'-20 followed by injections of α-30 (8.7 μM) and α'-25

(10 μM). A β'-20 concentration of 200 nM was picked to pre-occupy the surface capacity and reduce it to almost the same amount observed after the β' SDR and before the α' SDR in Table 2-2. The α' SDR yield was (50/82)*100 = 61 %. The value of 0.61 in the fifth column of Table 2-2 is adopted from the control experiment explained above. In a separate control experiment, a 3.0 μM β'-20 in 5x SSC hybridization (4, 2) generated about 363 RU signal.

Dose-response curves as functions of flow rates

Different concentrations of β'-20 in 5x SSC were injected for 3 min over a chip at a constant flow rate for three different flow rates (2, 10, and 30 μL/min). The same curves were built for α-30 and β'-41 to see how changing the DNA size from a 20-mer to a 30-mer and then a 41-mer would influence the mass transport to the chip surface.

Optimization of α' SDR yield

Flow rate studies: α-30 (2.0 μM) and α'-25 (10 μM) were in 5x SSC buffer. For varying flow rates (2, 10, and 30 μL/min) of α-30, the hybridization time (3 min) and α'-25 injection parameters (4, 2) were kept constant. For varying flow rates of α'-25 the injection time was always 2 min and the injection parameters (6, 2) of α-30 were kept the same.

Hybridization time studies: α-30 (2.0 μM) and α'-25 (10 μM) were in 5x SSC buffer. The flow rate was constant at 2.0 μL/min. When injection parameters needed to be kept constant, (6, 2) and (4, 2) were used for α-30 and α'-25, respectively. Different hybridization times (1, 2, 3, 5, 15 min) were obtained by changing the injection volumes.

Concentration studies: The flow rate was set to 2.0 μL/min and the hybridization times were 3 min and 2 min for α-30 and α'-25, respectively. The concentrations of α-30 and α'-25 were 2.0 μM and 10 μM, respectively, when kept constant.

α-30 Recapture

To perform the recapture experiment the first flow cell of a CM5 BIACORE chip was functionalized with β probes and the second flow cell with ε probes as described in

the reproducibility experiments. The ε probe is complementary to the second half of α-30 and shows no cross-hybridization to β'-20 fuel strand. α-30 (2.0 μM in 5x SSC) was captured on the first flow cell after a 3-min hybridization and later was released by injection of β'-20 (2.0 μM in 5x SSC) for 3 min at the same flow rate. This experiment was done at different flow rates. The ratio of the signals gained on the second flow cell to the first one yields the recapture efficiency.

The same experiment was repeated on a BIACORE 3000 instrument, where four flow cells are formed on the CM5 chip. This time the first flow cell was functionalized with β probes and the last two flow cells with ε probes.

(α-TgAb Conjugate + Tg) complex release on BIACORE X

All injections were done for 3 min at 5 μL/min on a CM5 chip functionalized with β probes. The chip surface was first passivated with a BSA solution (1.0 mg/mL) in HBS-P buffer and then, the α-TgAb conjugate (42 ug/mL) in HPN was injected. After another BSA passivation, Tg (225 ug/mL) in HBS-P was captured on the chip. Finally, α'-25 (5.0 μM) in HBS-P was injected to release the antibody-antigen complex.

α-TgAb conjugate recapture on BIACORE 3000

After a BSA passivation (50, 10), α-TgAb conjugate was captured (6, 2) on the first flow cell (517 RU signal). The flow path was then set to pass through flow cells 1 to 4. Flow cells 3-4 were already functionalized with ε probes. Injection (6, 2) of 1.0 μM β'-20 in HBS-P buffer released the conjugate from the first flow cell. It was partly recaptured later on flow cells 3-4 (90 RU signal).

(α-TgAb Conjugate + Tg) complex recapture on BIACORE 3000

The same procedure as the one described in the last section was used with the following changes: after the conjugate capture, Tg was injected and the total signal gain was 1092 RU. The release step was done using the same concentration of β'-20 for 3 min at 5 μL/min. 57 RU signal was gained in the recapture.

CHAPTER 3

DNA STRAND DISPLACEMENT REACTION FOR PROGRAMMABLE RELEASE OF BIOMOLECULES

Sample cleanup is a major processing step in many analytical assays, and the capture and subsequent release of the analyte from a solid phase is a common strategy. Here, we propose an approach to capture-and-release based on the DNA strand displacement reaction (SDR) and demonstrate its application to a fluoroimmunoassay on beads for a thyroid cancer biomarker, thyroglobulin. The DNA-directed immobilization of the primary thyroglobulin antibody on the silica microparticles is attained through its conjugation to a single-stranded DNA partially complementary to the DNA probes on the beads. Upon formation of a secondary, labeled antibody-antigen sandwich complex, the complex was specifically released via SDR for fluorimetry. The SDR-based cleanup showed no interference from matrix molecules in serum.

Introduction

The non-specific adsorption of matrix macromolecules in biological samples on solid supports often poses a big challenge to the accuracy and proficiency of assays through matrix effects [152,169]. Increased noise levels [153] and interferences with the analyte signal are common as a result [170]. Besides employing non-fouling surfaces [152,153], it can be effective to employ sample clean up steps prior to quantification [169]. One straightforward cleanup method is the specific capture and subsequent release of an analyte, for instance in solid phase extraction, or when using antibody-functionalized magnetic beads [171]. However, the significant change in solvent or

thermal conditions required for release means that many techniques still suffer from interference by matrix molecules, as they may also be released by the changed conditions. A methodology that involves highly specific binding and release, that does not require changed conditions (such as pH or ionic strength [172]) would be advantageous. Here, we exploit DNA hybridization, followed by a strand displacement reaction (SDR) as a very specific and programmable capture-and-release tool, which does not require changing buffer or temperature conditions. Instead, the specific release is achieved via SDR, a concept used in DNA biomolecular chemistry that provides rapid, isothermal dehybridization. SDR is one of the commonly used techniques in DNA nanotechnology [4] and molecular beacon-based sensing [14,15]. In the displacement reaction, two DNA single strands both complementary to the same template are used sequentially. The DNA strand with the larger number of matched nucleobases (also called a fuel strand) will replace the other strand already duplexed to the template [4,38], driven by forming a more thermodynamically stable duplex (Scheme 3-1). The nucleation site for the fuel on the template strand is sometimes referred to as the "toehold" [38]. The SDR is a fast, efficient, specific, and isothermal reaction and all these features are favorable in a sample cleanup technique.

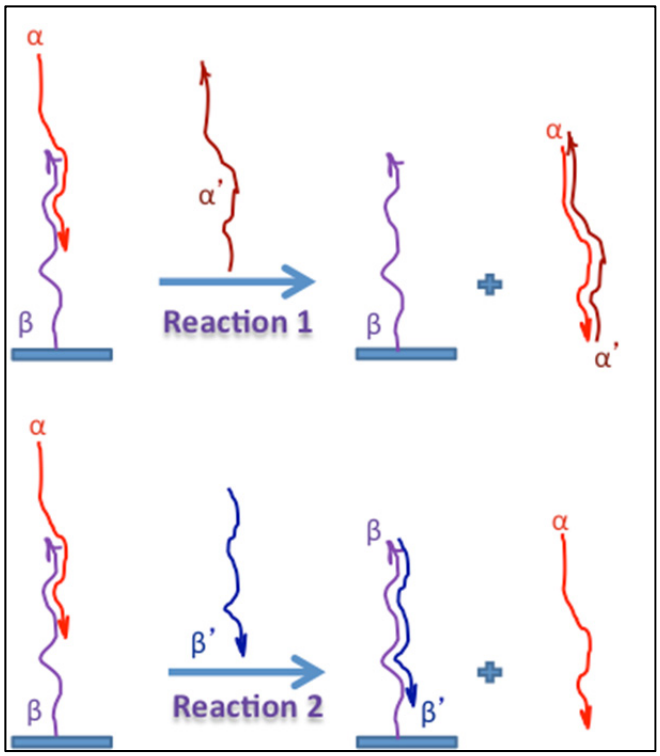

Scheme 3-1: Two possible ways of releasing the α capture strand off the surface using SDR. On the top, α is released as a duplex and at the bottom, as a single strand.

Fluoroimmunosorbent assays (FIA) [173] are well-established techniques in bioanalytical chemistry. They are negatively influenced by the matrix effect [134] and the background noise resulting on a solid support [174]. A highly specific release step in the assay, so that the signal reading could be done in solution ideally free of matrix molecules, would improve performance. We selected the challenging thyroid cancer biomarker, thyroglobulin (Tg) [165,166], immunoassay as the model to demonstrate the use of SDR for specific release of an immunosorbed complex. Tg is a challenging choice because it is huge (MW 660 kDa) and might exhibit a higher propensity for immunoprecipitation on beads even at low concentrations. The SDR was integrated into a sandwich FIA for thyroglobulin (Tg) [165,166], as a cleanup method. We first demonstrate that the SDR-mediated release scheme works effectively on silica microparticles functionalized with a relevant DNA probe. The thyroglobulin monoclonal antibody (TgAb) was conjugated to a capture DNA strand, α, [175,176] giving α-TgAb conjugate. It was immobilized on beads through duplex formation between capture and probe strands. An antibody-antigen-labelled antibody sandwich complex was

subsequently formed on the bead. The complex was then released from the beads using a SDR and was quantified in solution by fluorescence spectroscopy. The purpose of this study is to introduce use of the SDR process as a highly selective capture and release tool.

Results and discussion

To demonstrate that the SDR on beads is fast and efficient, the 2 μm carboxylated silica beads were first functionalized with neutravidin through the standard EDC/NHS chemistry [177,178]. The biotinylated probes were then fixed on the beads using the strong biotin-avidin interaction [179,180]. They were either partially complementary (β) or non-complementary (Ctrl) to the capture strand. The capture strand, α, labeled with carboxyfluorescein (FAM) was captured on 1.5 mg of beads in a hybridization step, followed by three washes. Finally, an incubation with the fuel strand, β', released the captured α strand via SDR. At the end of each step, the beads were pelleted by centrifugation and the supernatants were analyzed by fluorimetry. The beads were re-suspended at the beginning of each step using a bench-top vortex.

The SDR on beads happens fairly fast, with a high efficiency (90% when β' is the fuel strand), as indicated in Figure 3-1. The reproducibility of the process is very good and the RSD values for β' SDR capture and release are 2.8% and 5.6%, respectively. There is no detectable release off the control beads (Figure 3-1). These findings confirm the specific nature of the DNA sequence-mediated capture and release.

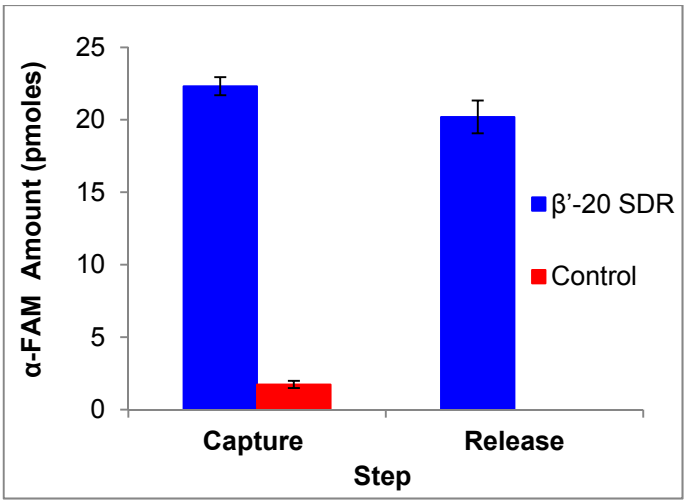

Figure 3-1: Proof of concept of SDR-mediated release on beads. The amounts of α-FAM (on y axis) were calculated based on its concentrations in the supernatants at the ends of both capture and release steps (on x axis) using the α-FAM calibration curve (Figure 3-7 in supplementary info). The captured amount in the control experiment was because of non-specific adsorption of α-FAM.

To integrate the SDR-mediated release with an immunofluorometric assay on beads, the primary antibody should be conjugated to the capture strand, α (Scheme 3-2). The steps needed to do such an assay include DNA-directed immobilization of the primary antibody on the beads, incubation of the antigen, then the labeled secondary antibody, and eventually release via hybridization of the fuel strand (Scheme 3-2). surface plasmon resonance (SPR) spectrometry was used to analyze the binding interactions, providing real time image of the binding events, and insights into the effects of non-specific adsorptions and steric hindrance on the SDR-mediated release of the complex. On a Biacore chip bearing the biotinylated β probes the α-TgAb conjugate was immobilized and the antigen (Human Tg) and the secondary antibody (TgAb-FAM) were subsequently added to form the immunosorbed sandwich complex. The beads were then subjected to the fuel strand α'-25, giving 49% release of the sandwich complex (Table 3-1 in supplementary info). (Figure 3-6 of supplementary info shows the SPR sensogram based on which Table 3-1 was compiled.) Notably, a prior surface passivation with bovine serum albumin (BSA) was necessary. SPR traces showed that BSA treatment as a prior surface passivation step significantly improved the SDR yield by suppressing non-specific adsorption of the α-TgAb conjugate, Tg, and TgAb-FAM. We also noted the SDR yield for removal of the α-TgAb conjugate (MW ~ 160 kDa) alone

was about 88%, in contrast to the 49% release for the sandwich complex (MW ~ 970 kDa). Such a significant drop in SDR yield may arise from reduced accessibility of the toehold for α'-25 or a much stronger barrier to mass transport, in the presence of the sandwich complex. Additionally, multivalent TgAb-Tg bindings, also known as "avidity" [181,182], may contribute to reduced release. Although TgAb used here is a monoclonal antibody, Tg is an oligomer comprised of several subunits and might contain several copies of the same epitope.

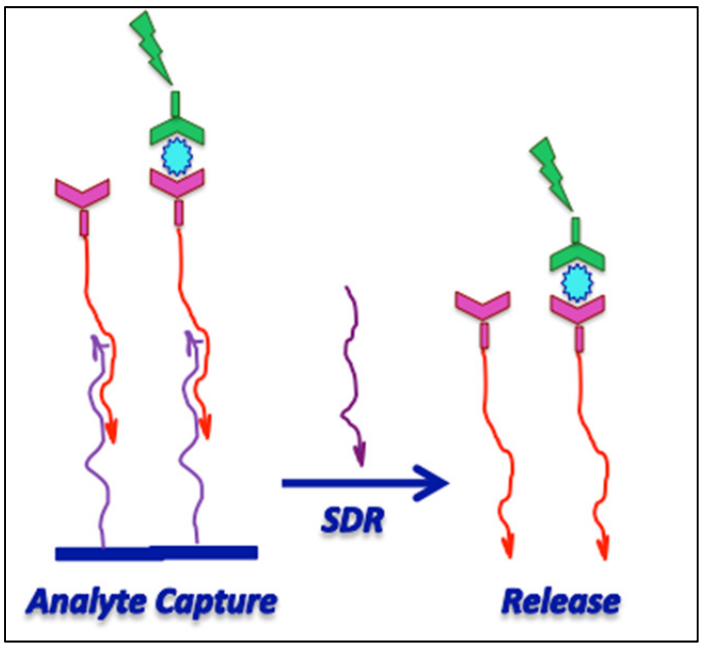

Scheme 3-2: SDR was integrated to a FIA on beads for sample cleanup.

The surface density of primary antibody on the beads is a potentially important factor in assay performance, and is governed by the concentration of the capture agent, α-TgAb conjugate, during surface loading with the conjugate. To optimize performance, we examined the capture and release profiles for sandwich complexes (α-TgAb/Tg/TgAb-FAM) as a function of different concentrations of the conjugate during surface loading. The sandwich complex release efficiency decreases significantly when the surface of the beads is overcrowded with conjugate; that is when conjugate is loaded on the beads at concentrations above 50 μg/mL (Figure 3-2). This may be due to the decreased accessibility of the toeholds on the probes to the fuel strand, or to more cooperativity in antibody-antigen binding (avidity) [181,182]. It is important to select a

conjugate concentration that gives rise to the optimal density of conjugates on the surface. Figure 3-2 shows that a solution concentration range of 20-50 μg/mL for the conjugate results in the highest release yield for the sandwich complex. (Figure 3-8 in the supplementary info includes the capture and release profiles used to prepare Figure 3-2).

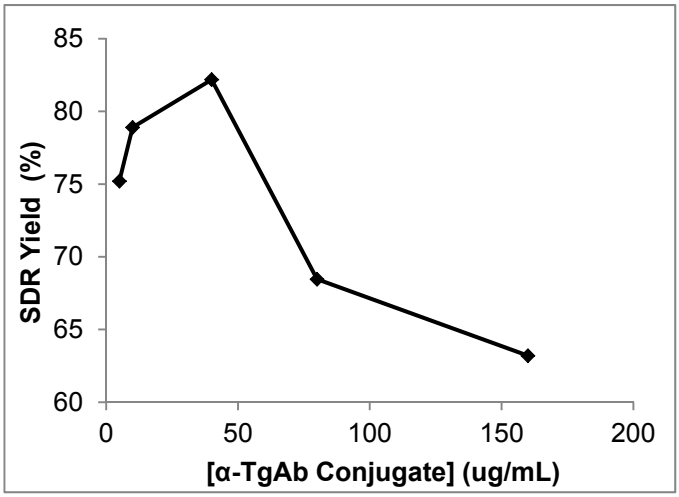

Figure 3-2: The DNA-directed immobilization of the conjugate on the beads makes its solution concentration dictate its surface density. The conjugate surface density, in turn, influences the SDR yields. The highest SDR yields lie in the α-TgAb conjugate concentration range of 20-50 μg/mL.

Ideally, the release yield should be independent of the concentration of antigen for a fixed surface loading concentration of the conjugate. To calculate the SDR release efficiencies, calibration curves for the capture and release of Tg were obtained (Figure 3-3). The capture curve and the release curve do not show a big difference in the saturation concentrations at which they reach their plateaus (Figure 3-3). (Figure 3-9 in the supplementary info examines the linear ranges of capture and release profiles shown in Figure 3-3.) This is consistent with the assumption that at a fixed solution concentration of the conjugate, its surface density has remained the same for all different concentrations of the antigen. In agreement with the results obtained from SPR, the SDR yield on beads for the labeled unconjugated α strand (90%) is larger than for the sandwich complex (63-82%) on beads.

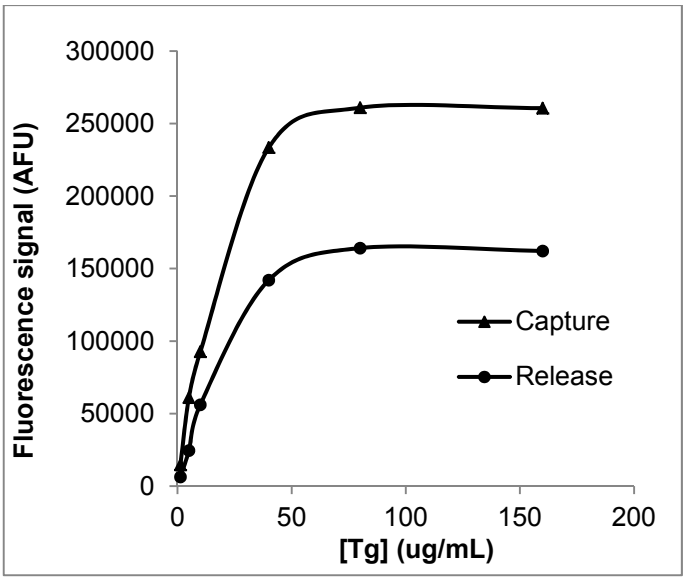

Figure 3-3: Capture and release profiles of the antigen, Tg, at the fix [α-TgAb] of 40 μg/mL were used to estimate the release yields in Figure 3-4.

As expected, the release to capture signal ratios stays almost constant at different concentrations of the antigen, although there is some difference at lower antigen concentrations (Figure 3-4). The non-specific portion of capture constitutes a significant fraction of the total capture signal at the lowest concentrations, leading to underestimation of the signal ratios at the lower end. The term "signal ratio" was used instead of the SDR yield because the non-specific capture was not subtracted from the total capture in this data set.

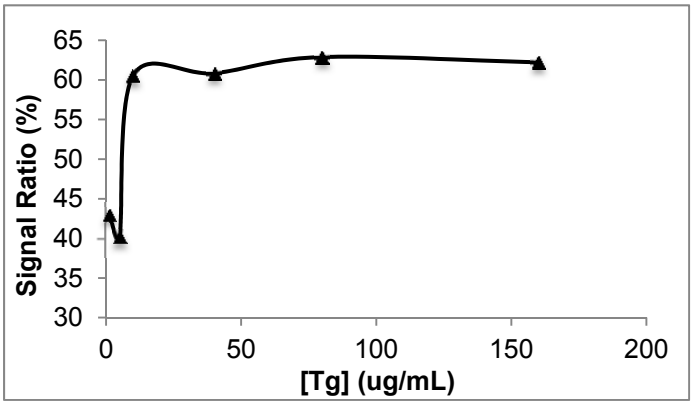

Figure 3-4: The release to capture signal ratios stay almost constant when the conjugate density on the surface is kept the same.

After the above study of the SDR-based capture in buffer, the performance was then tested in buffer and in serum spiked with Tg, with the release step performed in buffer. In data presented above, used to estimate the SDR yields, the concentration range for Tg was much higher than the clinically relevant one (above 2 ng/mL to μg/mL [167,168]). The calibration curves for Tg in both buffer and serum are shown in Figure 3-5. The presence of the complex matrix molecules clearly has no significant negative effect on the performance of the assay in serum. The linear range for the Tg detection is 12.6-2000 ng/mL for Tg in the serum (R2= 0.998) (Figure 3-5). The differences in signal intensities between the two curves stem from the slightly different solution concentrations of the α-TgAb conjugate during bead surface loading (20.0 μg/mL in case of buffer and 23.0 μg/mL for the spiked serum) (Table 3-2 in supplementary info). The RSD of release for the triplicate measurements of a Tg concentration (62.5 ng/mL) in the lower end of the spiked serum calibration curve was 4.2%. It was also observed that similar release efficiency was achievable with α'-25 as the fuel strand instead of β'-20 (Figures 3-12 and 3-13 in supplementary info).

It is also worth mentioning that the dynamic range of the assay could be shifted to a desired concentration range by changing the experimental conditions. This is evident from comparing Figure 3-5 with Figure 3-9, where changing the conjugate concentration and instrumental sensitivity led to a shift in dynamic range toward much less Tg concentrations.

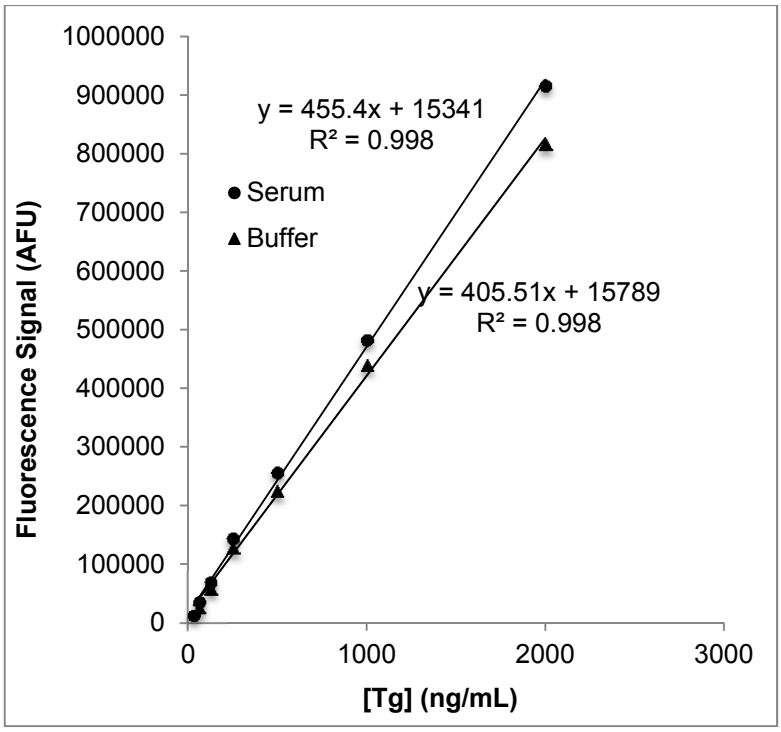

Figure 3-5: The calibration curve for Tg captured from spiked serum samples and released into a buffer shows a performance similar to the Tg in buffer samples.

Conclusions

We demonstrated the successful application of the DNA strand displacement reaction (SDR) to the sequential capture and release of an antigen, thyroglobulin, and its sandwich antibody complex. Addition of such a fast, efficient, and in situ cleanup mechanism to a conventional fluoroimmunosorbent assay on beads will provide an additional aid in overcoming non-specific adsorption. This sort of capture and release tool could potentially be integrated into other assay formats. It also lends itself to multiplexing given the sequence-specific nature of the DNA duplex formation.

Supplementary information

Characterization of the conjugate by surface plasmon resonance (SPR) measurements

To assure that the conjugates are comprised of the α-30 capture strand covalently attached to a still functional TgAb, interaction analyses were performed on a Biacore X

SPR instrument. A CM5 Biacore chip was functionalized with neutravidin using the standard EDC/NHS chemistry [183] and the biotinylated β-46 probes were immobilized on the chip. The surface was first passivated by injecting BSA 0.1% in HBS-P buffer and then the α-TgAb conjugate (91.5 μg/mL with respect to TgAb) was injected to the surface of the chip to immobilize the conjugate via duplex formation between the α-30 capture strand of the conjugate and the immobilized β probes on the chip. The Human Thyroglobulin (Tg) antigen (225 μg/mL) was then injected followed by the injection of the secondary antibody, TgAb-FAM, (180 μg/mL) to form the sandwich complex on the chip. The complex was released after injection of the fuel strand α'-25 (5.0 μM). It should be noted that α'-25 was used here because its sequence is orthogonal to the β probes on the surface and will not bind to surface to generate any signal. As a result of this, the signal loss observed upon injection of α'-25 is entirely due to the DNA strand displacement reaction. The same experiment was repeated without the antigen (Tg) injection step to examine the non-specific adsorption of TgAb-FAM and also the SDR yield of the α-TgAb conjugate alone. The SPR data in response units (RU) is shown in details in Table 3-1:

Step	Time (seconds)	Signal change in RU (experiment)	Time (seconds)	Signal change in RU (control)
BSA (1.0 mg/mL)	**900**	**- 5.0**	**5406**	**6.7**
α-TgAb conjugate (91.5 µg/mL)	**1563**	**2902**	**6092**	**2941**
BSA (1.0 mg/mL)	**2031**	**- 9.0**	**6755**	**- 9.4**
Tg (225 µg/mL)	**2665**	**1535**		**No injection**
BSA (1.0 mg/mL)	**3103**	**- 8.9**		**No injection**
TgAb-FAM (180 µg/mL)	**3788**	**410**	**7382**	**- 1.3**
α'-25 fuel (5.0 µM)	**4403**	**-2334**	**8120**	**- 2575**
Total Capture		**4824**		**2937**
α'-25 SDR Yield (%)		**48.4**		**87.7**

Table 3-1: SPR Signal level changes were calculated by subtracting the signal level before the injection from the one after the injection where the signal is fully stable. A negative value for the signal level change means the signal dropped by that amount. All injections were at 5.0 µL/min and the injection volume of 15.0 µL. The times columns correspond to the X axis of the sensogram shown in Figure 3-6.

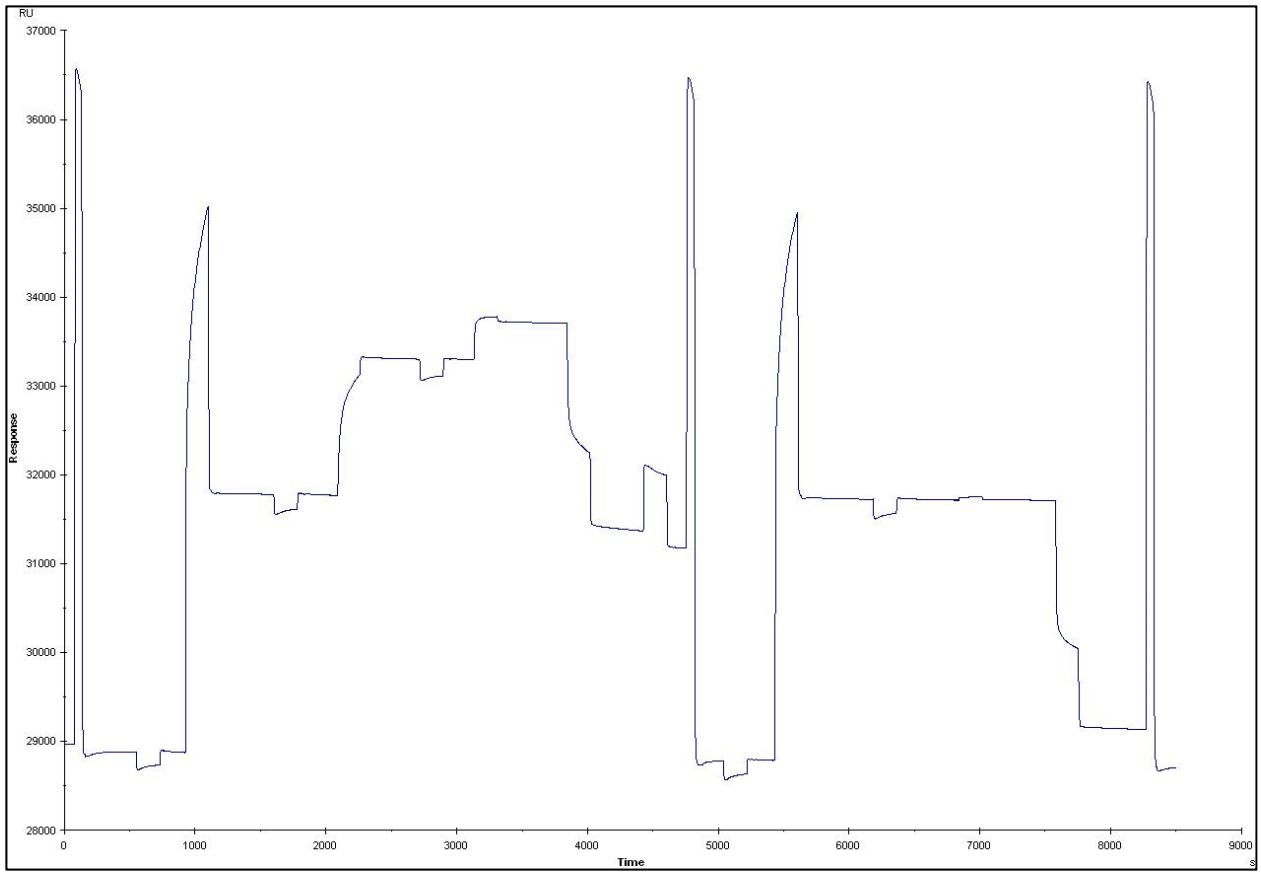

Figure 3-6: The SPR sensogram based on which Table 3-1 was composed. To find which peak relates to which step see Table 3-1.

In a separate control experiment, the α-30-SH capture strand and the unconjugated TgAb were mixed together and injected over the chip. Incubation of the antigen, Tg, in the next step produced no signal confirming that the covalent attachment of the capture strand, α-30, to TgAb is crucial to the successful immobilization of TgAb on the chip.

Calibration curve for α-FAM

To pick a concentration that falls in the linear range of α-FAM, a standard curve was obtained using different dilutions of the α-FAM stock:

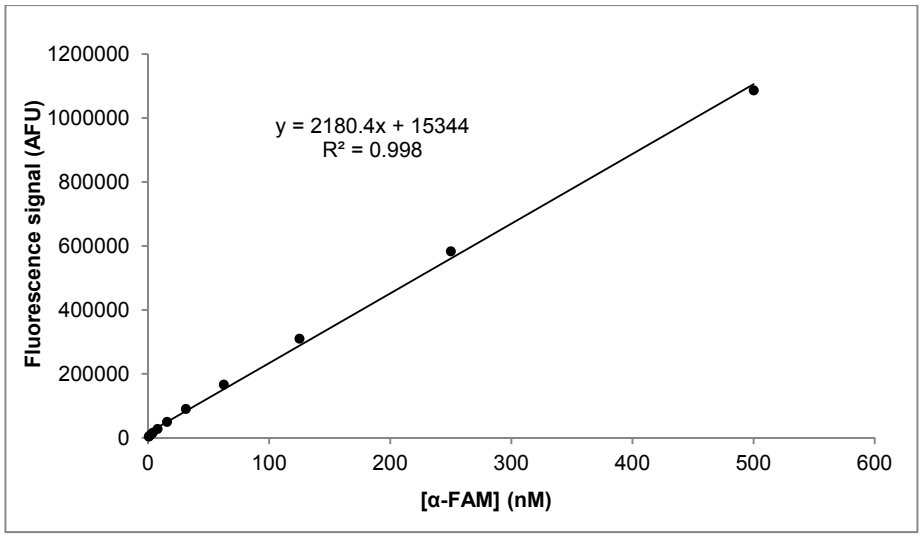

Figure 3-7: Standard curve for α-FAM.

The 500 nM concentration was taken for the experiment. This calibration curve was used to estimate the concentrations of α-FAM in the supernatants and thus calculate the captured and released amounts reported in Figure 3-1 in pmoles.

Optimization of α-TgAb conjugate concentration

The general procedure for FIA on beads (see experimental section) was adopted using five different concentrations of α-TgAb conjugate. For each concentration of the conjugate a replicate with the Ctrl probe-functionalized beads was done at the same time. The capture signal of the Ctrl beads was subtracted from the capture signal of its corresponding experiment to account for the capture resulted from non-specific adsorptions. The yield in percentage (in Figure 3-2) was the release signal divided by the Ctrl-subtracted capture signal at each conjugate concentration. Figure 3-8 shows the capture and release profiles as functions of α-TgAb conjugate concentration. This figure was used to obtain release yields in Figure 3-2.

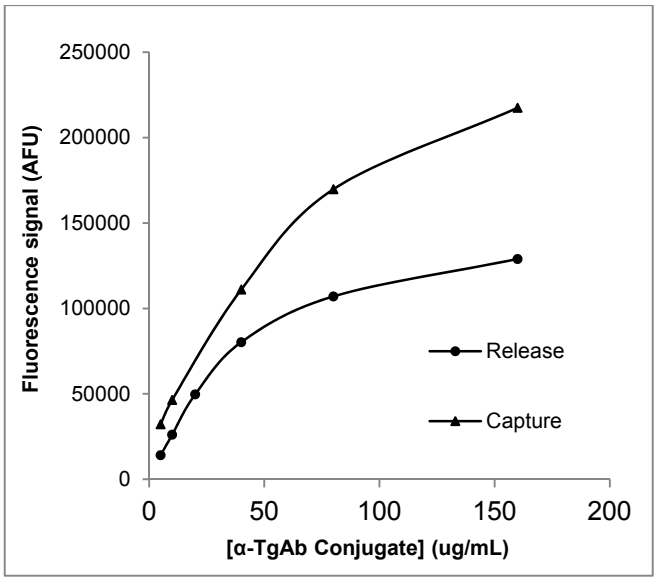

Figure 3-8: Capture and release profiles as functions of [α-TgAb conjugate].

Linearity of capture and release profiles at a fixed conjugate concentration

The linearity of capture and release profiles presented in Figure 3-3 was investigated in Figure 3-9. A calibration curve for TgAb-FAM was obtained using different concentrations of TgAb-FAM (Figure 3-10). The calibration curve for TgAb-FAM is a control to assure that the labeled secondary antibody behaves linearly in the concentration ranges studied.

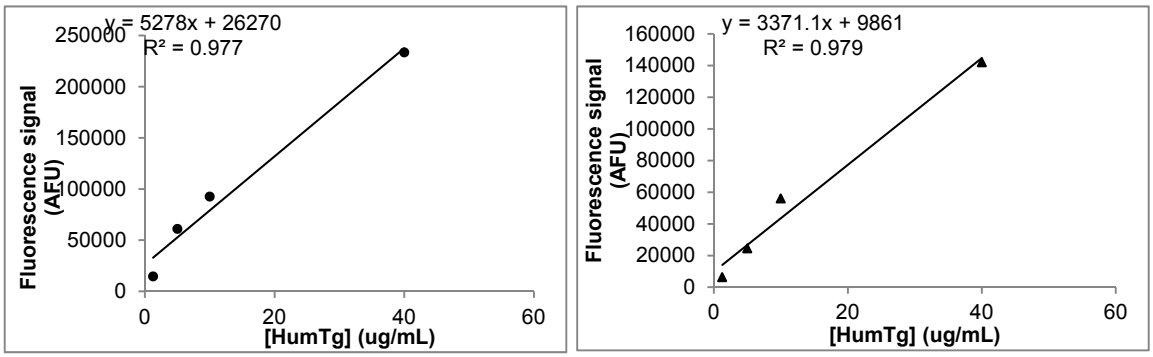

Figure 3-9: Examining the linear ranges of the capture (left) and release (right) profiles shown in Figure 3-3.

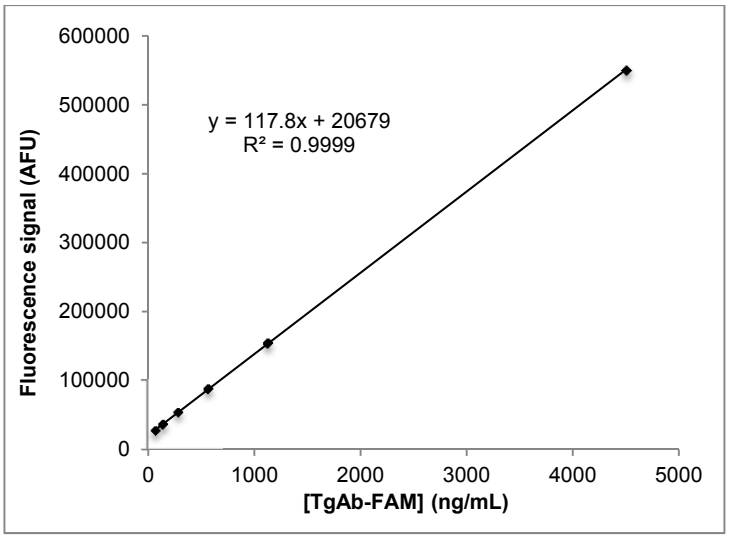

Figure 3-10: Calibration curve for TgAb-FAM in buffer indicates that the TgAb-FAM response is completely linear in the concentration range of interest.

The linearity of the capture and release profiles (Figure 3-9) is much worse than the one for TgAb-FAM (Figure 3-10) as is evident from the linear regression coefficients. Linearity depends on many factors including the non-specific adsorptions and how strong the multivalent antigen-antibody binding is across the concentration range examined, among the others. Both mentioned factors would improve at the lower Tg concentrations.

Comparison of calibration curves for Tg in serum versus Tg in buffer

The general procedure for FIA on beads was followed (see experimental section) with six different concentrations of Tg in buffer and in bovine serum to build the calibration curves in Figure 3-5. Of particular interest is the improvement observed with linearity in terms of the regression coefficients when compared to Figure 3-9. In Figure 3-5, a much lower concentration range (62.5-2000 ng/mL) for Tg was examined. The calibration curve for TgAb-FAM in buffer under the same instrumental setups establishes a control experiment (Figure 3-11), assuring that the labeled secondary antibody behaves linearly in the concentration ranges studied.

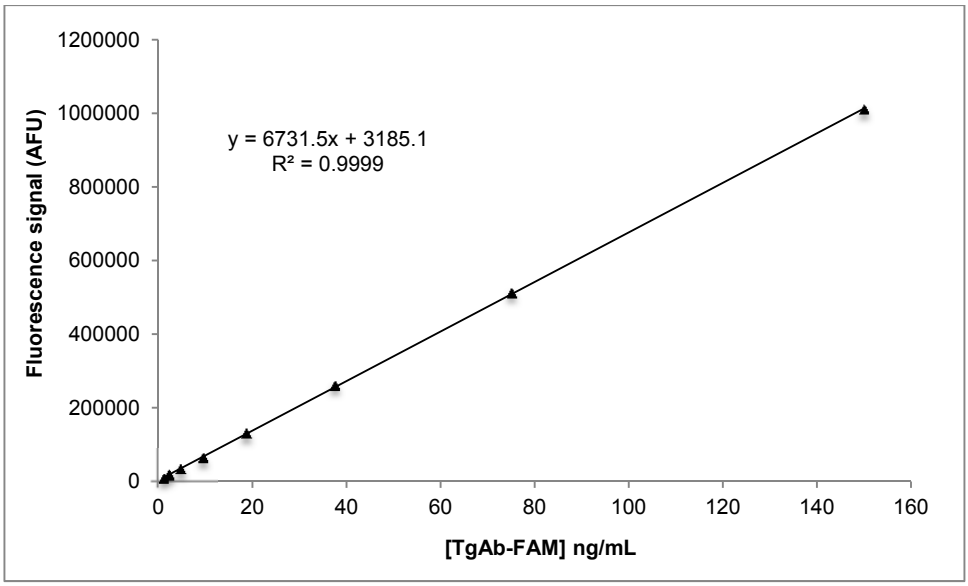

Figure 3-11: Calibration curve for TgAb-FAM in buffer shows a perfectly linear response for the labeled secondary antibody in the concentration range of interest.

Table 3-2 shows how an increase of roughly 15% in the solution concentration of the conjugate from the buffer to serum experiments manifests itself almost proportionately as higher release signals in serum. This is especially the case at the higher and intermediate concentrations of the calibration curves shown in Figure 3-5.

[Tg] (ng/mL)	Signal in buffer	Signal in serum	Signal ratio (serum/buffer)
2000	815997	916370	1.12
1000	439341	481915	1.10
500	224413	255673	1.14
250	127954	143233	1.12
125	57539	69018	1.20
62.5	26184	35377	1.35

Table 3-2: The signal ratios of release in serum to release in buffer indicate roughly the same magnitude of increase in probe densities when there was a 15% increase in the solution concentration of the conjugate.

SDR-mediated release using different fuel strands

Although all results shown so far were obtained using the β'-20 fuel strand, both SDR formats were found to work with almost similar yields as indicated in Figure 3-12. Following the general procedure for Tg FIA on beads and using Tg (1.0 μg/mL) in HBS-P buffer, three different release experiments were conducted using α'-25, β'-20, and α'-25+β'-20 as fuel strands. It should be noted that α'-25 and β'-20 have 13 complementary base pairs and form a partial duplex as soon as they are mixed together. Nonetheless, the release efficiency for the mixture remains almost the same as the ones for the each fuel strand alone (Figure 3-12), probably due to the higher resistance to the mass transport of the combined fuel strands to the surface.

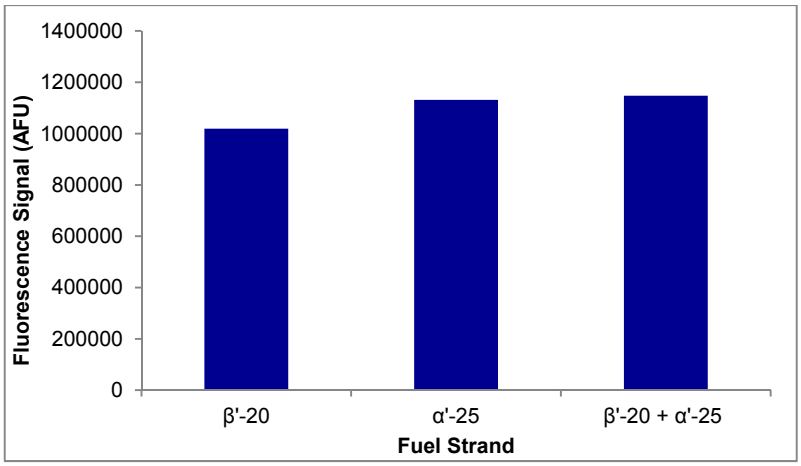

Figure 3-12: Both SDR formats will bring about very efficient releases at [Tg]= 1.0 µg/mL in buffer.

When the same experiments were repeated with Tg in the bovine serum at a much lower concentration of 62.5 µg/mL similar results were obtained (Figure 3-13). This indicates that the release efficiency does not depend on whether the toehold is embedded in the capture strand sequence or in the probe sequence, which is closer to the surface.

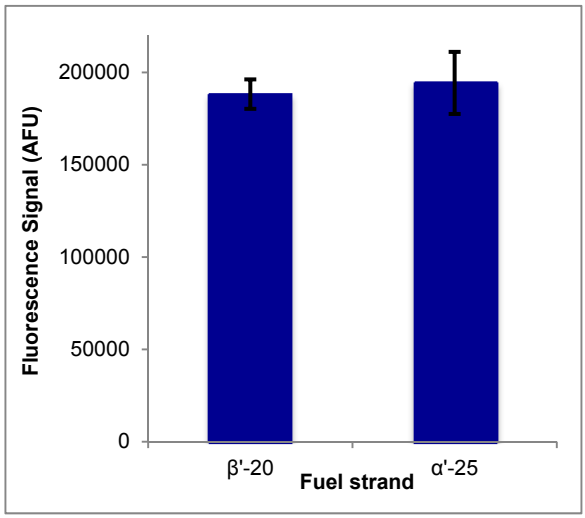

Figure 3-13: Effect of fuel strand type on the release signal at low [Tg] in serum.

Experimental section

Materials and methods

Integrated DNA Technology (IDT) synthesized all DNA strands. Human thyroglobulin was purchased from Sigma-Aldrich. The monoclonal anti-thyroglobulin antibody (clone number 5E6) and the FAM-labeled monoclonal anti-thyroglobulin secondary antibody (clone number 6F9) were from HyTest. NeutrAvidin was obtained from Pierce. Silica microparticles functionalized with carboxyl groups (2 μm mean diameter) were from Bang Laboratories. 1-Ethyl-3-[3-dimethylaminopropyl]carbodiimide hydrochloride (EDC) and N-hydroxysuccinimide (NHS) were from Sigma-Aldrich. Sulfosuccinimidyl-4-(N-maleimidomethyl)cyclohexane-1-carboxylate (Sulfo-SMCC) was from GBiosciences. 2-(N-morpholino)ethanesulfonic acid (MES) buffer, Phosphate buffer Saline (PBS), and Saline Sodium Citrate (SSC) buffer were made in the lab and their pH values were adjusted to 6.0, 7.2, and 7.4, respectively. The 10 mM HEPES buffer containing 150 mM NaCl and 0.005% P20 (HBS-P) at pH 7.4 already prepared, degassed, and filtered was from Biacore GE Healthcare. The HPN 0.5 M buffer was prepared by increasing the NaCl concentration of HBS-P to 500 mM. All DNA hybridizations were done at room temperature (21-24 °C). The ultrafiltration devices and Glen Gel-Pak DNA desalting columns were bought from Millipore and Glen Research, respectively. The NanoDrop ND-1000 UV-Vis spectrometer, Photon Technology International (PTI) Fluorometer, Biacore X SPR and Applied Biosystems Voyager MALDI-TOF-MS instruments were used. The CM5 Chips were from Biacore (now GE Healthcare). The BCA kit was from Pierce.

DNA Sequence design

Four DNA sequences were designed using the online packages DINAMelt (http://mfold.rna.albany.edu/?q=DINAMelt/software) and OligoAnalyzer 3.1 (http://www.idtdna.com/analyzer/Applications/OligoAnalyzer/). All sequences were checked for their melting points to make sure they were all above 45 C. The 5'-biotinylated probe strand, β, was made of 46 nucleotides; 13 of which at the 3' end

complementary to the first 13 nucleotides of the capture strand, α, at its 5' end. The last 10 nucleotides at the 5' end of β acted as a spacer stretch for better folding of the duplexes. Two displacing "fuel" strands, β' and α', were also designed to release the captured α strand. β' was composed of 20 nucleotides and a toehold of 7 nucleotides at the 5' end to form a 20 base pair duplex with the probe on the beads. The α' fuel strand had 25 bases complementary to α leaving a toehold of 12 nucleobases on α and 5 bases as a short spacer between the functional parts of α and the antibody conjugated to it at the 5' end. The sequences were optimized to be free of any significant secondary structure at room temperature (on DINAMelt) and any cross-hybridization involving a stretch of more than 4 nucleotides (OligoAnalyzer 3.1). All toeholds were larger than 7 nucleotides to assure a fast SDR kinetics. The sequences are shown below:

α-30: 5-/Thiol or FAM/ TGA GAG ATA GAA TGA GAG GGA GGT GGC GGA -3

α'-25: 5-TCC GCC ACC TCC CTC TCA TTC TAT C -3

β-46: 5-/Biotin/ TCA CAC ACT ATC ACC ACT TTC TTC CAT CCT CAC TCC GCC ACC TCC C -3

Ctrl-46: 5-/Biotin/ ACA CAC ACA CAC ACA CAC ACA ACA CAC ACA CAC ACA CAA CAC TAC T -3

β'-20: 5-GGG AGG TGG CGG AGT GAG GA -3

Immobilization of the DNA probes on silica beads

Each step described here involving a reaction or process on beads starts with re-suspending the beads after addition of buffers/reagents using a benchtop vortex and ends with spinning down the beads at 10,000 g for 3 min to remove the supernatant using a micropipette. The 2.0 μm silica microparticles already grafted with linkers containing carboxyl groups at their ends were from Bang Laboratories. For a typical NeutrAvidin immobilization [177,178,184-186], 30 mg beads were washed with 1.0 mL MilliQ water, and soaked in 1.0 mL MES buffer (pH= 6.0) for overnight. The beads were then centrifuged down again, the supernatant was discarded, 1.0 mL fresh MES was added and the suspension was sonicated for 90 min. 500 μL freshly prepared EDC (0.4M) was mixed with 500 μL freshly prepared NHS (0.4M) and the mixture was added immediately to the beads. After 10 minutes the beads were washed with 1.0 mL

MES6.0 buffer quickly. 750 µL NeutrAvidin (0.4 mg/mL) in MES6.0 buffer was added to the beads and incubated with them for 8 hours on vortex. To quench any unreacted activated NHS ester, 1.0 mL Ethanolamine 1.0 M (pH= 8.5) was used for 30 min on vortex. Two more washes each time with 1.0 mL 2.5x SSC for 1 min on vortex would make the beads ready for the immobilization of the probes. 1.20 mL DNA probes (either β-46 or Ctrl-46 biotinylated at their 5' ends, 2.5 µM) in 2.5x SSC buffer were mixed with the beads for 16 hours on vortex. Two washes each time with 1.0 mL HBS-P buffer for 1 min on vortex were done at the end and finally the bead suspensions were divided into 20 equal portions of each 1.5 mg.

Synthesis of the conjugate

Sulfo-SMCC was chosen as the small molecule linker between the DNA single strand and the Anti-Thyroglobulin primary antibody (TgAb). Sulfo-SMCC reacts with its NHS ester end to the amino groups on the amino acid side-chains of the antibody and through its Maleimide functionality to the thiolated α-30 capture strand. Hence, the synthesis is accomplished in three steps:

1) Sulfo-SMCC attachment to TgAb

The kinetics of the reaction depends on the concentrations of the reagents, the molar ratio, and the reaction time. The procedure should be customized for each antibody, as they might be very different in reactivity as a result of their sources, clonality, post-translational modifications and hosts. The recipe presented here was compiled based on previously reported [175,176,187-189] procedures and was specifically optimized for TgAb.

For a typical reaction, 100 µg TgAb (clone # 5E6) was used. The antibody is supplied in PBS buffer containing 0.1% Sodium Azide as a preservative. Since an azide could act as a nucleophile, it is necessary to remove it before the reaction. Three filtrations and buffer exchanges with PBS pH 7.2 on an Amicon ultrafiltration device (MWCO 50 kDa) at 14000 g (for 3 min each time) removes the azides efficiently. Sulfo-SMCC was dissolved in PBS pH 7.2 to yield a concentration of 1.0 mg/mL. 100 µL TgAb (1.0 mg/mL, 666.7 pmole) was then reacted to the 8x molar excess of Sulfo-SMCC (5.33 nmole, 1.0 mg/mL) for 30 min on vortex. After 30 min, the reaction mixture was

centrifuged at 21000 g for 2 min to make sure no precipitation has occurred. Ultrafiltration and buffer exchange with PBE for three times (at 14000 g, 3min each time) using an Amicon filter (MWCO 50 kDa) removed the unreacted/ hydrolyzed Sulfo-SMCC and small-molecule by-products. The functionalized TgAb was quantified by a NanoDrop UV-Vis spectrometer.

2) Disulfide bond reduction of α-30 capture strand

The thiolated α-30 capture strand from IDT (α-30-Thiol) bears a disulfide bond at its 5' end with a C6 linker. Thus, it is necessary to reduce that bond to obtain nucleophilic thiol groups. The DTT reduction procedure could be carried out using 10-300 mM DTT at pH 8.0 to 8.5 for 30 min [190-193]. It should be noted that pKa for the thiol group is about 8.3 and therefore, pH of PBE used in this work was set to 8.3. 250.0 µL α-30-Thiol (10.0 µM) in PBE pH 8.3 was used to dissolve 11.6 mg DTT (making the final concentration of 300 mM DTT) and the reaction was run at room temperature on the vortex for 4 hours. A Glen Gel-Pak gravity column for DNA desalting was used to purify the reduced α-30-Thiol and remove the small molecule by-products and unreacted DTT based on size exclusion chromatography. The reduced α-30-Thiol collected from the column was quantified by NanoDrop and used immediately in the next reaction to minimize the chance of re-oxidation.

3) Conjugation of the reduced α-30-Thiol strand to the maleimide group of TgAb-SulfoSMCC

To obtain a DNA:Ab ratio of around 1.0 in the product, an experimental ratio of 1.2 DNA:Ab was established. Different optimization attempts also indicated that the initial concentrations of TgAb-SulfoSMCC and the reduced α-30-Thiol should be approximately 1.0 µM each. In a typical reaction, 144 µL TgAb-SulfoSMCC (0.84 mg/mL, 805 pmole) was diluted to 644 µL using PBE buffer pH 7.2 and was added to it 212 µL reduced α-30-Thiol (4.56 µM, 967 pmole) in PBE buffer pH 7.2. The reaction time was 30 min on vortex and centrifugation at 21000 g for 2 min at the end showed no precipitation. The unreacted reduced α-30-Thiol was removed using an Amicon ultrafiltration device (MWCO 50 kDa) by three filtrations (at 14000 g each time for 3 min) and buffer exchange with HBS-P buffer containing 500 mM NaCl (HPN). The

concentration of α-TgAb conjugate was measured by UV-Vis spectrometry and the DNA:Ab ratio was calculated to be 0.98 using the molar extinction coefficients of TgAb and α-30-Thiol at 260 nm and 280 nm. The BCA protein assay for a number of conjugated products made in different batches was in a very good agreement with the values calculated from the UV-Vis measurements.

Characterization of the conjugate by SPR measurements

To assure that the conjugates are comprised of the α-30 capture strand covalently attached to a still functional TgAb, interaction analyses were performed on a Biacore X SPR instrument. A CM5 Biacore chip was functionalized with neutravidin using the standard EDC/NHS chemistry [183] and the biotinylated β-46 probes were immobilized on the chip. The surface was first passivated by injecting BSA 0.1% in HBS-P buffer and then the α-TgAb conjugate (91.5 μg/mL with respect to TgAb) was injected to the surface of the chip to immobilize the conjugate via duplex formation between the α-30 capture strand of the conjugate and the immobilized β probes on the chip. The Human Thyroglobulin (Tg) antigen (225 μg/mL) was then injected followed by the injection of the secondary antibody, TgAb-FAM, (180 μg/mL) to form the sandwich complex on the chip. The complex was released after injection of the fuel strand α'-25 (5.0 μM). The SPR data in response units (RU) is shown in details in Table 3-1.

SDR-based release of α-FAM

Each step described from this point on starts with re-suspending the silica beads functionalized with β probes in the reaction solution, vortexing for a specified period of time, and centrifugation of the suspension at 10000 g for 3 min to remove the supernatant.

To pick a concentration that falls in the linear range of α-FAM, a standard curve was obtained using different dilutions of the α-FAM stock (Figure 3-7). The 500 nM concentration was taken for the experiment. The calibration curve was used to estimate the concentrations of α-FAM in the supernatants and thus calculate the captured and released amounts in pmoles.

1.5 mg β-functionalized beads were sonicated in 300 μL HPN buffer (pH=7.4) for 45 min and were incubated with 150.0 μL α-FAM (500 nM) in HPN for 5 min. The

beads were washed twice with 150.0 μL HPN buffer each time for 1 min. The third wash was also with 150.0 μL HPN but for 15 min. Finally, the release step included incubation with 150.0 μL β'-20 fuel strand (2.50 μM) in HPN for 15 min. All supernatants were saved after each step for fluorescent measurements. A control experiment was done at the same time on 1.5 mg silica microparticles functionalized with Ctrl-46, a DNA probe that has no stretch complementary to α-FAM.

SDR-based FIA on beads

Each step again starts with adding a given reagent to 1.5 mg beads, re-suspending and incubating for a period time on vortex, and centrifugation at 10,000 g for 3 min to remove the supernatant before going to the next step. The general procedure is as follows: 1.5 mg beads were suspended in 300 μL HPN buffer and sonicated for 60 min followed by incubation in 2.0 mg/mL BSA in HPN for 5 min. Resuspension of the beads in 100.0 μL α-TgAb conjugate (concentration varies with the type of experiments) in HPN for 15 min puts a layer of primary TgAb on the surface of the beads via DNA-directed immobilization. After two washes with 150.0 μL HBS-P buffer for 3 min and another 5 min incubation with 150.0 μL 2.0 mg/mL BSA in HBS-P buffer, 150.0 μL Tg (concentration depends on the experiment) in HBS-P buffer containing 2.0 mg/mL BSA was added and incubated for 30 min. The two washes and BSA incubation steps were repeated as described above. 150.0 μL TgAb-FAM (9.0 μg/mL) in HBS-P buffer containing 2.0 mg/mL BSA was then reacted for 30 min to form the sandwich complex. The supernatants of this step were saved for fluorescence measurements to obtain the capture signal. The first wash with 150.0 μL HBS-P was only for 1 min and was repeated once more. Incubation with 150.0 μL BSA 2.0 mg/mL in HBS-P for 45 min completed the wash steps between the capture and release. The release step was accomplished by resuspending the beads in 150.0 μL β'-20 fuel strand (5.0 μM) in HBS-P buffer containing 2.0 mg/mL BSA for 45 min. The supernatant of this step was also saved to measure the release signal.

Optimization of α-TgAb conjugate concentration

The general procedure was adopted with the following changes: the volume at the conjugate incubation step was reduced from 100.0 μL to 50.0 μL and five different

concentrations were used. For each concentration of the conjugate, 50.0 μL Tg (100 μg/mL) in HBS-P buffer containing 2.0 mg/mL BSA was used. For each concentration of the conjugate a replicate with the Ctrl probe-functionalized beads was done at the same time. The average capture signal of the Ctrl beads was subtracted from the capture signal of its corresponding experiment to account for the capture resulted from the non-specific adsorptions. The yield in percentage was the release signal divided by the Ctrl-subtracted capture signal at each conjugate concentration.

Estimation of the SDR yields at a fixed conjugate concentration

The general procedure was adopted with the following changes: the conjugate concentration of 40.0 μg/mL was used for all experiments. 100.0 μL Tg at six different concentrations were used to build the calibration curve.

Comparison of calibration curves for Tg in serum versus Tg in buffer

The general procedure was followed with different concentrations of Tg in buffer and in bovine serum with the following changes: the conjugate concentrations of 20.0 μg/mL and 23.0 μg/mL were used for the buffer and bovine serum experiments, respectively. 150.0 μL Tg at six different concentrations were used to build the calibration curves. The second and third washes after TgAb-FAM incubation were done for 45 min and 15 min. Of particular interest is the improvement observed with linearity in terms of the regression coefficients when a much lower concentration range (62.5-2000 ng/mL) for Tg was examined.

SDR-mediated release using different fuel strands

Although all results shown so far were obtained using the β'-20 fuel strand, both SDR formats were found to work with almost similar yields as indicated in Figure 3-12. Following the general procedure for Tg FIA on beads and using 100.0 μL conjugate (20 μg/mL) in HPN and 150.0 μL Tg (1.0 μg/mL) in HBS-P, three different release experiments were conducted using α'-25, β'-20, and α'-25+β'-20 as fuel strands (all at 5.0 μM). The same experiments were repeated with Tg in the bovine serum at a much lower concentration of 62.5 μg/mL (Figure 3-13).

CHAPTER 4

IDCAPT: A DNA-BASED TOOLBOX TO STUDY TRANSCRIPTION FACTORS

Transcription factors (TFs) are DNA-binding proteins that play a pivotal role in regulation of gene expression, by binding to particular sequences of genomic DNA called transcription factor binding sites (TFBSs). They are often present in cells in very small amounts and dilute concentrations, posing large challenges in their discovery, identification, purification, and assay. The majority of techniques developed to address these challenges chiefly focus on either proteomics, by starting from a purified TF, or genomics using TFBSs on DNA [194-197]. A limited number of strategies taking an integrative genomic-proteomic characterization approach such as "proteomics of isolated chromatin segments" (PICh) [138] and "protein binding microarrays" (PBM) are often composed of many steps, complicated, and difficult to multiplex. Multiplexing purification of TFs using the conventional DNA affinity chromatography techniques [195,196] is hampered by the non-specific modes of elution of all TFs captured on the column.

Here, the well-established concept called the DNA strand displacement reaction (SDR) is applied to the use of selective capture on beads for purification of TFs. This approach furnishes us with a specific mechanism of release that only depends on the programmed sequence of DNA, avoiding any drastic changes in the physicochemical properties of the environment, such as ionic strength or temperature. Moreover, our method preserves the information regarding the DNA sequences of the transcription factor binding sites (TFBSs) while affording a straightforward and scalable system capable of multiplexing. Our technique could be used to discover and quantify TFs with minimal co-purification of the unwanted matrix proteins in the nuclear extract. We have given our strategy the acronym IDCAPT (for Integrated Discovery,

Characterization, Assay and Purification of TFs), since it could be customized to accomplish one of the functions mentioned in the acronym or to perform the sequence of those functions integrated together.

Introduction

Characterization and purification of TFs are essential to studying their biological functions and structures. There is a plethora of TF purification and characterization techniques and a wide variety of them could be classified into three major categories; the proteomics, genomics, and combined integrated approaches. The proteomics-oriented techniques take advantage of the protein purification methods to isolate TFs from nuclear extracts. The genomics-based methodologies, on the other hand, start from a collection of DNA sequences that are plausible as the target binding sites for TFs.

The electrophoretic mobility shift assay (ESMA) or simply gel shift/ retardation assay has been traditionally one of the major techniques for discovery and characterization of TFs [196,198]. ESMA works on the premise that the TF-DNA binding shifts the electrophoretic mobility of the labeled DNA. A mixture of promising DNA sequences, also known as putative TFBSs, is mixed with the nuclear extract and the mixture is analyzed by gel electrophoresis. The TFBSs thus characterized could be used for the large-scale purification of TFs using DNA affinity chromatography. There are also other TF discovery methods involving DNA immobilization on solid supports for surface-enhanced laser desorption/ ionization mass spectrometry (SELDI-MS) [199-201], matrix-assisted laser desorption/ ionization mass spectrometry (MALDI-MS) [202], SPR chips [203], or microfluidic devices [204].

The alternative approach to DNA-centered methods is purification of TFs by the standard protein separation methods such as gel electrophoresis, ion exchange chromatography, gel filtration chromatography, and reverse phase high performance liquid chromatography [195]. The purified TF is then characterized in terms of both structure and its TFBSs, for instance using mass spectrometry and southwestern blotting [172,196,198]. Finally, the integrative genomics-proteomics approaches mostly crosslink TFs to their TFBSs using UV or formaldehyde. Chromatin immunoprecipitation (ChIP) methods [205] are the classic examples of isolation of TF-

TFBS complexes using an integrative approach. However, they often focus on characterization of either a TF (such as PICh [138] or GENECAPP [204]) or a TFBS (for example ChIP-Seq [194,206-208], SABE [209], and ChIP-Exo [210]) at the end.

There is a long list of techniques for characterization of the TF-TFBS bindings both *in vitro* [197,211-213] and *in vivo* [194,214] plus *in silico* [215,216]. The protein binding microarray (PBM) method is one of the most comprehensive *in vitro* characterization techniques. In PBM [136,137,217], all possible "k-mer" sequences of DNA (where k is an integer, usually 8 or 10) as putative TFBSs are synthesized and spotted on microarray slides. The TF of interest is expressed as a fusion protein to an epitope tag, such as glutathione S-transferase (GST). The epitope-tagged TF is then incubated with DNA sequences and its binding sites are characterized through the fluorescence signal of the Anti-GST antibody and the positions of spots. While PBM is a strong *in vitro* [197] experimental technique, due to the fact that it does not need prior knowledge of the TFBSs, it was designed to only identify the binding sites of a single purified TF. It relies on the expression of epitope-tagged TFs and is narrow and cumbersome to multiplex for TFs.

The "proteomics of isolated chromatin segments" (PICh) technique is a refined ChIP method for the *in vivo* TF characterization [138]. After the formaldehyde crosslinking of TFs to their TFBSs, the genome is fragmentated and the crosslinked TF-TFBS complexes are captured on the avidin magnetic beads using complementary DNA probes functionalized with desthiobiotin. To release the TF-TFBS complexes enriched on the beads, biotin is added replacing the desthiobiotinylated DNA probes on the beads. This release strategy, though more specific than changing pH or ionic strength, is still very non-discriminative and all the captured materials are released at once, making the technique very restricted for multiplexed TF characterization. The final analyses of DNA-binding proteins using SDS-PAGE or mass spectrometry often result in losing information on the TFBSs.

The conventional solid phase DNA affinity chromatography of TFs, whether done on beads or columns [196], presents many challenges. Co-detection and purification of the matrix proteins of nuclear extracts non-specifically adsorbed to the solid phase [196] and parallelization of the process are the two main obstacles. The common methods of elution of TFs off the DNA affinity supports such as utilization of high salt

concentrations [195,196], heparin [195], high temperature [195], disulfide bond exchange [218], His tag [219], photocleavable linkers [220], and even the biotin-desthiobiotin exchange in PICh [138] operate on generic release mechanisms leading to co-release of the matrix proteins and a subsequent need for purification. These methods are not amenable to parallelization, because all captured TFs co-elute, meaning the information linking the TFs to their TFBSs is lost.

We hereby propose a new method called IDCAPT to address the challenges of non-discriminative release and multiplexing of TFs. The IDCAPT strategy utilizes DNA for both molecular recognition and for specific release. Specific release is achieved through encoding DNA sequences to exhibit a function called DNA strand displacement reaction (SDR). The displacement reaction is a well-established concept in DNA Nanotechnology [4] and molecular beacon technology [14,15]. In SDR, a template DNA single strand already in a partial DNA duplex is reacted with a second DNA single strand, also known as the "fuel" strand, to form a more thermodynamically stable duplex, containing a larger number of DNA base pairs. The nucleation site on the template for the hybridization of the fuel strand is called a "toehold", from which the fuel strand starts unzipping its competitor via branch migration. Initiation of the displacement reaction leads to complete release of the DNA strand that initially formed a partial duplex with a portion of the template strand. As will be outlined below, SDR is exploited in this work as an isothermal, fast, and sequence-specific release mechanism as well as a method to preserve the TFBS sequence information and to eventually multiplex the assay, purification, and characterization of TFs.

IDCAPT functions on two main principles; that the SDR is a programmable and specific release mechanism and the TF binding to its TFBS will prevent the SDR proceeding to completion. The experimental evidence for the latter requirement comes from a FRET assay designed for a transcription factor, NFκβ [221]. One of the two DNA single strands forming the binding sites for NFκβ was labeled with a fluorophore and the other with a quencher [221]. In the absence of NFκβ, a SDR removed the quencher strand leading to high fluorescence. In the presence of NFκβ, however, the SDR was inhibited and the fluorescent signal stayed quenched [221].

The IDCAPT concept is comprised of two main setups. The first setup could be used for discovery, characterization, and assay (DCA) of TFs and therefore, we call it the DCA setup (Schemes 4-1 and 4-2). The second approach accomplishes purification of TFs only and is referred to as the P setup (Scheme 4-3). Scheme 4-1 shows the DCA setup in the presence of a transcription factor. Beads functionalized with single stranded DNA probes, β, capture a multi-segment DNA strand, α, bearing the TFBS. As illustrated in Scheme 4-1, there is also a toehold domain, α_R, present between the TFBS and the α end that forms a partial duplex with the bound probes, β. The capture strand, α, already hybridized to a short complementary strand, C, to form the TFBS duplex is first incubated with the nuclear extract and then with beads to immobilize the TFs associated to their binding sites:

$\alpha + C \rightarrow [\alpha\text{-}C]$ (in solution)

$[\alpha\text{-}C] + TF \rightarrow [\alpha\text{-}C\text{-}TF]$ (in solution)

$[\alpha\text{-}C\text{-}TF] + \text{Beads} \rightarrow [\alpha\text{-}C\text{-}TF]_{im}$ (the subscript "im" means immobilized)

After a few washes, a "marker" strand, M, is added with a universal adaptor stretch at one end and a segment complementary to the toehold (α_R) of the capture strand at the other end. The universal adaptor stretch is complementary to a short, FAM-labeled, universal DNA signal strand, U (Scheme 4-1). When M is added to the beads, there are two possibilities; in the presence of a TF, the toehold on the capture strand hybridizes to the marker strand but the SDR is blocked by the TF (Scheme 4-1):

$[\alpha\text{-}C\text{-}TF]_{im} + M \rightarrow [\alpha\text{-}C\text{-}TF\text{-}M]_{im}$

After a few wash cycles, the next step is to add the "interrogator" strand, I, complementary to the marker strand except for its universal adaptor segment. By taking advantage of the exposed toehold on M, when a transcription factor is present, the "I" strand releases M back into solution. This release occurs only if there is a TF bound to the capture strand via the exposed toehold, M_I, on M and thus, provides a signal-ON assay for the TF of interest:

$[\alpha\text{-}C\text{-}TF\text{-}M]_{im} + I \rightarrow M\text{-}I + [\alpha\text{-}C\text{-}TF]_{im}$

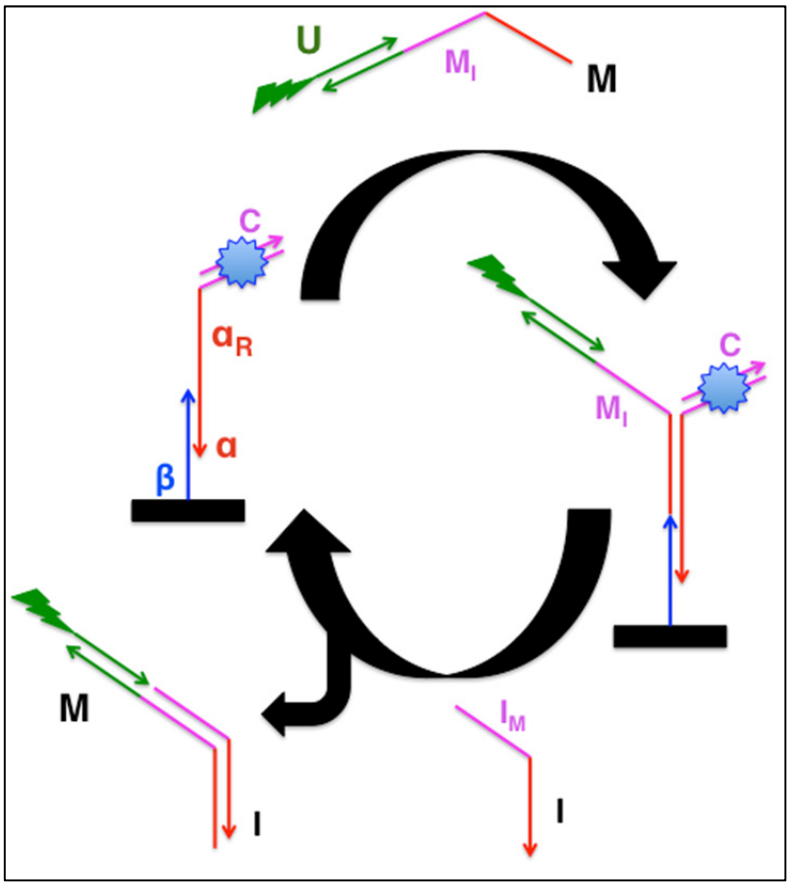

Scheme 4-1: The DCA setup of the IDCAPT strategy in the presence of a TF (blue 12-point star): a marker strand, M, with a universal adaptor at its 3' end complementary to a fluorescently labeled short strand, U (in green) is added. The 5' end of M will sit on the toehold ($\boldsymbol{\alpha_R}$) of the capture strand, α, but cannot replace the complementary strand (C, in pink) since C is a part of TFBS bound to the TF. The marker strand is thus immobilized on the beads while its pink segment is exposed as a toehold (M_C). A second SDR will release the I-M complex back into the solution upon adding the interrogator strand, I, and its binding to the toehold on M (M_I). The original toehold on α, namely $\boldsymbol{\alpha_R}$, is re-exposed and available for a third SDR discussed in Scheme 4-3.

The other possibility is depicted in Scheme 4-2, when there is no TF bound to a putative binding site. In this case, after addition of the marker strand, M, the SDR on strand C can proceed to completion. This gives rise to irreversible capture of M on beads and, unlike Scheme 4-1, no release of the marker strand back into solution, since the interrogator strand does not encounter an open toehold on M:

$[\alpha\text{-C}]_{im} + M \rightarrow [\alpha\text{-M}]_{im} + C$

$[\alpha\text{-M}]_{im} + I \rightarrow$ No reaction

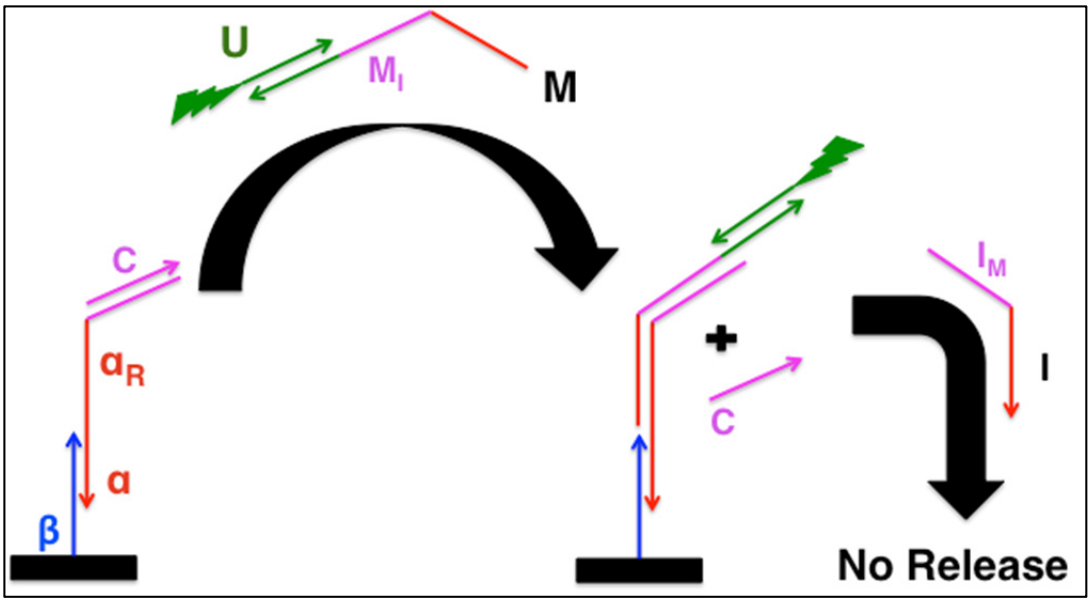

Scheme 4-2: The DCA setup of the IDCAPT strategy in the absence of a TF: when there is no TF bound to a TFBS, the marker strand, M, will be captured on the beads through a SDR but because its toehold, M_I, is bound to the capture strand, α, addition of the interrogator strand, I, will not result in any release.

In the end, if the fluorescence signal in the supernatant indicates that there is a TF bound to a particular TF binding site, the "release" strand, R, is added to recover the TF in its native state for further analysis or purification (Scheme 4-3). The "release" strand, R, is simply another fuel strand doing a SDR on the capture strand, α, to dehybridize it from the immobilized probes. R initiates the final SDR by sitting on the toehold, α_R, re-exposed only in the presence of a TF (Scheme 4-3). The TF/ TFBS release can be multiplexed by utilizing many different unique R, and correspondingly α and β, sequences. The use of various unique R strands retains the information as to which TFBS/ TF was released:

$[\alpha\text{-C-TF}]_{im} + R \rightarrow [\alpha\text{-C-TF-R}]_{su}$ (the subscript "su" means "in supernatant")

$[\alpha\text{-M}]_{im} + R \rightarrow$ No reaction

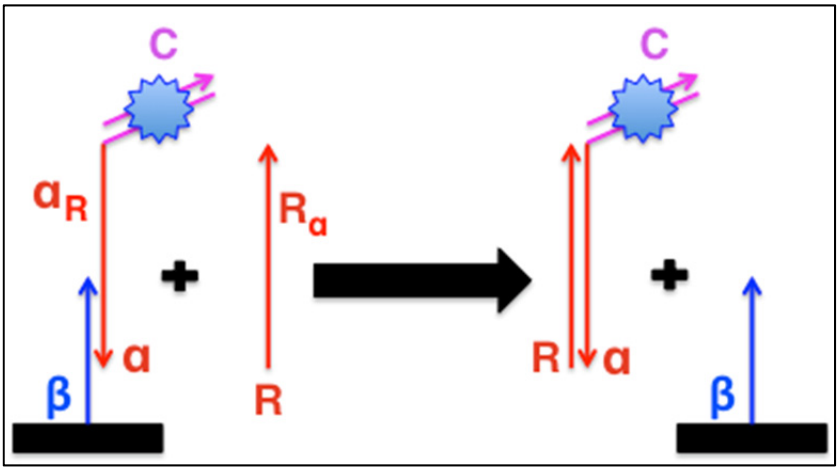

Scheme 4-3: The P setup of the IDCAPT strategy for purification of a TF (blue 12-point star): a promising TFBS identified in Scheme 4-1 would release its TF through another SDR in which R is the fuel strand this time.

IDCAPT utilizes a radar-like propensity to identify its target TFs. It sends off a signal-bearing strand, M, to be captured and examines whether its binding could be reversed through the interrogator strand, I. The SDR-mediated release of M is TF-dependent. In the absence of a TF, M would be captured irreversibly. In the context of computer science, such a behavior represents an "AND" logical gate [4], where presence of two inputs together is necessary to generate an output. Analogously, the release strand, R, and a TF are the inputs and the output is the marker strand, M, in our chemical system.

The IDCAPT methodology enjoys versatility at different levels. If the goal is to discover and identify new TFs and TFBSs, one might take a similar approach to the protein binding microarrays (PBM) [136,137,217]. As discussed earlier, PBM screens an array of possible DNA sequences against a known TF expressed as a fusion protein to an epitope. PBM is therefore, very powerful at multiplexed identification of all possible TFBSs *in vitro* for a single TF, but is very limited in terms of multiplexing the procedure for many TFs. Our proposed method, on the other side, could use the same "k-mer" strategy on beads instead of microarray slides to explore a large binding sequence space, but it can selectively release the TFs bound to a given DNA sequence (TFBS), allowing for a route to multiplex the testing and isolation of TFs. Additionally, IDCAPT could simultaneously discover and identify many TFs in their native states plus their major

binding sites using nuclear extracts, without any need for protein expression or tagging. However, IDCAPT is certainly less capable of high throughput configuration than DNA microarray technology. IDCAPT is also equipped with a simple *in situ* fluorescence reporter system based on SDR that could be used qualitatively or quantitatively. This eliminates the need for any downstream assays using molecular beacons [221-223], labeled antibodies [224,225], or mass spectrometry [226].

Unlike the conventional TF purification methods, our IDCAPT technique could be focused on the parallel purification of multiple TFs. The SDR-mediated sequential release of each TF guarantees the sequences of TFBSs remain retrievable and co-elution of the unwanted non-specifically adsorbed molecules is minimized. The latter is achieved using the same buffer and physicochemical environment throughout the capture, wash, and release steps. The multiplexing capability of IDCAPT could also be employed for *in vivo* study of TFs using a methodology similar to PICh.

Results and discussion

To prove the concept of SDR-mediated multiplexing on silica beads, three orthogonal (no stretch of more than 5 nucleotides can cross-hybridize) sets of biotinylated probes, with their fuel and capture strands were designed. The capture strand in each SDR set was labeled with a unique fluorophore (FAM, TAMRA, or TYE-665). The SDR sets were designed such that they would show minimal cross-hybridization with one another, and the melting points were all above 45 °C.

Three different types of beads, each functionalized with one of the three probes (β1, β2, β3), were mixed together in equal amounts and then incubated with the mixture of capture strands (FAM-α1, TAMRA-α2, TYE-α3). After three wash cycles, the fuel strands fully complementary to the probes (β'1, β'2, β'3) were incubated one at a time. The captured and released amounts (in pmoles) were determined by fluorescence measurements of the supernatants in each step, combined with the calibration curve for each labeled capture strand (Figures 4-10 to 4-12 in the supplementary info). It was assumed that the signal intensity at the maximum emission wavelength of each fluorophore exclusively represented that fluorophore and there was no significant spectral interference from the other two fluorophores. Such an assumption was

validated by spectral analyses of the three fluorophores. The concentrations of labeled αs in supernatants were obtained using the appropriate calibrations curves. The captured amounts were determined by subtracting concentration of the labeled α in the supernatant of capture step from its concentration before mixing with beads. The relative amount released in each step (in percentage) was obtained by dividing the amount quantified in the supernatant (in pmoles) by the captured amount (in pmoles) for each set (21.6, 55.3, and 35.0 pmoles for FAM-α1, TAMRA-α2 and TYE-α3, correspondingly). Sequential release of the captured strands using β' fuel strands was achieved in high yields and with cross talk of 0-4 % among the three sets (Figure 4-1).

A similar set of experiments using α' fuel strands, which are complementary to the labeled capture strands instead of β probes, resulted in the same efficiency of multiplexing with almost no cross talk among the three sets. Notably, this approach leaves single stranded β probes on the bead surface, allowing them to be used if that is desired.

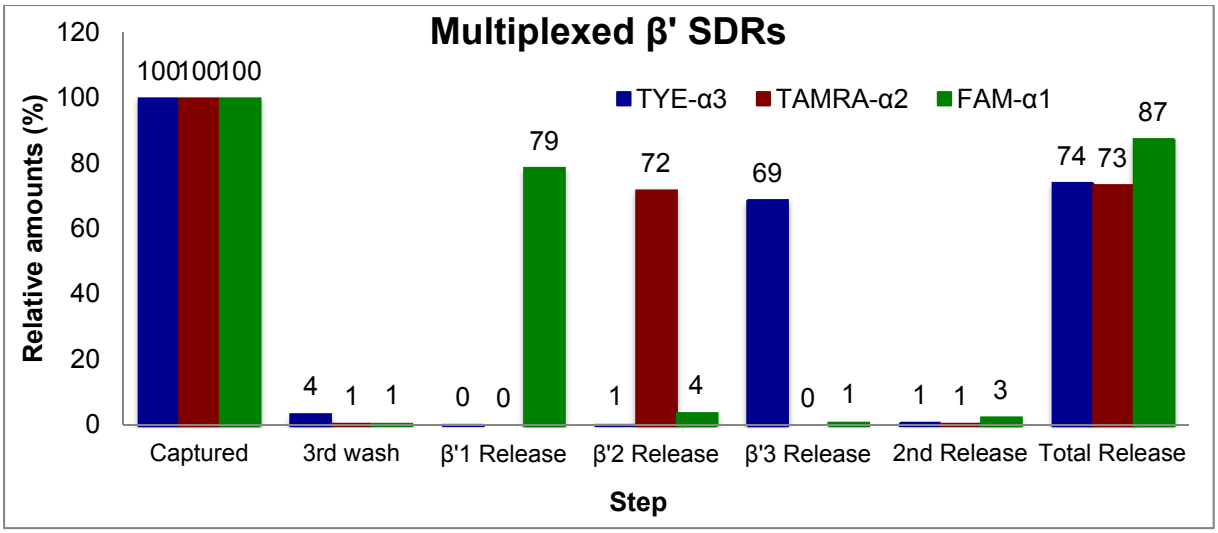

Figure 4-1: SDR-mediated release could be multiplexed through orthogonal sequence designs as demonstrated by three sets above. A mixture of three labeled strands was captured on beads but only the appropriate complementary strand was released depending on which fuel strand, β', was used. The release of labeled αs is shown following the capture. Results of the third wash step are shown as they are controls to the three-step first release followed by the effects of sequentially treating the beads with a single type of β' strand in each step of the first release. For the second release, though, a mixture of β'1, β'2, and β'3 was used [$(\alpha_i + \alpha_j + \alpha_k) + (\beta_i + \beta_j + \beta_k) + (\beta'_i$ then $\beta'j$ then $\beta'_k) + (\beta'_i + \beta'_j + \beta'_k)$].

Different control experiments demonstrated the sequence-specific nature of the release, where a given capture strand was not released in the presence of the wrong probe or fuel strand (Figures 4-2 to 4-5). The first control experiment was designed, in which a mixture of two labeled capture strands ($\alpha_i + \alpha_j$), with concentrations equal to the ones used for Figure 4-1, were hybridized with only one bead type bearing a non-complementary probe (β_k) (Figures 4-2 and 4-3). The complementary fuel strand (β'_k) was used in the release step.

Figure 4-2 compares the amounts (in pmoles) captured specifically in Figure 4-1 and non-specifically in the first control. As seen in Figure 4-2, the absolute amounts captured non-specifically for TAMRA-α2 and TYE-α3 were much smaller than the specific ones observed in Figure 4-1. However, it was observed that FAM-α1 had a huge non-specific adsorption (Figure 4-2). The large amount of FAM-α1 non-specifically captured was initially concerning, but the data of control 1 (Figure 4-3) and subsequent controls showed that it was readily removed in the wash steps.

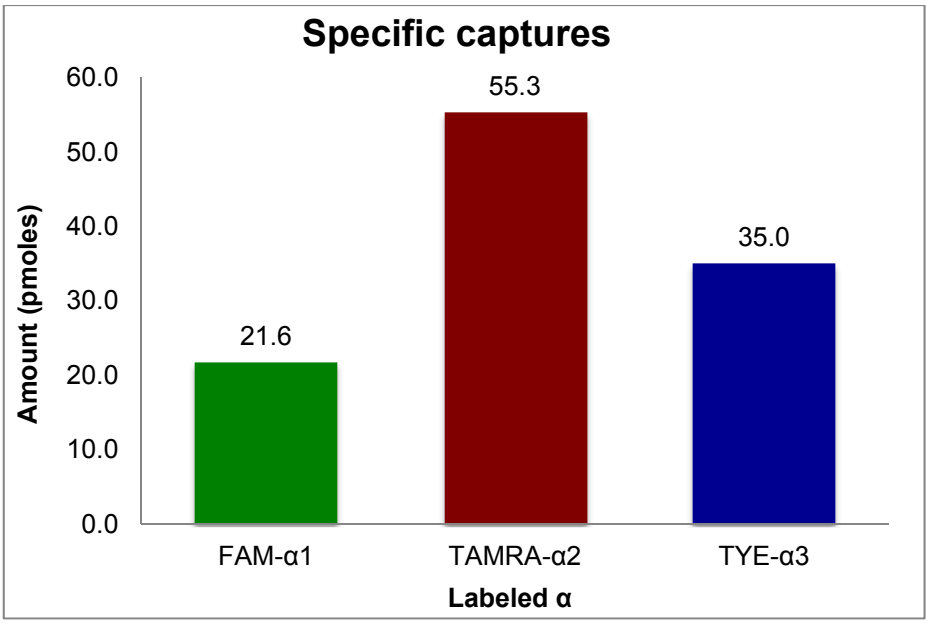

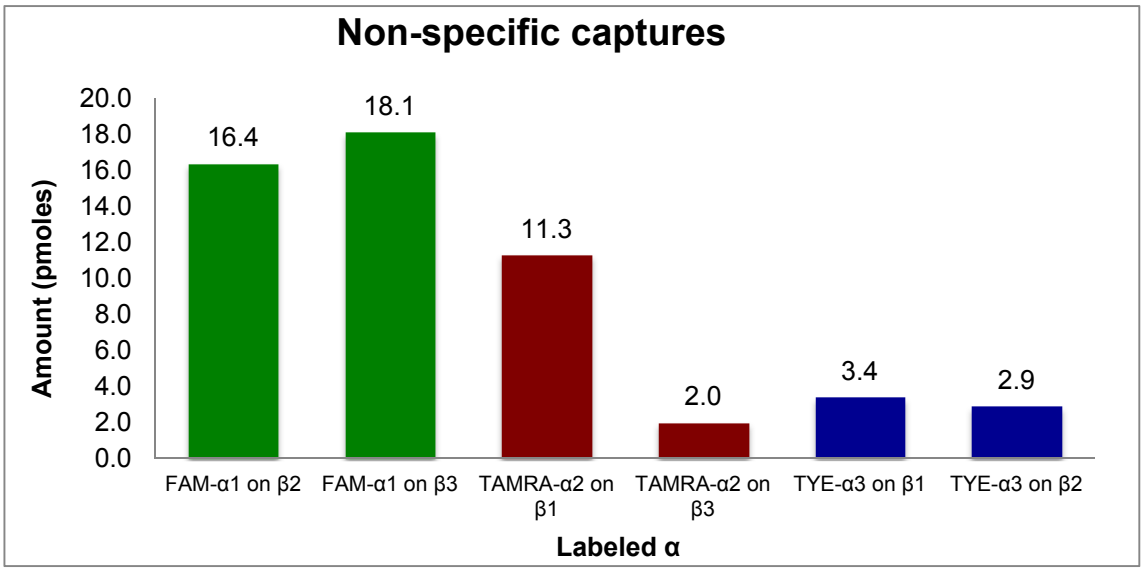

Figure 4-2: Comparison of absolute amounts of specific capture for α_i from Figure 4-1 (on top) with the non-specific captures described in control 1 (see Figure 4-3 for details).

Figure 4-3 presents the relative release in each step of control 1. The relative release percentages were obtained by normalizing the released pmoles in each step with respect to the amounts of α_i non-specifically captured in control 1 (also presented as the non-specific capture values in Figure 4-2). Despite huge non-specific captures of FAM-α1 found in Figure 4-2, its final non-specific release by either β'2 or β'3 is minimal (Figure 4-3). The three washes between the capture and release steps proved completely

effective in removing non-specifically adsorbed materials for all three sets. This is evident from the undetectable values of release in the third washes (Figure 4-3). It should be noted that signal readings from the supernatant of the first wash should always be interpreted cautiously as there is varying degrees of carryover from the capture step. The wash steps include both carryover of α_i in the loading solution, if any, plus any release from the surface during the wash. Additionally, the third wash provides a control for the release since it uses the same buffer as the release step for the same incubation time.

It was found that the release efficiencies for the non-specific captures were almost zero for TAMRA-α2 and TYE-α3 and only 1 % for FAM-α1 (Figure 4-3). This control proves that when the mode of capture is non-specific, the surface remodeling due to the fuel strand hybridization is not able to effectively release any significant amounts of bound materials.

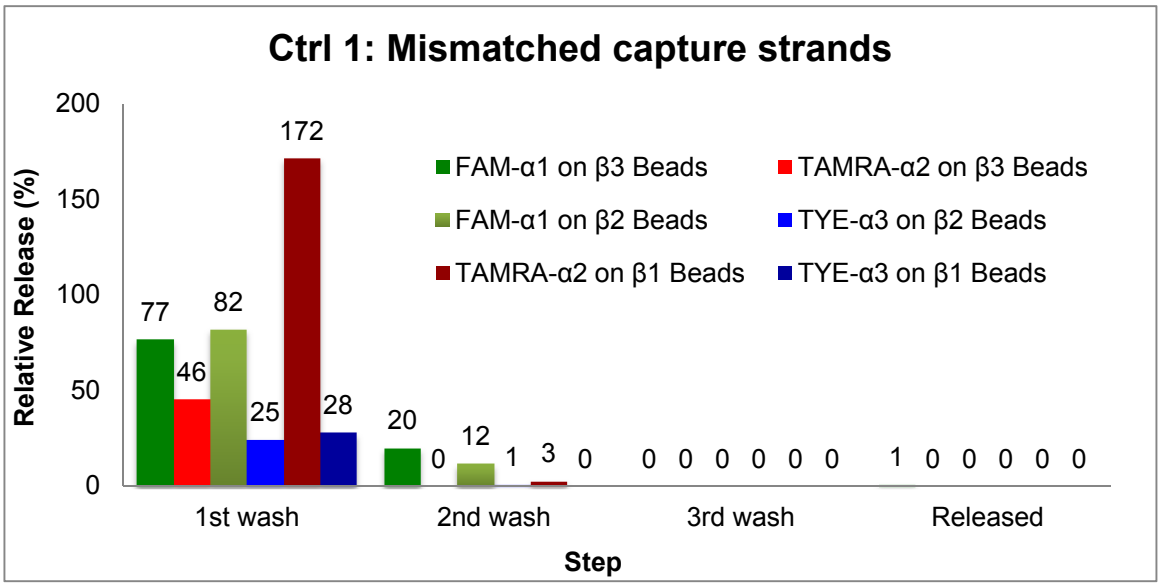

Figure 4-3: The first control experiment (Capture ☒, Release ☑): a non-specific capture using mismatched capture strands and a specific release $((\alpha_i + \alpha_j) + \beta_k + \beta'_k)$.

In the second control experiment shown in Figure 4-4, the labeled capture strand, α_j, and the probe, β_j, were complementary and thus, the capture was specific. This time, however, a mixture of two fuel strands, $(\beta'_i + \beta'_k)$, which are mismatched to

the immobilized probe on the beads, β_j, were used to estimate the magnitude of sequence-independent non-specific release. The relative release in percent was obtained using the pmoles of specific capture of α_i in this control experiment (19.4, 21.5, and 51.0 pmoles for FAM-α1, TAMRA-α2 and TYE-α3, respectively) as the reference values. As expected, the non-specific release was very modest in all three sets in the range of 0- 5.6 % (Figure 4-4). This control gives an estimation of the non-specific adsorption of fuel strands to the non-complementary probes via cross-hybridizations. It should be also noticed that the relative release of FAM-α1 in the first wash step of Figure 4-4 is much smaller than in Figure 4-3, due to the specific mode of capture in the former.

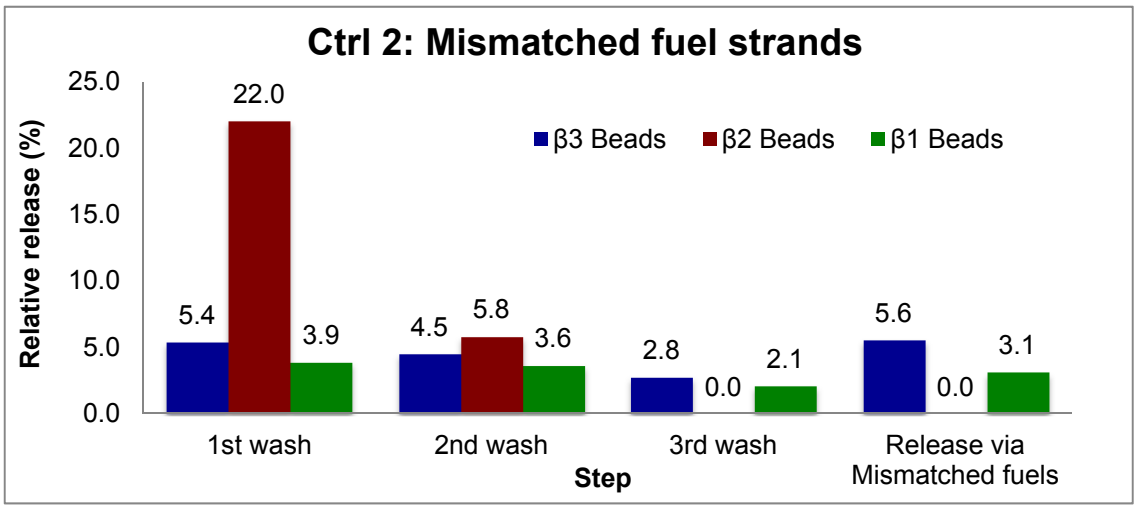

Figure 4-4: The second control experiment (Capture ☑, Release ☒): a specific capture using capture strands matched to the probes but a non-specific release through using mismatched fuel strands ($\alpha_j + \beta_j + (\beta'_i+\beta'_k)$).

The third control experiment examined release after both non-specific capture and release. A mixture of two mismatched capture strands, ($\alpha_i + \alpha_k$), was mixed with a non-complementary bead type, β_j. In the release step a mixture of two fuel strands, ($\beta'_i + \beta'_k$), mismatched to the probes was added. The relative release was obtained by taking the absolute amounts of non-specific capture of α_i in this control experiment (for FAM-α1 7.0 and 11.6 pmoles, for TAMRA-α2 3.3 and 1.1 pmoles, and for TYE-α3 3.3 and 2.7 pmoles) as the references. As seen in Figure 4-5, there is only a 0-5 % non-specific release following a non-specific capture.

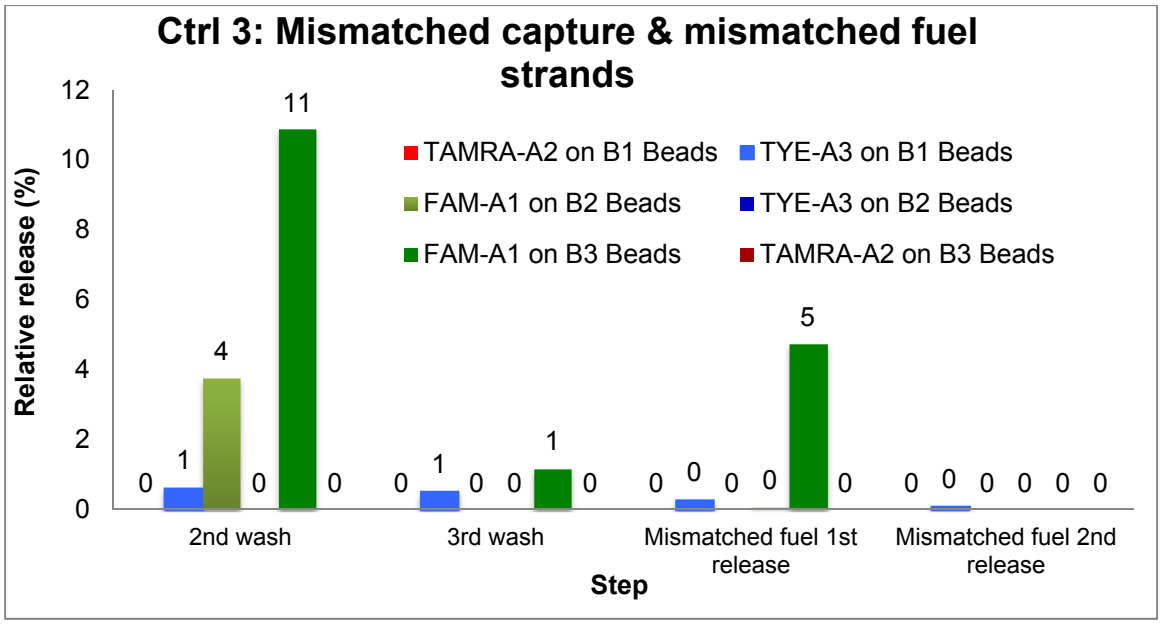

Figure 4-5: The third control experiment (Capture ☒, Release ☒): a non-specific capture using capture strands mismatched to the probes and a non-specific release through using mismatched fuel strands ($(\alpha_i + \alpha_k) + \beta_j + (\beta'_i + \beta'_k)$).

The last control experiment looked into whether presence of the other two capture strands would change the kinetics and therefore, efficiency of capture for a given third capture strand in a mixture. To test this, all steps of a capture and release were compared between two duplicate experiments with both specific capture and release; one of them used a capture strand alone and the other used the same strand in a mixture with the other two mismatched capture strands. The results showed no large differences between the two (Figure 4-6).

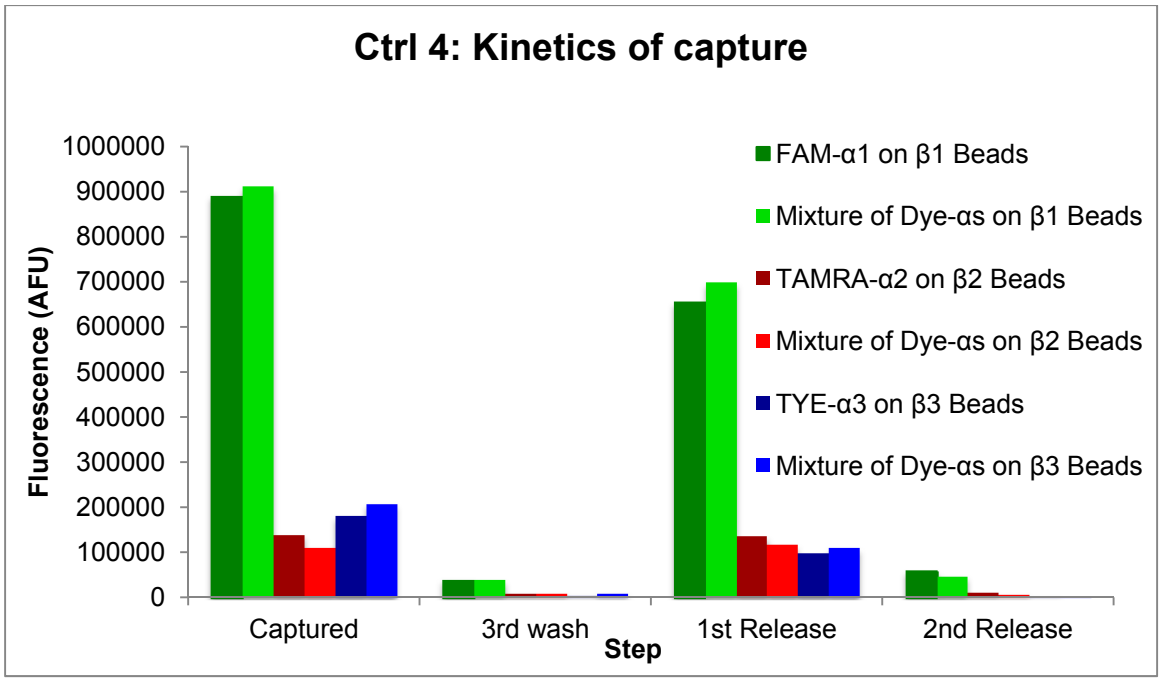

Figure 4-6: The fourth control experiment (Capture ☑, Release ☑): Kinetics of capture is not affected significantly by the presence of other capture strands ($[(\alpha_i + \alpha_j + \alpha_k) + \beta_j + \beta'_j]$ vs. $[\alpha_j + \beta_j + \beta'_j]$).

A similar procedure as the one used for Figure 4-1 was adopted for triplicate experiments to examine the reproducibility of multiplexing. The reproducibility of SDRs in the multiplexed format is very good (Figure 4-7). Unsurprisingly, the relative standard deviation (RSD) values for specific capture and release are much smaller than the ones for the non-specific releases during the washes (Figure 4-7).

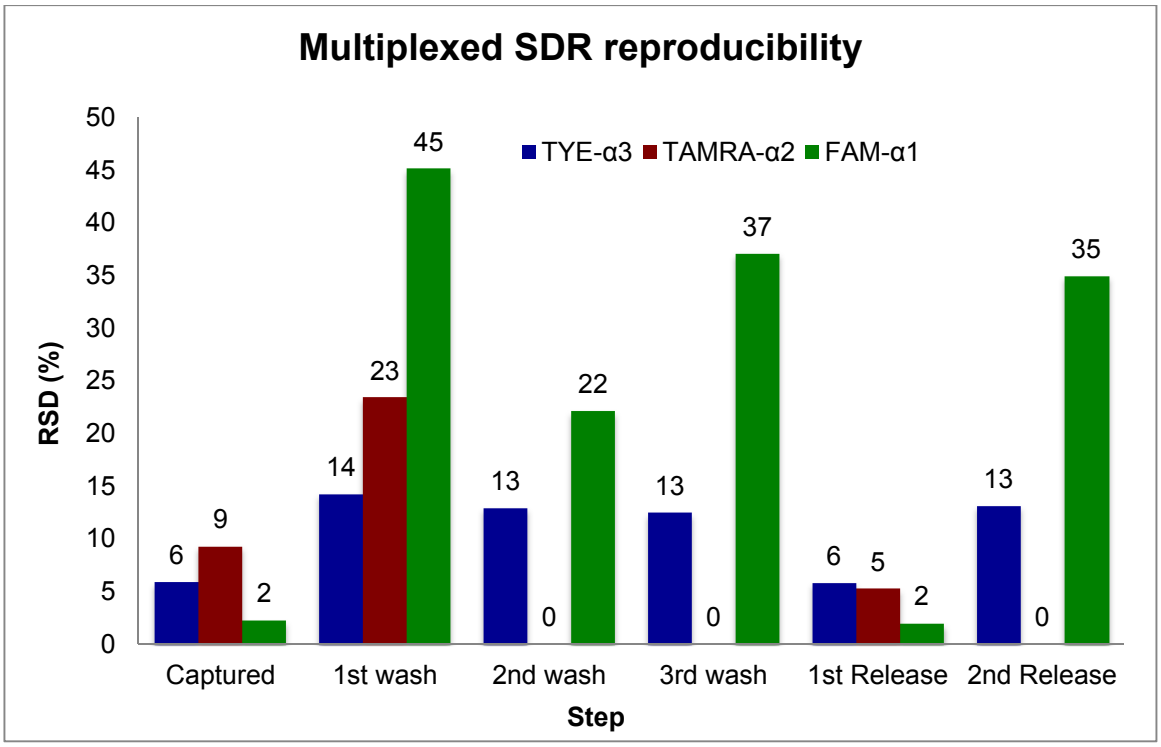

Figure 4-7: Reproducibility of multiplexed SDRs.

To examine how a prototypic IDCAPT design could be used for the capture and release of a TF, a model transcription factor, NFκβ, was chosen. Both NFκβ and its binding sites are well characterized [227-232]. As discussed earlier, the reporter system in IDCAPT works based on sequential SDRs and indicates whether there is a TF bound to a particular TFBS. It could also be used as a quantification method without any need for antibodies against TFs by taking advantage of the blockage created by the TF binding to DNA to prevent the SDR from proceeding. The blockage could be used in two configurations; in the signal-off format two toeholds are flanking the TFBS. As depicted in Scheme 4-4, the TFBS for NFκβ is formed by hybridization of an adaptor strand, N, to a complementary strand, C. The capture strand, α, is labeled with TAMRA and binds to N through its complementary domain, α_N. The αNC complex is then incubated with NFκβ and is subsequently immobilized on beads. The NFκβ binding event will result in failure of the SDR initiated by a fuel strand, F, from its toehold on N (N_F) to expose a second toehold, α_N, on α already hidden downstream of the TFBS. The second toehold

(α_N) must be available to release the fluorescently labeled capture strand into the solution (Scheme 4-4).

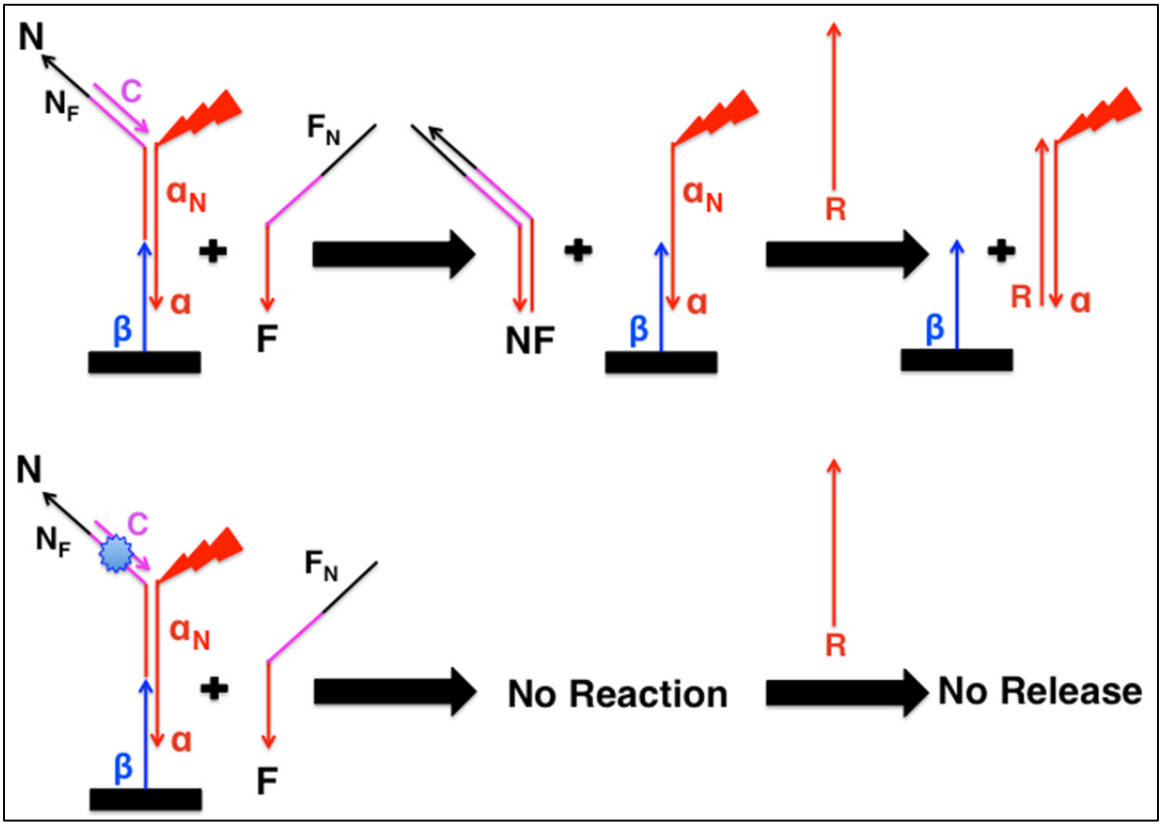

Scheme 4-4: Signal-off format for an SDR-based TF assay. In the absence of a bound TF (NFκβ here) two consecutive SDRs will release the labeled capture strand (on the top). When a TF is bound, the first SDR fails leading to the toehold for the second SDR to be inaccessible. Therefor, no labeled capture strand could be released (bottom).

Figure 4-8 proves the signal-off assay concept discussed in Scheme 4-4. Polystyrene beads were used instead of silica, because the negative charge of silica might cause an extensive non-specific adsorption of mostly positively charged proteins in the nuclear extract. The negative control involves no incubation with NFκβ resulting in the maximum release signal in Figure 4-8. Skipping NFκβ and fuel strand, F, incubation steps lead to the minimal release signal and constitute the positive control. Finally, incubation with NFκβ generates a release signal within the signal range established by the control experiments (Figure 4-8). The signal for NFκβ depends on its concentration

and in Figure 4-8, it seems that the functional NFκβ in the sample does not have a large enough concentration to fully suppress the signal to the level observed in the positive control. Still, its signal is 14 % less than the negative control which is much higher than the 5 % RSD of release observed in Figure 4-7. It should be added that the release signal for the positive control could be set to zero by assuring equimolar amounts of N, C, and TAMRA-α are mixed together.

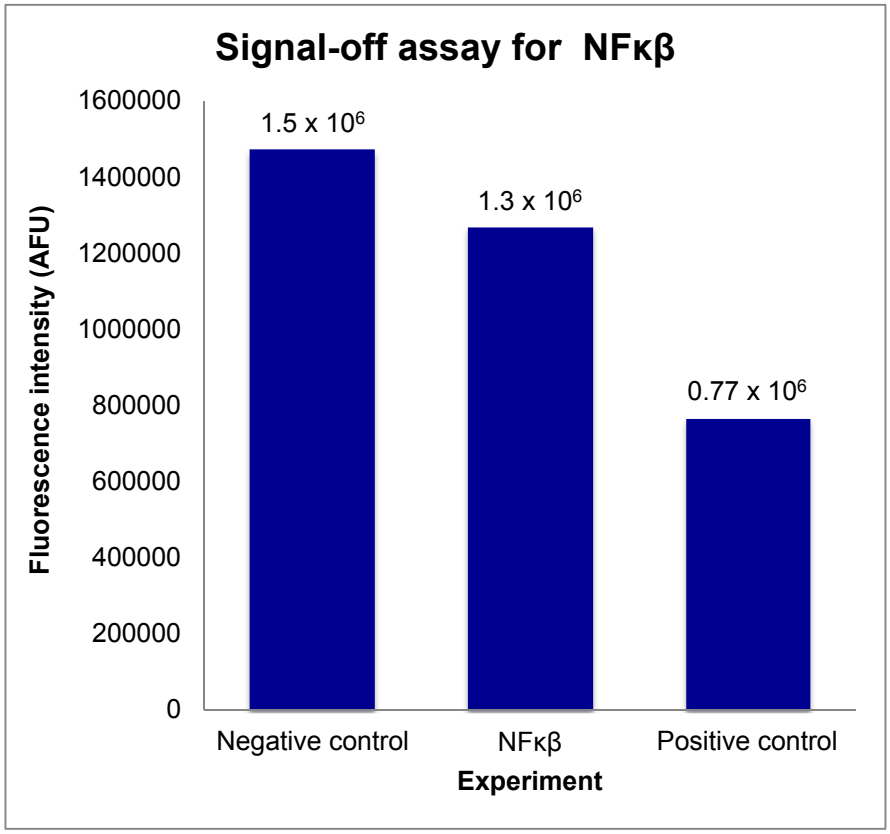

Figure 4-8: Proof of concept for signal-off assay of NFκβ. In the negative control no NFκβ was used and in the positive control no fuel strand, F. The NFκβ experiment was performed using 1.0 μM NFκβ and 200 nM αNC complex.

While the signal-off format requires a simpler design, it needs a rigorous and simultaneous calibration for each set to define the signal level in the absence of a TF. The signal-on configuration in analytical assays is often more reliable, since the signal generated is compared to the background noise instead of the very large signal level in the absence of the analyte in the signal-off format. The signal-on design should be

particularly useful for interrogating the TFs, especially those present in very small concentrations. The signal-on methodology could be used in a quantitative assay, or as a reporter system for qualitative response in a screening mode for promising TFBSs. The signal-on assay was, therefore, chosen for the IDCAPT technique. The signal-on configuration employs two toeholds downstream of the TFBS and three sequential SDRs to survey the binding status of a TFBS, as depicted in Scheme 4-1. It is possible to use a fluorescently labeled capture strand instead of the universal labeled tag assembled with the marker strand, M. However, labeling many capture strands for a parallel assay is required, being a great disadvantage. Schemes 4-5 and 4-6 are variation of Schemes 4-1 and 4-2 with a few drawbacks. In Scheme 4-5 the TF-TFBS complex is released before interrogation of the TF binding event. This problem has been corrected in the designs of Schemes 4-1 and 4-2, in which the use of a universal fluorescently tagged strand, U, also eliminates the need for labeling many different α sequences. Schemes 4-5 and 4-6 could be considered a preliminary version of the IDCAP design (Schemes 4-1 and 4-2). Since we already had the reagents needed for Schemes 4-5 and 4-6, we used these schemes to establish the core idea of a signal-on assay in IDCAPT. We therefore, used a capture strand, α, labeled with TAMRA as laid out in Scheme 4-5. The adaptor strand, N, bears the TFBS at its 3' end and both toeholds are located on the same side of the TFBS. As described for Scheme 4-4, the αNC complex is formed and incubated with NFκβ in solution, and is then immobilized on polystyrene beads. The first SDR is initiated by addition of the first fuel strand, D, and goes to completion only if there is no TF bound (Scheme 4-5):

$$[\alpha\text{-N-C}]_{im} + D \rightarrow [\alpha\text{-N-D}]_{im} + C$$

Upon completion, fuel D blocks the toehold on N (the green domain in Scheme 4-5) permanently inhibiting the next three SDRs and the toehold-dependent release mechanism of the labeled capture strand, α. The following three SDRs are identified in Scheme 4-6 as is the process in the presence of NFκβ.

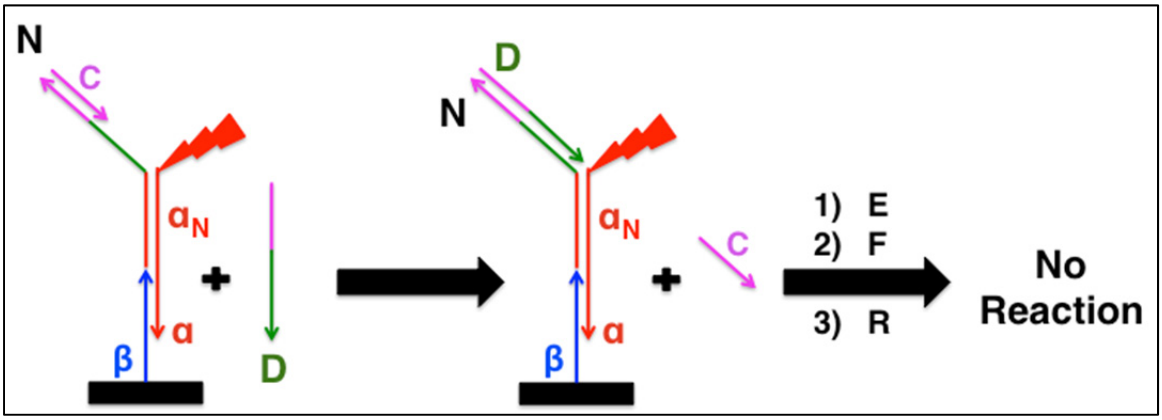

Scheme 4-5: Signal-on assay in the absence of NFκβ. See text for the detailed explanations.

In the presence of a bound TF (NFκβ in this case), the first SDR will make only the first half of D form a duplex with the toehold on N (N_F) leaving its other half single stranded because of the blockage by the bound TF (Scheme 4-6, step 1):

$[\alpha\text{-N-C-TF}]_{im} + D \rightarrow [\alpha\text{-N-C-TF-D}]_{im}$

When the second fuel strand, E, is added, which is fully complementary to D, it will remove D and expose the toehold, N_F, back again on N (Scheme 4-6, step 2):

$[\alpha\text{-N-C-TF-D}]_{im} + E \rightarrow [\alpha\text{-N-C-TF}]_{im} + E\text{-D}$

Note that while steps 1-2 (incubations with D and E strands) are redundant in Scheme 4-6, they are required to prevent signal generation in the absence of the TF, as shown in Scheme 4-5. The third fuel strand, F, is then added to release N as the NF duplex, exposing a new toehold, α_N, on the capture strand, α (Scheme 4-6, step 3):

$[\alpha\text{-N-C-TF}]_{im} + F \rightarrow [\alpha]_{im} + [\text{N-C-TF-F}]_{su}$

Finally, addition of the fourth fuel strand, R, will release the labeled capture strand (Scheme 4-6, step 4-4):

$[\alpha]_{im} + R \rightarrow [\alpha\text{-R}]_{su}$

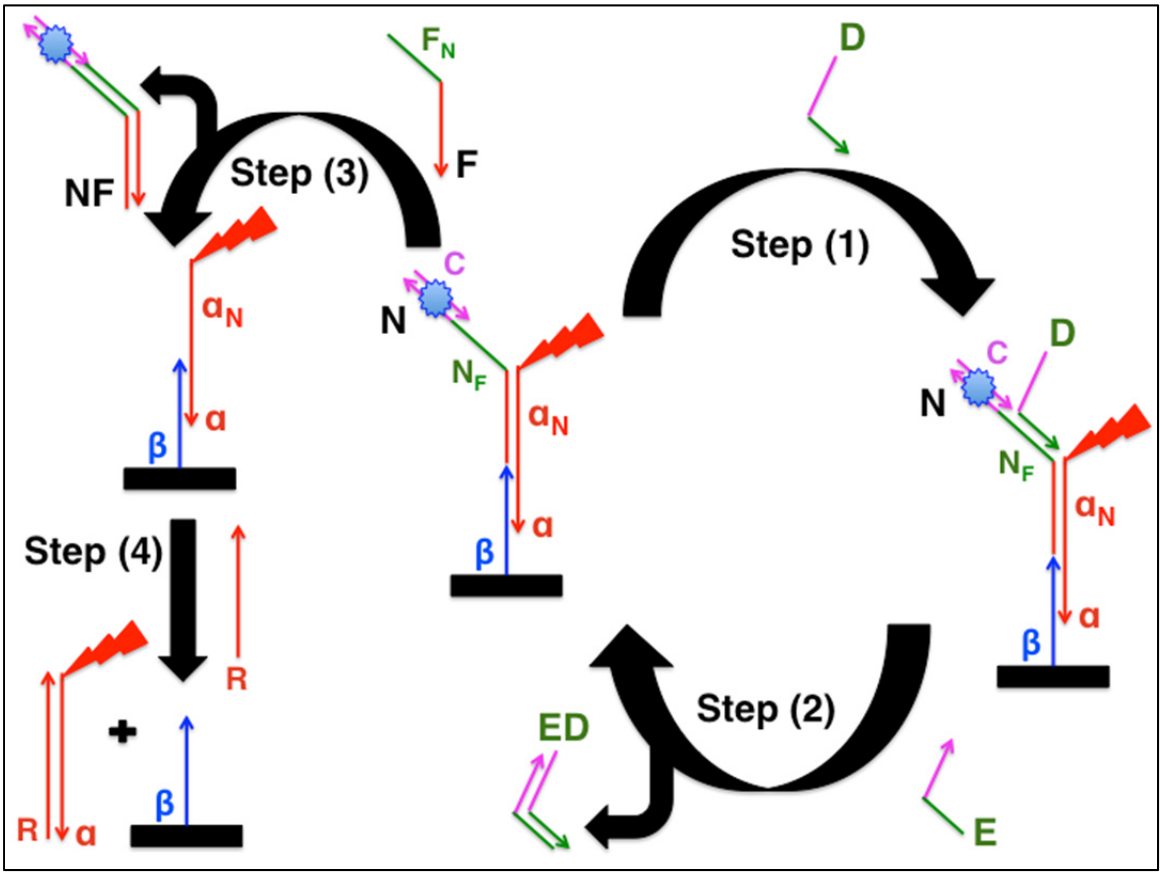

Scheme 4-6: Signal-on assay in the presence of NFκβ (blue 12 point star). See text for the detailed explanations.

Figure 4-9 presents the experimental proof of Schemes 4-5 and 4-6. Two negative control experiments and one positive were conducted, all of them without any NFκβ incubation step. The first negative control contained no incubation with NFκβ yielding the minimal release signal. The second negative control involved no incubation with the third fuel strand, F, producing again the same minimal release signal. The positive control included no incubation with the first fuel strand, D, in which the release signal was maximum. The main experiment in the presence of NFκβ generated a signal significantly higher than the minimal levels observed with the negative controls and less than the maximum signal in the positive control (Figure 4-9). NFκβ generated 11 % more signal than the negative controls, which is higher than the RSD value of 5 % for TAMRA-α2 release in Figure 4-7. Furthermore, 11 % signal change for the signal-on assay is in agreement with 14 % in the signal-off, for the same concentration of NFκβ.

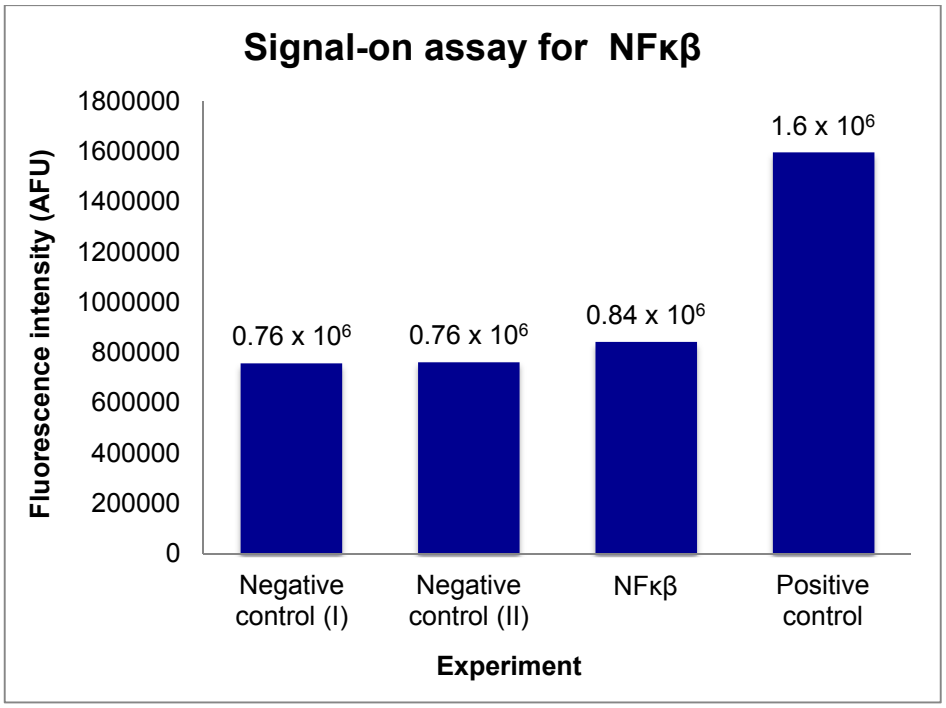

Figure 4-9: Proof of concept for signal-on assay of NFκβ. Negative control (I) includes no NFκβ incubation step. Negative control (II) has no incubation step with the third fuel strand, F, and the positive control involves no incubation with the first fuel strand, D. The NFκβ experiment was performed using 1.0 μM NFκβ and 200 nM αNC complex.

Conclusions

In conclusion, we developed a customizable strategy, IDCAPT, for discovery, purification, and quantification of transcription factors based on the programmability of DNA in sequential strand displacement reactions. IDCAPT is highly capable of parallelization and takes advantage of straightforward experimental designs to integrate multiple functions of great importance in studying transcription factors. NFκβ was used as a model transcription factor to prove the core concept of IDCAPT method. However, a larger number of model TFs (such as ATF3 and SP1) are to be tested to fully demonstrate the multiplexing power of the IDCAPT technique. The calibration curves using different concentrations of NFκβ should also be determined for both signal-on and signal-off assays.

Supplementary information

A calibration curve for each labeled α strand (Figures 4-10 to 4-12) was built and used to quantify the amount of labeled αs in supernatants.

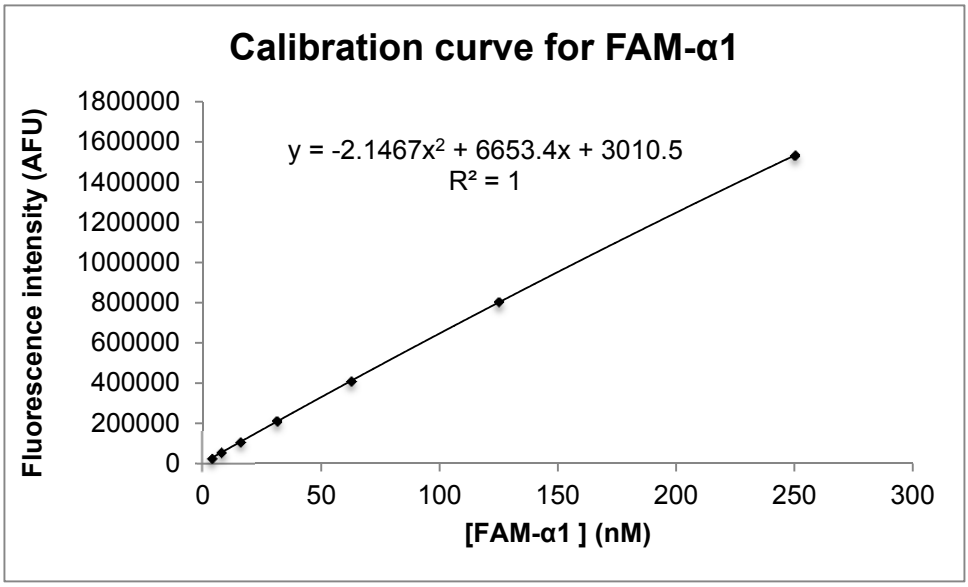

Figure 4-10: Calibration curve for FAM-α1.

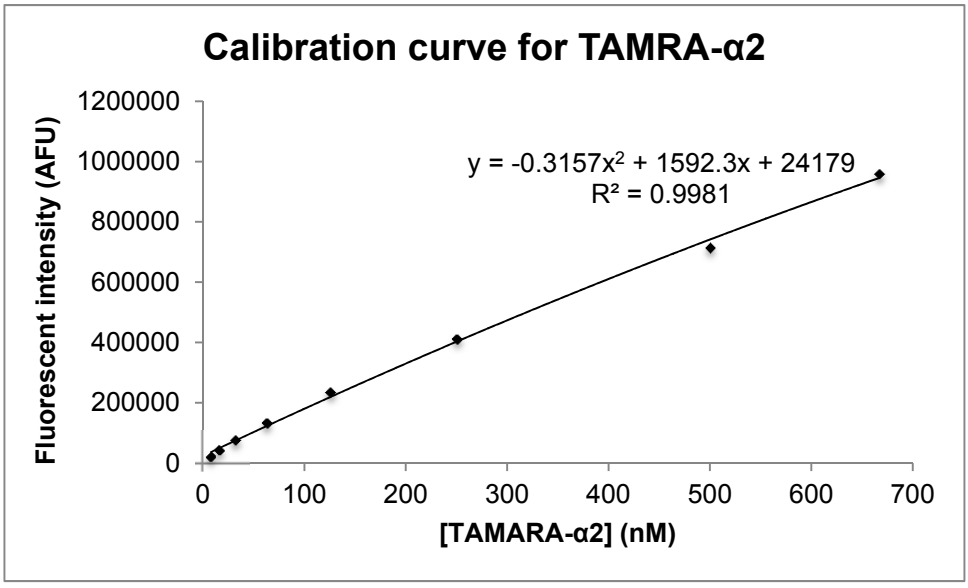

Figure 4-11: Calibration curve for TAMRA-α2.

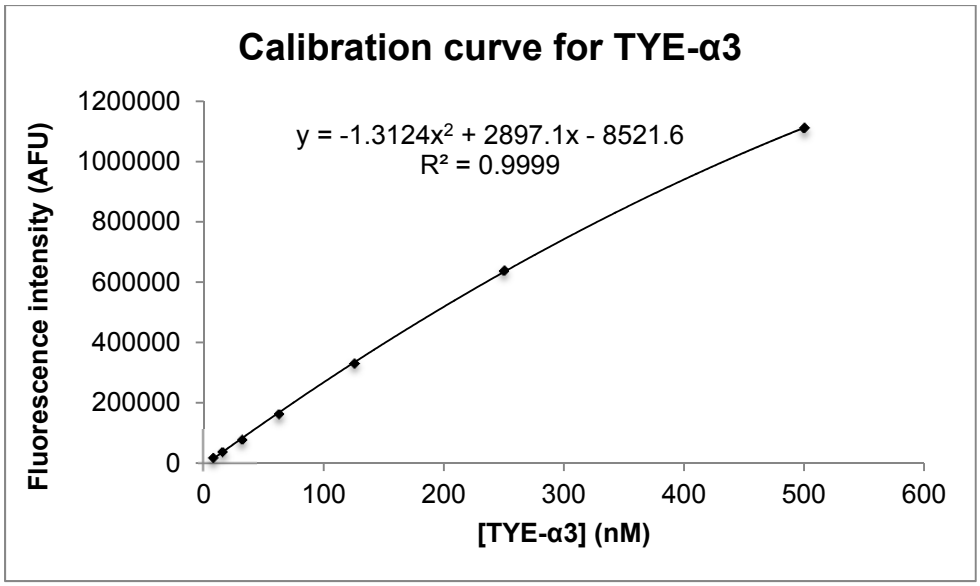

Figure 4-12: Calibration curve for TYE-α3.

An example of overlaid spectra for control 1 performed on mixture of FAM-α1 and TYE-α3, upon incubation with β2 beads is shown in Figure 4-13. The blue spectrum is for the mixture of labeled αs before mixing with β2 beads and the red trace relates to the supernatant after the capture step. The difference between the two is indicative of the non-specifically captured amounts of FAM-α1 and TYE-α3. As seen in Figure 4-13, the non-specific capture for FAM-α1 is much larger than TYE-α3. The green spectrum shows specific release of each labeled α into the supernatant after incubation with β'2.

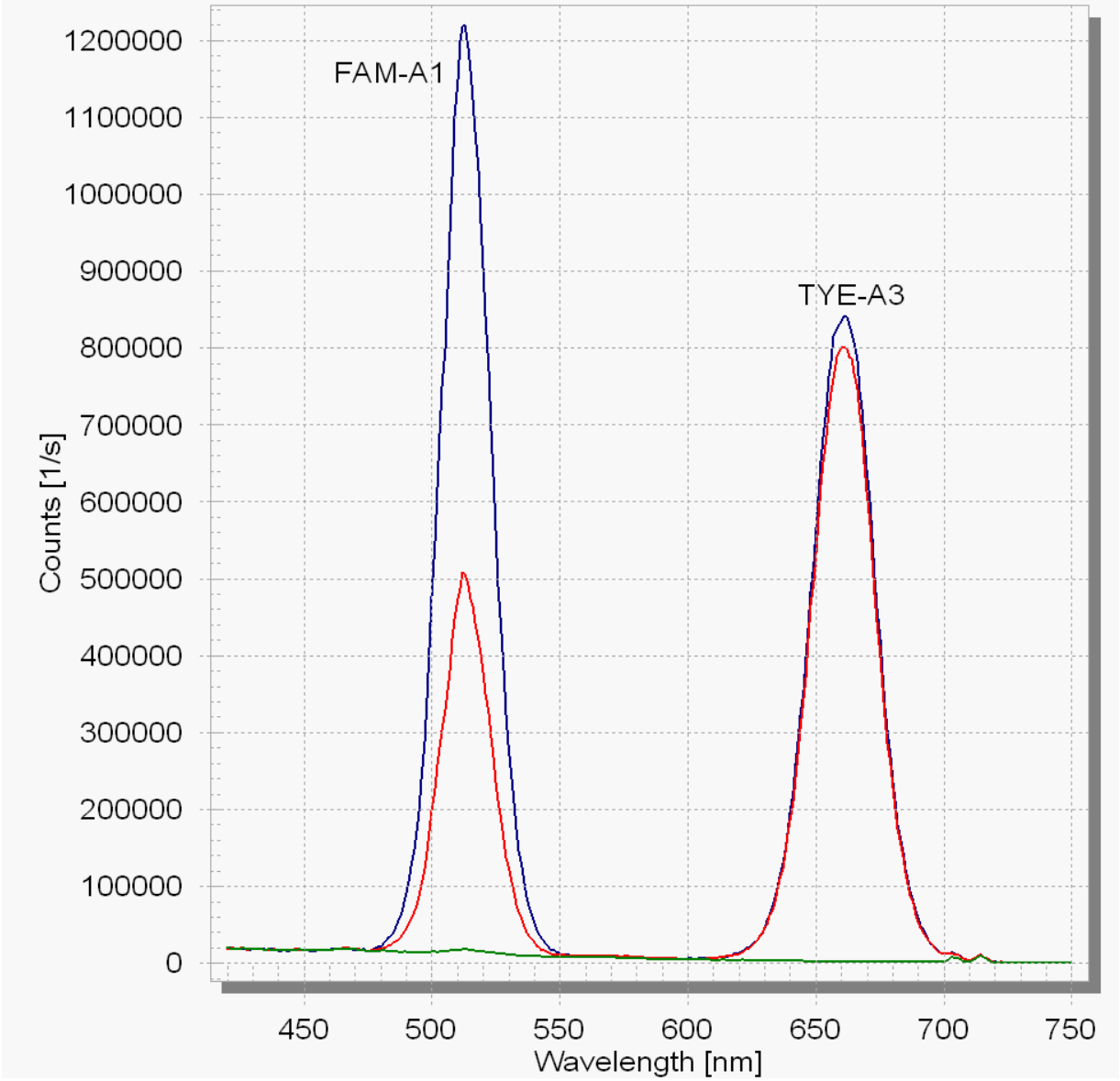

Figure 4-13: Overlaid spectra of the α mixture before mixing with β2 beads (blue), after mixing with β2 beads (red), and after release using β'2 (green).

Experimental section

Materials and methods

Integrated DNA Technology (IDT) synthesized all DNA strands. NFκβ was purchased from Adipogen. NeutrAvidin was obtained from Pierce. Silica microparticles functionalized with carboxyl groups (2.0 μm mean diameter) and carboxyl-functionalized polystyrene microparticles were from Bang Laboratories. 1-Ethyl-3-[3-

dimethylaminopropyl]carbodiimide hydrochloride (EDC) and N-hydroxysuccinimide (NHS) were from Sigma-Aldrich. 2-(*N*-morpholino)ethanesulfonic acid (MES) buffer, Tris HCl buffer, and Saline Sodium Citrate (SSC) buffer were made in the lab and their pH values were adjusted to 6.0, 7.8, and 7.4, respectively. The 10 mM HEPES buffer containing 150 mM NaCl and 0.005% P20 (HBS-P) at pH 7.4 already prepared, degassed, and filtered was from Biacore GE Healthcare. All DNA hybridizations were done at room temperature (21-24 °C). The NanoDrop ND-1000 UV-Vis spectrometer and Photon Technology International (PTI) Fluorometer were used.

DNA Sequence design

All DNA sequences were designed using the online packages DINAMelt (http://mfold.rna.albany.edu/?q=DINAMelt/software) and OligoAnalyzer 3.1 (http://www.idtdna.com/analyzer/Applications/OligoAnalyzer/). All sequences were checked for their melting points to make sure they were above 45 °C. Three SDR sets were designed each containing a 30-mer capture strand, α, a 5'-biotinylated probe, β, and two fuel strands, β' and α'. The 5'-biotinylated probe strand, β, in each SDR set was made of 35 nucleotides; 15 of which at the 3' end complementary to the first 15 nucleotides of the capture strand, α, at its 5' end. The last 10 nucleotides at the 5' end of β acted as a spacer stretch for better folding of the duplexes. The α capture strand of each SDR set was labeled with a unique fluorophore (α1 with FAM, α2 with TAMRA, and α3 with TYE665) at its 5' end. Two displacing "fuel" strands, β' and α', were also designed for each set to release the captured α strand. β' was composed of 25 nucleotides and a toehold of 10 nucleotides at the 5' end to form a 25 base pair duplex with the β probe on the beads. The α' fuel strand had 25 bases complementary to α, leaving a toehold of 10 nucleobases on α and 5 bases as a short spacer between the functional domains of α and the fluorescent label attached to it at the 5' end.

For the signal-off assay of NFκβ the adaptor strand, N, was a 42-mer single strand bearing the NFκβ binding site with the consensus sequence 5'-GGGACTTTCC-3'. The first 14 nucleotides of N from its 5' end were complementary to the first 15 nucleotides of TAMRA-α2 at its 5' end, leaving out a single nucleotide spacer between TAMRA and Nα2 duplex. The complementary strand, C, was a 20-mer matched to the

nucleotides 15-34 of N from its 5' end forming the duplex binding site for NFκβ. The first 8 nucleotides from the 3' end of N formed the toehold N_F for the fuel strand, F, which is fully complementary to N. The 25-mer "release" strand, R, in Scheme 4-4 is actually α'2 described earlier.

For the signal-on assay of NFκβ the adaptor strand, N, was a 44-mer single strand bearing the NFκβ binding site with the consensus sequence 5'-GGGACTTTCC-3'. Again, the first 14 nucleotides of N from its 5' end were complementary to the first 15 nucleotides of TAMRA-α2 at its 5' end, leaving out a single nucleotide spacer between TAMRA and the Nα2 duplex. For this assay format, however, the complementary strand, C, was a 20-mer matched to the first 20 nucleotides of N from its 5' end. This time, nucleotides 15-24 of N from its 5' end created a 10-mer toehold, N_F, in the middle of N, between the TFBS and Nα2 duplex. The first fuel strand, D, was a 30-mer complementary to the first 30 nucleotides of N from the 3' end. The second fuel strand, E, was fully complementary to D. The third fuel strand, F, was complementary to the first 24 nucleotides of N from the 3' end in this signal-on design. The fourth fuel strand, R, was α'2 described earlier.

The sequences were optimized to be free of any significant secondary structure at room temperature (on DINAMelt) and, wherever possible, any cross-hybridization involving a stretch of more than 4 nucleotides (OligoAnalyzer 3.1). All toeholds were larger than 7 nucleotides to assure a fast SDR kinetics. The sequences are shown below:

FAM-α1: 5-/FAM/ AGAGATAGAAGTAGTGGGAGGTGGTGGAGT-3

α'1: 5- ACTCCACCACCTCCCACTACTTCTA-3

β1: 5-/Biotin/ TCACACACTATTCCATCCTCACTCCACCACCTCCC-3

β'1: 5- GGGAGGTGGTGGAGTGAGGATGGAA-3

TAMRA-α2: 5-/TAMRA/ AGATGAAGAGTTAGAGGGTGAAAGAGGGTA-3

α'2: 5- TACCCTCTTTCACCCTCTAACTCTT-3

β2: 5-/Biotin/ TCACACACTATCCGCCTAACTACCCTCTTTCACCC-3

β'2: 5- GGGTGAAAGAGGGTAGTTAGGCGGA-3

TYE-α3: 5-/TYE665/ GAAGAAGGTGTTAAGAGAGAGAATATTGAT-3

α'3: 5- ATCAATATTCTCTCTCTTAACACCT -3

β3: 5-/Biotin/ TCACACACTCACACAACCACATCAATATTCTCTCT-3

β'3: 5- AGAGAGAATATTGATGTGGTTGTGT-3

N^{off}: 5- TCTAACTCTTCATCTACATGTGGGACTTTCCTGATTCTGTGT-3

C^{off}: 5- TCAGGAAAGTCCCACATGTA-3

F^{off}: 5- ACACAGAATCAGGAAAGTCCCACATGTAGATGAAGAGTTAGA-3

N^{on}: 5- TCTAACTCTTCATCGACTATTACTTGTGGGACTTTCCTATCTCA-3

C^{on}: 5- TGAGATAGGAAAGTCCCACA-3

D: 5- TGAGATAGGAAAGTCCCACAAGTAATAGTC-3

E: 5- GACTATTACTTGTGGGACTTTCCTATCTCA-3

F^{on}: 5- AGTAATAGTCGATGAAGAGTTAGA-3

Immobilization of the DNA probes on the carboxyl-bearing beads

Each step described here involving a reaction or process on beads starts with re-suspending the beads after addition of buffers/reagents using a benchtop vortex and ends with spinning down the beads at 10,000 g for 3 min to remove the supernatant using a micropipette. The 2.0 μm silica microparticles already grafted with linkers containing carboxyl groups at their ends were a dry powder, whereas the 3.0 μm polystyrene microparticles were in a 16.4 % suspension. For a typical NeutrAvidin immobilization [177,178,184-186], 30 mg beads were washed with 1.0 mL MilliQ water, and soaked in 1.0 mL MES buffer (pH= 6.0) for overnight. The beads were then centrifuged down again, the supernatant was discarded, 1.0 mL fresh MES was added and the suspension was sonicated for 90 min. 500 μL freshly prepared EDC (0.4M) was mixed with 500 μL freshly prepared NHS (0.4M) and the mixture was added immediately to the beads. After 10 minutes the beads were washed with 1.0 mL MES6.0 buffer quickly. 750 μL NeutrAvidin (0.4 mg/mL) in MES6.0 buffer was added to the

beads and incubated with them for 8 hours on vortex. To quench any unreacted activated NHS ester, 1.0 mL Ethanolamine 1.0 M (pH= 8.5) was used for 30 min on vortex. Two more washes each time with 1.0 mL 2.5x SSC for 1 min on vortex would make the beads ready for the immobilization of the probes. 1.20 mL DNA probes (either β1, β2, or β3 biotinylated at their 5' ends, 2.5 μM) in 2.5x SSC buffer were mixed with the beads for 16 hours on vortex. Two washes each time with 1.0 mL HBS-P buffer for 1 min on vortex were done at the end and finally the bead suspensions were divided into 20 equal portions of each 1.5 mg.

SDR-mediated multiplexing on silica beads

Each step described from this point on starts with re-suspending silica beads functionalized with β probes in the reaction solution, vortexing for a specified period of time, and centrifugation of the suspension at 10000 g for 3 min to remove the supernatant.

Multiplexed β' SDRs

1.5 mg β1 beads were added to 3.0 mg β2 and 1.5 mg β3 beads. A mixture of three labeled α strands was prepared in HBS-P buffer with the final concentrations of 167 nM, 667 nM, and 333 nM with respect to FAM-α1, TAMRA-α2, and TYE-α3, respectively. The mixture of β1-3 beads was sonicated in 450.0 μL HBS-P buffer for 5 min and 140.0 μL mixture of labeled αs described above was added for 5 min. Three washes using 450.0 μL HBS-P buffer were done; the first wash for 1 min, second for 5 min, and the third for 15 min. The sequential release was performed by a 15-min incubation with 140.0 μL β'3 (2.00 μM in HBS-P), a wash with 450.0 μL HBS-P buffer for 1 min, another 15-min incubation with β'2 (2.00 μM in HBS-P), a wash with 450.0 μL HBS-P buffer for 1 min, a 15-min incubation with β'1 (2.00 μM in HBS-P) followed by a wash with 450.0 μL HBS-P buffer for 1 min. For the second release, a mixture of β'1, β'2, and β'3 was prepared in HBS-P buffer with a final concentration of 667 nM with respect to each β'. The mixture of β's was then incubated with the mixture of beads for 45 min to simultaneously release everything left over on beads after the first sequential releases. The supernatants of all steps were saved for the fluorescent measurements. A calibration

curve for each labeled α strand (Figures 4-10 to 4-12) was built and used to quantify the amount of labeled αs in supernatants.

The fluorescence intensities at 512 nm, 578 nm, and 661 nm were used for FAM-α1, TAMRA-α2, and TYE-α3, respectively. It was assumed that there were no spectral overlaps among the three fluorophores at their maximum emission wavelengths. The spectra were obtained using the "synchronous scan" acquisition method, in which both excitation and emission wavelengths are scanned with a fixed wavelength difference (here, 20 nm). The concentrations of labeled αs in supernatants were obtained using above calibrations curves. The captured amounts were determined by subtracting concentration of the labeled α in the supernatant of capture step from the its concentration before mixing with beads. Figure 4-1 shows the analyzed data of multiplexed β' SDRs.

Control 1 ($(\alpha_i + \alpha_j) + \beta_k + \beta'_k$)

Control 1 was done on a single bead type (1.5 mg). A mixture of two labeled αs non-complementary to the probes on the beads was prepared in HBS-P buffer making the final concentrations of 167 nM, 667 nM, and 333 nM with respect to FAM-α1, TAMRA-α2, and TYE-α3, respectively. The beads were sonicated in 300.0 μL HBS-P buffer for 15 min and 140.0 μL mixture of the two appropriate labeled α in HBS-P was added for 5 min. Three washes using 300.0 μL HBS-P buffer were done; the first wash for 1 min, second for 5 min, and the third for 15 min. The release was performed by a 15-min incubation with 140.0 μL related β' (2.0 μM in HBS-P) complementary to the probe on beads. The supernatants of all steps were saved for the fluorescent measurements and the concentrations of labeled αs were obtained using the corresponding calibration curves.

Control 2 ($\alpha_j + \beta_j + (\beta'_i + \beta'_k)$)

The same procedure as the one for control 1 was followed. In this control, a single type of labeled α was captured on a single bead type with complementary β probes to α. The release was done using a mixture of two non-complementary β's (final concentrations of 2.00 μM in HBS-P).

Control 3 ($(\alpha_i + \alpha_k) + \beta_j + (\beta'_i+\beta'_k)$)

The same procedure as the one for control 2 was followed. In this control, two types of labeled α (final concentrations were the same as control 1 except for TAMRA-α2 which was 500 nM) were mixed with a single bead type with non-complementary β probes to αs. The release was done using a mixture of two non-complementary β's (final concentrations of 2.00 μM in HBS-P). After a short wash with 300.0 μL HBS-P buffer for 1 min, the release step was repeated for 15 min.

Control 4 ($[(\alpha_i + \alpha_j + \alpha_k) + \beta_j + \beta'_j]$ vs. $[\alpha_j + \beta_j + \beta'_j]$)

The same procedure as the one for control 3 was followed. In this control, a mixture of all three types of labeled α were mixed with a single bead type (1.5 mg) with complementary β probes to only one of the labeled α strands. The release was done using a single β' (final concentrations of 2.00 μM in HBS-P) complementary to the probes. After a short wash with 300.0 μL HBS-P buffer for 1 min, the release step was repeated for 15 min.

An identical procedure was used for a duplicate experiment for each labeled α strand. The only difference was that the labeled α of interest was added to the complementary bead type alone and the non-complementary αs were not present.

Reproducibility of multiplexed β' SDRs

Three bead types were mixed together (each 1.5 mg). On three mixtures of beads, the same procedure as the one described for multiplexed SDRs of Figure 4-1 was repeated with the following changes: in the mixture of three labeled αs, the final concentration of TAMRA-α2 was 333 nM. All washes were done in 300.0 μL HBS-P buffer. The second release was done for 15 min.

Multiplexed α' SDRs

The same procedure as the one for reproducibility of β' SDRs was followed. This experiment was done once and in the release steps α's (2.00 μM in HBS-P) were used instead of β' fuel strands.

Signal-off assay of NFκβ

1.5 mg polystyrene beads functionalized with β2 probes were used in each experiment. Three experiments were conducted (a positive and a negative control plus the main experiment with NFκβ). The binding buffer contained Tris HCl (20.0 mM), NaCl (50.0 mM), $MgCl_2$ (1.0 mM), and bovine serum albumin (BSA) (0.10 mg/mL). The pH of binding buffer was adjusted to 7.8. Adding N^{off}, C^{off}, and TAMRA-α2 together assembled the αNC complex in the binding buffer, such that the final concentration with respect to each constituent was 400 nM. The αNC complex was incubated at 90 °C for 15 min and then at room temperature for an extra 35 min. 80.0 μL NFκβ (2.0 μM in the binding buffer) was added to 80.0 μL assembled αNC complex and was incubated at room temperature for 70 min over vortex. Instead of NFκβ, 80.0 μL binding buffer was added to 80.0 μL αNC complex for the control experiments. 1.5 mg beads suspended in 150.0 μL binding buffer containing BSA (1.0 mg/mL) were sonicated for 10 min. 150.0 μL mixture of NFκβ-αNC complex (for controls only αNC complex) was then captured on beads for 10 min. After three 1-min washes with 150.0 μL binding buffer, 150.0 μL fuel strand F^{off} (1.0 μM in binding buffer) was added for 20 min. For the positive control, however, 150.0 μL binding buffer was added instead of F^{off}. After another three quick washes with the binding buffer, 150.0 μL α'2 (500 nM in binding buffer) was incubated for 30 min to release the labeled αNC complex unbound to NFκβ back to the solution. The supernatants of the release step were analyzed by fluorimetry.

Signal-on assay of NFκβ

1.5 mg polystyrene beads functionalized with β2 probes were used in each experiment. Two negative controls and a positive control were done in addition to the main experiment with NFκβ. The binding buffer contained Tris HCl (20.0 mM), NaCl (50.0 mM), $MgCl_2$ (1.0 mM), and bovine serum albumin (BSA) (0.10 mg/mL). The pH of binding buffer was adjusted to 7.8. Adding N^{on}, C^{on}, and TAMRA-α2 together assembled the αNC complex in the binding buffer, such that the final concentration with respect to each constituent was 400 nM. The αNC complex was incubated at 90 °C for 15

min and then at room temperature for an extra 35 min. 80.0 μL NFκβ (2.0 μM in the binding buffer) was added to 80.0 μL assembled αNC complex and was incubated at room temperature for 70 min over vortex. Instead of NFκβ, 80.0 μL binding buffer was added to 80.0 μL αNC complex for the control experiments. 1.5 mg beads suspended in 150.0 μL binding buffer containing BSA (1.0 mg/mL) were sonicated for 10 min. 150.0 μL mixture of NFκβ-αNC complex (for controls only αNC complex) was then captured on beads for 10 min. After three 1-min washes with 150.0 μL binding buffer, 150.0 μL fuel strand D (1.0 μM in binding buffer) was added for 20 min. For the positive control, however, 150.0 μL binding buffer was added instead of D. After another three quick washes with the binding buffer, 150.0 μL E (1.0 μM in binding buffer) was added for 20 min. Three quick washes were done and then 150.0 μL F^{on} (1.0 μM in binding buffer) was incubated with beads for 20 min except for one of the negative controls to which 150.0 μL binding buffer was added (the other negative control included all steps but addition of NFκβ). After another three quick washes with the binding buffer, 150.0 μL α'2 (500 nM in binding buffer) was incubated for 30 min to release the labeled αNC complex bound to NFκβ back to the solution. The supernatants of the release step were analyzed by fluorimetry.

CHAPTER 5

CONCLUSIONS AND FUTURE PROSPECTS

Strand displacement reaction (SDR) is so simple in principles that it is hard to imagine there could be such a vast repertoire of applications for it. Yet, when compared to applications of DNA hybridization itself, we notice that the simple molecular recognitions existing among the four DNA nucleobases give rise to the incredible complexity we refer to as "life". In this PhD work we expanded the scope of SDR applications by demonstrating how it could be customized for cleanup of biomolecules and parallel purification and assay of transcription factors. The inherent data storage nature of DNA allows for programming it through its sequence to perform parallel tasks and execute computations. The programmability brings forward the notion of specific in contrast to non-specific release of molecules and involves at least three different layers. The idea of adding an "effector" molecule to trigger the specific release of a target molecule is superior to the traditional approach of altering physicochemical properties of the buffer or solvent, for instance by adjusting pH or polarity. The conventional non-specific release methodologies often lack enough tunability and target a big class of compounds. The second layer of specific release through SDR is the ability to narrow down the target of release virtually to a single molecule. The limiting factor here is not the SDR-mediated release but specificity of the molecular recognition device (antibody, aptamer, carbohydrate, etc.) employed. Many "molecule-triggered" release systems are known such as imidazole in polyhistidine tag purification and immobilized metal ion affinity chromatography (IMAC) [219] in general, disulfide exchange [218], or heparin elution in DNA affinity chromatography [195]. These systems cannot achieve the second layer of specificity SDR offers since they carry out the release all at once, which, in turn, is because they are not amenable to storing information. Chapters 2-3 set forth and optimized the experimental parameters needed to establish the first and second layers of SDR-mediated specificity.

The third dimension of sequence-encoded specific release, multiplexability, is a corollary of the second layer of specificity discussed above. It was evinced in chapter 4, where three independent SDR sets were mixed together and showed no crosstalk among them. A versatile scheme called IDCAPT was conceived in which sequence addressability of DNA underpins parallel purification, characterization and quantification of transcription factors (TFs). This chapter also showcased a rudimentary DNA computation via implementing a TF-DNA logical gate that surveys the presence of a TF by sequential SDRs and releases an output signal DNA strand. The great advantage of IDCAPT is that it could be disposed to concentrate on one task or integrate multiple tasks. It is, however, needless to mention that a considerable body of work is still to be done to validate IDCAPT and test whether it lives up to the anticipations.

The results of chapter 2 proved that using a two-dimensional chip surface for DNA probe immobilization suffers from very limited mass transfer to the surface. The fraction of molecules captured on the surface could be very small compared to the total amounts in the bulk of solution. Our group has developed the methodology for packing crystalline arrays of nanoparticles inside the channels of microfluidic chips for the separation of biomolecules in the last decade [233]. Nanoparticles provide an extensive surface area and therefore, the capture efficiencies over them is expected to be much greater due to less resistance to mass transfer. Multiplexing on chip is prone to automation, very small amounts of reagent consumption, and considerable flexibility in customization built-in to the current mature microfluidic technology.

The SDR-based FIA on beads discussed in chapter 3 could be redesigned in a multiplex format for assays on chip. The same design paradigm could be adopted for mRNA [234,235] and siRNA profiling [236-238] on chip. It is also possible to test aptamers, antibody fragments, or carbohydrates as the molecular recognition device instead of antibodies.

There is plenty of room to refine and mature the IDCAPT strategy into a viable technology. In the context of multiplexing, IDCAPT should withstand rigorous testing for its application to purifications of two more TFs (for example SP1 and ATF3). To validate it for a full scale technological challenge, several tens of capture strands for characterized TFs in yeast or HeLa cells could be designed using the catalogues of TFs published [239] or the online TFBS databases (such as JASPAR, TRANSFAC,

UniPROBE, TFBSshape, TFBS, RegulanDB, HOCOMOCO, PAZAR, PRODORIC, and TRRD among many others). Designing manually a large number of orthogonal SDR sets is a formidable task but the web-based programming language for designing complex SDR circuits powered by Microsoft (see http://research.microsoft.com/en-us/projects/dna/ and http://boson.research.microsoft.com/webdna/) could be used in this case. The sensitivity and performance of IDCAPT for detection, purification, and identification of TFs is thus to be examined and optimized. It is worth mentioning that while the SDR set design could be optimized to be free of any major cross-hybridization, the cross-reactivity of TFs for different TFBSs is an intrinsic limitation of such an *in vitro* binding process. Nature, on the other side, has many complicated cell signaling pathways to ensure the selectivity and specificity of TF binding to the TFBSs inside the cell. For instance, when a TF needs to bind to its binding site in the nucleus, only the related segment of genome becomes exposed and accessible by the gene expression machinery of the cell.

If IDCAPT could be combined with microfluidics through the nanoparticle-in-channel packing approach described earlier, it would be possible to build upon many technical advances already established on the chip. Mass spectrometry (MS) is one of the major methods of characterization of proteins in general and TFs as well. There has been a substantial progress with interfacing capillary electrophoresis with MS [240,241], which might inspire designing similar setups on chips [242,243]. Moreover, our group is already in the process of developing a thin film substrate fabrication technology for surface enhanced laser desorption ionization mass spectrometry (SELDI-MS) [244] and interfacing it to microchips. If realized, the functional on-chip IDCAPT interfaced to MS seems like a promising multifaceted commercial product.

As elaborated on in chapter 4, the design fluidity of IDCAPT allows it to be tailored for a single application. As a proof of customizability, the TFBS length in terms of number of nucleotides could be characterized using different length of the "interrogator" strand. The kinetics of release gets slower as the length of toehold on the interrogator strand approaches zero. However, this tactic works directionally and identifies the boundary of TFBS on the 3' end. To evaluate the 5' end, a second toehold should be incorporated to the 5' end of the capture strand with the corresponding marker and interrogator strands designed.

As a brief afterword, I would like to put finishing touches on my dissertation by expressing what I have learned in terms of philosophy of science in a pithy and synoptic statement:

Science boils down to finding and making educated assumptions and testing which ones are valid.

BIBLIOGRAPHY

1. Seeman NC: **Nucleic acid junctions and lattices**. *Journal of theoretical biology* 1982, **99**:237-247.

2. Seeman NC, Wang H, Yang X, Liu F, Mao C, Sun W, Wenzler L, Shen Z, Sha R, Yan H: **New motifs in DNA nanotechnology**. *Nanotechnology* 1998, **9**:257.

3. Seeman NC: **An overview of structural DNA nanotechnology**. *Mol Biotechnol* 2007, **37**:246-257.

4. Zhang D, Seelig G: **Dynamic DNA nanotechnology using strand-displacement reactions**. *Nature Chemistry* 2011, **3**:103-113.

5. Fox MS: **On the mechanism of integration of transforming deoxyribonucleate**. *The Journal of General Physiology* 1966, **49**:183-196.

6. Holliday R: **The induction of mitotic recombination by mitomycin C in Ustilago and Saccharomyces**. *Genetics* 1964, **50**:323.

7. Liberi G, Foiani M: **The double life of Holliday junctions**. *Cell Res* 2010, **20**:611-613.

8. Green C, Tibbetts C: **Reassociation rate limited displacement of DNA strands by branch migration**. *Nucleic Acids Res* 1981, **9**:1905-1918.

9. Vary CP, McMahon FJ, Barbone FP, Diamond SE: **Nonisotopic detection methods for strand displacement assays of nucleic acids**. *Clinical Chemistry* 1986, **32**:1696-1701.

10. Collins M, Fritsch EF, Ellwood MS, Williams JI, Brewen JG: **A novel diagnostic method based on DNA strand displacement**. *Molecular and Cellular Probes* 1988, **2**:15-30.

11. Ellwood MS, Collins M, Fritsch EF, Williams JI, Diamond SE, Brewen JG: **Strand displacement applied to assays with nucleic acid probes**. *Clinical Chemistry* 1986, **32**:1631-1636.

12. Vary CP: **A homogeneous nucleic acid hybridization assay based on strand displacement**. *Nucleic Acids Res* 1987, **15**:6883-6897.

13. Gelfand CA, Plum GE, Mielewczyk S, Remeta DP, Breslauer KJ: **A quantitative method for evaluating the stabilities of nucleic acids**. *Proc. Natl. Acad. Sci. USA* 1999, **96**:6113-6118.

14. Li Q, Luan G, Guo Q, Liang J: **A new class of homogeneous nucleic acid probes based on specific displacement hybridization**. *Nucleic Acids Research* 2002, **30**:e5.

15. Tyagi S, Kramer F: **Molecular beacons: Probes that fluoresce upon hybridization**.

Nature Biotechnology 1996, **14**:303-308.
16. Meserve D, Wang Z, Zhang DD, Wong PK: **A double-stranded molecular probe for homogeneous nucleic acid analysis**. *Analyst* 2008, **133**:1013-1019.
17. Mo ZH, Yang XC, Guo KP, Wen ZY: **A nanogold-quenched fluorescence duplex probe for homogeneous DNA detection based on strand displacement**. *Anal Bioanal Chem* 2007, **389**:493-497.
18. Zhang Y, Tian J, Li H, Wang L, Sun X: **A novel single fluorophore-labeled double-stranded oligonucleotide probe for fluorescence-enhanced nucleic acid detection based on the inherent quenching ability of deoxyguanosine bases and competitive strand-displacement reaction**. *J Fluoresc* 2012, **22**:43-46.
19. Kolpashchikov DM: **An elegant biosensor molecular beacon probe: challenges and recent solutions**. *Scientifica* 2012, **2012**:928783.
20. Rajkowitsch L, Schroeder R: **Coupling RNA annealing and strand displacement: a FRET-based microplate reader assay for RNA chaperone activity**. *BioTechniques* 2007, **43**:304-310.
21. Huang F, You M, Han D, Xiong X, Liang H, Tan W: **DNA branch migration reactions through photocontrollable toehold formation**. *J Am Chem Soc* 2013, **135**:7967-7973.
22. Tang W, Wang H, Wang D, Zhao Y, Li N, Liu F: **DNA tetraplexes-based toehold activation for controllable DNA strand displacement reactions**. *J Am Chem Soc* 2013, **135**:13628-13631.
23. Zhu J, Zhang L, Li T, Dong S, Wang E: **Enzyme-free unlabeled DNA logic circuits based on toehold-mediated strand displacement and split G-quadruplex enhanced fluorescence**. *Adv Mater* 2013, **25**:2440-2444.
24. Gidwani V, Riahi R, Zhang DD, Wong PK: **Hybridization kinetics of double-stranded DNA probes for rapid molecular analysis**. *Analyst* 2009, **134**:1675-1681.
25. Wang Z, Zhang K, Wooley KL, Taylor JS: **Imaging mRNA Expression in Live Cells via PNA.DNA Strand Displacement-Activated Probes**. *J Nucleic Acids* 2012, **2012**:962652.
26. Rothlingshofer M, Gorska K, Winssinger N: **Nucleic acid-templated energy transfer leading to a photorelease reaction and its application to a system displaying a nonlinear response**. *J Am Chem Soc* 2011, **133**:18110-18113.
27. Liang M, Liu X, Cheng D, Nakamura K, Wang Y, Dou S, Liu G, Rusckowski M, Hnatowich DJ: **Optical antisense tumor targeting in vivo with an improved fluorescent DNA duplex probe**. *Bioconjugate Chem* 2009, **20**:1223-1227.
28. He F, Feng F, Duan X, Wang S, Li Y, Zhu D: **Selective and homogeneous fluorescent**

DNA detection by target-induced strand displacement using cationic conjugated polyelectrolytes. *Analytical Chemistry* 2008, **80**:2239-2243.

29. Huang S, Salituro J, Tang N, Luk KC, Hackett JJ, Swanson P, Cloherty G, Mak WB, Robinson J, Abravaya K: **Thermodynamically modulated partially double-stranded linear DNA probe design for homogeneous real-time PCR**. *Nucleic Acids Res* 2007, **35**:e101.

30. Duwensee H, Jacobsen M, Flechsig GU: **Electrochemical competitive hybridization assay for DNA detection using osmium tetroxide-labelled signalling strands**. *Analyst* 2009, **134**:899-903.

31. Mir M, Lozano-Sanchez P, Katakis I: **Towards a target label-free suboptimum oligonucleotide displacement-based detection system**. *Anal Bioanal Chem* 2008, **391**:2145-2152.

32. Xiao Y, Lubin AA, Baker BR, Plaxco KW, Heeger AJ: **Single-step electronic detection of femtomolar DNA by target-induced strand displacement in an electrode-bound duplex**. *Proc Natl Acad Sci U S A* 2006, **103**:16677-16680.

33. Bertolino C, Macsweeney M, Tobin J, O'Neill B, Sheehan MM, Coluccia S, Berney H: **A monolithic silicon based integrated signal generation and detection system for monitoring DNA hybridisation**. *Biosens Bioelectron* 2005, **21**:565-573.

34. Zhu J, Feng X, Lou J, Li W, Li S, Zhu H, Yang L, Zhang A, He L, Li C: **Accurate Quantification of microRNA via Single Strand Displacement Reaction on DNA Origami Motif**. *PLOS ONE* 2013, **8**:e69856.

35. Zangmeister RA, Tarlov MJ: **DNA displacement assay integrated into microfluidic channels**. *Anal. Chem.* 2004, **76**:3655-3659.

36. Xu P, Huang F, Liang H: **Real-time study of a DNA strand displacement reaction using dual polarization interferometry**. *Biosens Bioelectron* 2013, **41**:505-510.

37. Liu L, Dong X, Lian W, Peng X, Liu Z, He Z, Wang Q: **Homogeneous competitive hybridization assay based on two-photon excitation fluorescence resonance energy transfer**. *Anal Chem* 2010, **82**:1381-1388.

38. Zhang D, Winfree E: **Control of DNA Strand Displacement Kinetics Using Toehold Exchange**. *Journal of the American Chemical Society* 2009, **131**:17303-17314.

39. Baker BA, Milam VT: **Hybridization kinetics between immobilized double-stranded DNA probes and targets containing embedded recognition segments**. *Nucleic Acids Res* 2011, **39**:e99.

40. Genot A, Zhang D, Bath J, Turberfield A: **Remote toehold: a mechanism for flexible**

control of DNA hybridization kinetics. *Journal of the American Chemical Society* 2011, **133**:2177-2182.

41. Zhang D, Chen S, Yin P: **Optimizing the specificity of nucleic acid hybridization**. *Nature Chemistry* 2012, **4**:208-214.

42. Qian L, Winfree E, Bruck J: **Neural network computation with DNA strand displacement cascades**. *Nature* 2011, **475**:368-372.

43. Chen Y, Dalchau N, Srinivas N, Phillips A, Cardelli L, Soloveichik D, Seelig G: **Programmable chemical controllers made from DNA**. *Nature Nanotechnology* 2013, **8**:755-762.

44. Muscat RA, Strauss K, Ceze L, Seelig G: **DNA-based molecular architecture with spatially localized components**. In *Proceedings of the 40th Annual International Symposium on Computer Architecture*: ACM: 2013:177-188.

45. Zhang Y, Yu H, Qin J, Lin B: **A microfluidic DNA computing processor for gene expression analysis and gene drug synthesis**. *Biomicrofluidics* 2009, **3**:44105.

46. Phillips A, Cardelli L: **A programming language for composable DNA circuits**. *Journal of the Royal Society Interface* 2009, **6**:S419-S436.

47. Lakin MR, Youssef S, Cardelli L, Phillips A: **Abstractions for DNA circuit design**. *J R Soc Interface* 2012, **9**:470-486.

48. Livstone MS, Weiss R, Landweber LF: **Automated Design and Programming of a Microfluidic DNA Computer**. *Natural Computing* 2006, **5**:1-13.

49. Lee SH, van Noort D, Yang KA, Lee IH, Zhang BT, Park TH: **Biomolecular theorem proving on a chip: a novel microfluidic solution to a classical logic problem**. *Lab Chip* 2012, **12**:1841-1848.

50. Soloveichik D, Seelig G, Winfree E: **DNA as a universal substrate for chemical kinetics**. *Proceedings of the National Academy of Sciences of the United States of America* 2010, **107**:5393-5398.

51. Sainz de Murieta I, Rodriguez-Paton A: **DNA biosensors that reason**. *Biosystems* 2012, **109**:91-104.

52. Yang J, Shen L, Ma J, Schlaberg HI, Liu S, Xu J, Zhang C: **Fluorescent nanoparticle beacon for logic gate operation regulated by strand displacement**. *ACS Appl Mater Interfaces* 2013, **5**:5392-5396.

53. Lake A, Shang S, Kolpashchikov DM: **Molecular logic gates connected through DNA four-way junctions**. *Angew Chem Int Ed Engl* 2010, **49**:4459-4462.

54. Senum P, Riedel M: **Rate-Independent Constructs for Chemical Computation**. *Plos*

One 2011, **6**:e21414.

55. Cardelli L: **Strand algebras for DNA computing**. Edited by: Springer; 2009:12-24.

56. Seelig G, Soloveichik D: **Time-complexity of multilayered DNA strand displacement circuits**. Edited by: Springer; 2009:144-153.

57. Hazarika P, Ceyhan B, Niemeyer CM: **Reversible switching of DNA-gold nanoparticle aggregation**. *Angew Chem Int Ed Engl* 2004, **43**:6469-6471.

58. Zhang Z, Cheng Q, Feng P: **Selective removal of DNA-labeled nanoparticles from planar substrates by DNA displacement reactions**. *Angewandte Chemie-International Edition* 2009, **48**:118-122.

59. Tison C, Milam V: **Reversing DNA-mediated adhesion at a fixed temperature**. *Langmuir* 2007, **23**:9728-9736.

60. Song T, Liang H: **Synchronized assembly of gold nanoparticles driven by a dynamic DNA-fueled molecular machine**. *J Am Chem Soc* 2012, **134**:10803-10806.

61. Duose D, Schweller R, Hittelman W, Diehl M: **Multiplexed and Reiterative Fluorescence Labeling via DNA Circuitry**. *Bioconjugate Chemistry* 2010, **21**:2327-2331.

62. Duose DY, Schweller RM, Zimak J, Rogers AR, Hittelman WN, Diehl MR: **Configuring robust DNA strand displacement reactions for in situ molecular analyses**. *Nucleic Acids Res* 2012, **40**:3289-3298.

63. Chandran H, Rangnekar A, Shetty G, Schultes E, Reif J, LaBean T: **An autonomously self-assembling dendritic DNA nanostructure for target DNA detection**. *Biotechnology Journal* 2013, **8**:221-227.

64. Zhang DY, Turberfield AJ, Yurke B, Winfree E: **Engineering entropy-driven reactions and networks catalyzed by DNA**. *Science* 2007, **318**:1121-1125.

65. Chen X, Briggs N, McLain J, Ellington A: **Stacking nonenzymatic circuits for high signal gain**. *Proceedings of the National Academy of Sciences of the United States of America* 2013, **110**:5386-5391.

66. Dirks RM, Pierce NA: **Triggered amplification by hybridization chain reaction**. *Proc Natl Acad Sci U S A* 2004, **101**:15275-15278.

67. Shimron S, Wang F, Orbach R, Willner I: **Amplified detection of DNA through the enzyme-free autonomous assembly of hemin/G-quadruplex DNAzyme nanowires**. *Anal Chem* 2012, **84**:1042-1048.

68. Seelig G, Yurke B, Winfree E: **Catalyzed relaxation of a metastable DNA fuel**. *Journal of the American Chemical Society* 2006, **128**:12211-12220.

69. Wang F, Elbaz J, Willner I: **Enzyme-free amplified detection of DNA by an**

autonomous ligation DNAzyme machinery. *J Am Chem Soc* 2012, **134**:5504-5507.
70. Bi S, Zhang J, Hao S, Ding C, Zhang S: **Exponential amplification for chemiluminescence resonance energy transfer detection of microRNA in real samples based on a cross-catalyst strand-displacement network**. *Anal Chem* 2011, **83**:3696-3702.
71. Niu S, Qu L, Zhang Q, Lin J: **Fluorescence detection of thrombin using autocatalytic strand displacement cycle reaction and a dual-aptamer DNA sandwich assay**. *Anal Biochem* 2012, **421**:362-367.
72. Zimak J, Schweller RM, Duose DY, Hittelman WN, Diehl MR: **Programming in situ immunofluorescence intensities through interchangeable reactions of dynamic DNA complexes**. *Chembiochem* 2012, **13**:2722-2728.
73. Zhang DY, Winfree E: **Robustness and modularity properties of a non-covalent DNA catalytic reaction**. *Nucleic Acids Res* 2010, **38**:4182-4197.
74. Walker GT: **Empirical aspects of strand displacement amplification**. *PCR Methods Appl.* 1993, **3**:1-6.
75. Ehses S, Ackermann J, McCaskill JS: **Optimization and design of oligonucleotide setup for strand displacement amplification**. *J Biochem Biophys Methods* 2005, **63**:170-186.
76. Paul P, Apgar J: **Single-molecule dilution and multiple displacement amplification for molecular haplotyping**. *Biotechniques* 2005, **38**:553-560.
77. Hellyer T, Nadeau J: **Strand displacement amplification: a versatile tool for molecular diagnostics**. *Expert Review of Molecular Diagnostics* 2004, **4**:251-261.
78. Walker G, Fraiser M, Schram J, Little M, Nadeau J, Malinowski D: **Strand displacement amplification—an isothermal, in vitro DNA amplification technique**. *Nucleic Acids Research* 1992, **20**:1691-1696.
79. Baker BA, Mahmoudabadi G, Milam VT: **Using double-stranded DNA probes to promote specificity in target capture**. *Colloids Surf B Biointerfaces* 2013, **102**:884-890.
80. Kim K, Yang H, Park S, Lee D, Kim S, Lim Y, Kim Y: **Washing-free electrochemical DNA detection using double-stranded probes and competitive hybridization reaction**. *Chemical Communications* 2004:1466-1467.
81. Zhang Z, Zeng D, Ma H, Feng G, Hu J, He L, Li C, Fan C: **A DNA-Origami chip platform for label-free SNP genotyping using toehold-mediated strand displacement**. *Small* 2010, **6**:1854-1858.
82. Wang D, Chen G, Wang H, Tang W, Pan W, Li N, Liu F: **A reusable quartz crystal**

microbalance biosensor for highly specific detection of single-base DNA mutation. *Biosens Bioelectron* 2013, **48**:276-280.

83. Wang X, Zou M, Huang H, Ren Y, Li L, Yang X, Li N: **Gold nanoparticle enhanced fluorescence anisotropy for the assay of single nucleotide polymorphisms (SNPs) based on toehold-mediated strand-displacement reaction**. *Biosens Bioelectron* 2013, **41**:569-575.

84. Wang D, Tang W, Wu X, Wang X, Chen G, Chen Q, Li N, Liu F: **Highly selective detection of single-nucleotide polymorphisms using a quartz crystal microbalance biosensor based on the toehold-mediated strand displacement reaction**. *Anal Chem* 2012, **84**:7008-7014.

85. Wang HQ, Liu WY, Wu Z, Tang LJ, Xu XM, Yu RQ, Jiang JH: **Homogeneous label-free genotyping of single nucleotide polymorphism using ligation-mediated strand displacement amplification with DNAzyme-based chemiluminescence detection**. *Anal Chem* 2011, **83**:1883-1889.

86. Hirata K, Sato Y, Kano A, Akaike T, Maruyama A: **Nucleation-synchronized strand displacement for highly sensitive DNA analysis**. In *Nucleic Acids Symposium Series*: Oxford Univ Press: 2004:267-268.

87. Chen SX, Zhang DY, Seelig G: **Conditionally fluorescent molecular probes for detecting single base changes in double-stranded DNA**. *Nat Chem* 2013, **5**:782-789.

88. Khodakov DA, Khodakova AS, Linacre A, Ellis AV: **Toehold-mediated nonenzymatic DNA strand displacement as a platform for DNA genotyping**. *J Am Chem Soc* 2013, **135**:5612-5619.

89. Das SK, Austin MD, Akana MC, Deshpande P, Cao H, Xiao M: **Single molecule linear analysis of DNA in nano-channel labeled with sequence specific fluorescent probes**. *Nucleic Acids Res* 2010, **38**:e177.

90. Pourmand N, Caramuta S, Villablanca A, Mori S, Karhanek M, Wang SX, Davis RW: **Branch migration displacement assay with automated heuristic analysis for discrete DNA length measurement using DNA microarrays**. *Proc Natl Acad Sci U S A* 2007, **104**:6146-6151.

91. He Y, Liu DR: **A sequential strand-displacement strategy enables efficient six-step DNA-templated synthesis**. *J Am Chem Soc* 2011, **133**:9972-9975.

92. McKee ML, Milnes PJ, Bath J, Stulz E, Turberfield AJ, O'Reilly RK: **Multistep DNA-templated reactions for the synthesis of functional sequence controlled oligomers**. *Angew Chem Int Ed Engl* 2010, **49**:7948-7951.

93. Yin P, Choi H, Calvert C, Pierce N: **Programming biomolecular self-assembly pathways**. *Nature* 2008, **451**:318-322.
94. Chen X: **Expanding the rule set of DNA circuitry with associative toehold activation**. *J Am Chem Soc* 2012, **134**:263-271.
95. Zhang DY, Hariadi RF, Choi HM, Winfree E: **Integrating DNA strand-displacement circuitry with DNA tile self-assembly**. *Nat Commun* 2013, **4**:1965.
96. Maune H, Han S, Barish R, Bockrath M, Goddard W, Rothemund P, Winfree E: **Self-assembly of carbon nanotubes into two-dimensional geometries using DNA origami templates**. *Nature Nanotechnology* 2010, **5**:61-66.
97. Li Z, Ke Y, Lin C, Yan H, Liu Y: **Subtractive assembly of DNA nanoarchitectures driven by fuel strand displacement**. *Chemical Communications* 2008:4318-4320.
98. Lubrich D, Green SJ, Turberfield AJ: **Kinetically Controlled Self-Assembly of DNA Oligomers**. *J. Am. Chem. Soc.* 2009, **131**:2422-2423.
99. Wei B, Ong LL, Chen J, Jaffe AS, Yin P: **Complex reconfiguration of DNA nanostructures**. *Angew Chem Int Ed Engl* 2014, **53**:7475-7479.
100. Han D, Pal S, Liu Y, Yan H: **Folding and cutting DNA into reconfigurable topological nanostructures**. *Nature Nanotechnology* 2010, **5**:712-717.
101. Zhang F, Nangreave J, Liu Y, Yan H: **Reconfigurable DNA origami to generate quasifractal patterns**. *Nano Lett* 2012, **12**:3290-3295.
102. Zhang C, Tian C, Li X, Qian H, Hao C, Jiang W, Mao C: **Reversibly switching the surface porosity of a DNA tetrahedron**. *J Am Chem Soc* 2012, **134**:11998-12001.
103. Yurke B, Turberfield A, Mills A, Simmel F, Neumann J: **A DNA-fuelled molecular machine made of DNA**. *Nature* 2000, **406**:605-608.
104. Venkataraman S, Dirks RM, Rothemund PW, Winfree E, Pierce NA: **An autonomous polymerization motor powered by DNA hybridization**. *Nat Nanotechnol* 2007, **2**:490-494.
105. Green SJ, Lubrich D, Turberfield AJ: **DNA hairpins: fuel for autonomous DNA devices**. *Biophys J* 2006, **91**:2966-2975.
106. Chen Y, Mao C: **Putting a brake on an autonomous DNA nanomotor**. *Journal of the American Chemical Society* 2004, **126**:8626-8627.
107. You M, Huang F, Chen Z, Wang R-W, Tan W: **Building a Nanostructure with Reversible Motions Using Photonic Energy**. *ACS Nano* 2012, **6**:7935-7941.
108. Simmel FC, Dittmer WU: **DNA nanodevices**. *Small* 2005, **1**:284-299.
109. Zhang Z, Olsen EM, Kryger M, Voigt NV, Torring T, Gultekin E, Nielsen M,

MohammadZadegan R, Andersen ES, Nielsen MM, et al.: **A DNA tile actuator with eleven discrete states**. *Angew Chem Int Ed Engl* 2011, **50**:3983-3987.

110. Elbaz J, Wang ZG, Wang F, Willner I: **Programmed dynamic topologies in DNA catenanes**. *Angew Chem Int Ed Engl* 2012, **51**:2349-2353.

111. Lohmann F, Ackermann D, Famulok M: **Reversible light switch for macrocycle mobility in a DNA rotaxane**. *J Am Chem Soc* 2012, **134**:11884-11887.

112. Chhabra R, Sharma J, Liu Y, Yan H: **Addressable molecular tweezers for DNA-templated coupling reactions**. *Nano Letters* 2006, **6**:978-983.

113. Tian Y, He Y, Chen Y, Yin P, Mao C: **A DNAzyme that walks processively and autonomously along a one-dimensional track**. *Angew Chem Int Ed Engl* 2005, **44**:4355-4358.

114. Liu M, Fu J, Hejesen C, Yang Y, Woodbury NW, Gothelf K, Liu Y, Yan H: **A DNA tweezer-actuated enzyme nanoreactor**. *Nat Commun* 2013, **4**:2127.

115. Gianneschi NC, Ghadiri MR: **Design of molecular logic devices based on a programmable DNA-regulated semisynthetic enzyme**. *Angew Chem Int Ed Engl* 2007, **46**:3955-3958.

116. Erkelenz M, Kuo CH, Niemeyer CM: **DNA-mediated assembly of cytochrome P450 BM3 subdomains**. *J Am Chem Soc* 2011, **133**:16111-16118.

117. Liang JC, Smolke CD: **Rational design and tuning of ribozyme-based devices**. *Methods Mol Biol* 2012, **848**:439-454.

118. Endo M, Miyazaki R, Emura T, Hidaka K, Sugiyama H: **Transcription regulation system mediated by mechanical operation of a DNA nanostructure**. *J Am Chem Soc* 2012, **134**:2852-2855.

119. Rudchenko M, Taylor S, Pallavi P, Dechkovskaia A, Khan S, Butler V, Rudchenko S, Stojanovic M: **Autonomous molecular cascades for evaluation of cell surfaces**. *Nature Nanotechnology* 2013, **8**:580-586.

120. Seelig G, Soloveichik D, Zhang D, Winfree E: **Enzyme-free nucleic acid logic circuits**. *Science* 2006, **314**:1585-1588.

121. Li W, Yang Y, Yan H, Liu Y: **Three-input majority logic gate and multiple input logic circuit based on DNA strand displacement**. *Nano Lett* 2013, **13**:2980-2988.

122. Qian L, Winfree E: **Scaling up digital circuit computation with DNA strand displacement cascades**. *Science* 2011, **332**:1196-1201.

123. Xing Y, Yang Z, Liu D: **A responsive hidden toehold to enable controllable DNA strand displacement reactions**. *Angew Chem Int Ed Engl* 2011, **50**:11934-11936.

124. Wieland M, Benz A, Haar J, Halder K, Hartig J: **Small molecule-triggered assembly of DNA nanoarchitectures**. *Chemical Communications* 2010, **46**:1866-1868.
125. Han D, Zhu Z, Wu C, Peng L, Zhou L, Gulbakan B, Zhu G, Williams KR, Tan W: **A logical molecular circuit for programmable and autonomous regulation of protein activity using DNA aptamer-protein interactions**. *J Am Chem Soc* 2012, **134**:20797-20804.
126. Douglas SM, Bachelet I, Church GM: **A logic-gated nanorobot for targeted transport of molecular payloads**. *Science* 2012, **335**:831-834.
127. Amir Y, Ben-Ishay E, Levner D, Ittah S, Abu-Horowitz A, Bachelet I: **Universal compting by DNA origami robots in a living animal**. *Nature Nanotechnology* 2014, **9**:353-357.
128. Hazarika P, Kukolka F, Niemeyer CM: **Reversible binding of fluorescent proteins at DNA-gold nanoparticles**. *Angew Chem Int Ed Engl* 2006, **45**:6827-6830.
129. Kooyman R, Schasfoort R, Tudos A: **Physics of Surface Plasmon Resonance**. In *Handbook of Surface Plasmon Resonance*. Edited by; 2008:15-34.
130. Homola J, Piliarik M: **Surface plasmon resonance (SPR) sensors**. In *Surface Plasmon Resonance Based Sensors*. 2006:45-67. vol 4.
131. Cooper MA: **Optical biosensors in drug discovery**. *Nat Rev Drug Discov* 2002, **1**:515-528.
132. Homola J, Yee S, Gauglitz G: **Surface plasmon resonance sensors: review**. *Sensors and Actuators B-Chemical* 1999, **54**:3-15.
133. Schasfoort R, McWhirter A: **SPR instrumentation**. In *Handbook of Surface Plasmon Resonance*. Edited by; 2008:35-80.
134. ISHIKAWA E, HASHIDA S, KOHNO T: **DEVELOPMENT OF ULTRASENSITIVE ENZYME-IMMUNOASSAY REVIEWED WITH EMPHASIS ON FACTORS WHICH LIMIT THE SENSITIVITY**. *Molecular and Cellular Probes* 1991, **5**:81-95.
135. Vinson C, Chatterjee R, Fitzgerald P: **Transcription factor binding sites and other features in human and Drosophila proximal promoters**. *Subcell Biochem* 2011, **52**:205-222.
136. Berger MF, Philippakis AA, Qureshi AM, He FS, Estep PWr, Bulyk ML: **Compact, universal DNA microarrays to comprehensively determine transcription-factor binding site specificities**. *Nat Biotechnol* 2006, **24**:1429-1435.
137. Berger MF, Bulyk ML: **Universal protein-binding microarrays for the comprehensive characterization of the DNA-binding specificities of transcription factors**. *Nat Protoc* 2009, **4**:393-411.
138. Dejardin J, Kingston RE: **Purification of proteins associated with specific genomic**

Loci. *Cell* 2009, **136**:175-186.
139. Marre S, Jensen KF: **Synthesis of micro and nanostructures in microfluidic systems**. *Chem Soc Rev* 2010, **39**:1183-1202.
140. Yeo LY, Chang HC, Chan PP, Friend JR: **Microfluidic devices for bioapplications**. *Small* 2011, **7**:12-48.
141. Lenshof A, Laurell T: **Continuous separation of cells and particles in microfluidic systems**. *Chem Soc Rev* 2010, **39**:1203-1217.
142. Shapiro MS, Haswell SJ, Lye GJ, Bracewell DG: **Microfluidic Chromatography for Early Stage Evaluation of Biopharmaceutical Binding and Separation Conditions**. *Separation Science and Technology* 2010, **46**:185-194.
143. Su X, Young EW, Underkofler HA, Kamp TJ, January CT, Beebe DJ: **Microfluidic cell culture and its application in high-throughput drug screening: cardiotoxicity assay for hERG channels**. *J Biomol Screen* 2011, **16**:101-111.
144. Homola Jr, Yee SS, Myszka D, Dc P: *Surface plasmon resonance biosensors*: Amsterdam, The Netherlands: Elsevier; 2002.
145. LIEDBERG B, LUNDSTROM I, STENBERG E: **Principles of biosensing with an extended coupling matrix and surface plasmon resonance**. *Sensors and Actuators B-Chemical* 1993, **11**:63-72.
146. HUTCHINSON A: **Evanescent wave biosensors. Real-time analysis of biomolecular interactions.** *Molecular Biotechnology* 1995, **3**:47-54.
147. Janshoff A, Steinem C: **Quartz crystal microbalance for bioanalytical applications**. *Sensors update* 2001, **9**:313-354.
148. Su X, Wu YJ, Knoll W: **Comparison of surface plasmon resonance spectroscopy and quartz crystal microbalance techniques for studying DNA assembly and hybridization**. *Biosens Bioelectron* 2005, **21**:719-726.
149. Kurosawa S, Aizawa H, Tozuka M, Nakamura M, Park J: **Immunosensors using a quartz crystal microbalance**. *Measurement Science & Technology* 2003, **14**:1882-1887.
150. Kanazawa K, Cho N-J: **Quartz Crystal Microbalance as a Sensor to Characterize Macromolecular Assembly Dynamics**. *Journal of Sensors* 2009, **2009**:1-17.
151. Xiaodi SU, Fook Tim CHEW, Sam FY: **Design and application of piezoelectric quartz crystal-based immunoassay**. In *Analytical sciences*. 2000. vol 16.
152. Gong P, Grainger DW: **Nonfouling surfaces: a review of principles and applications for microarray capture assay designs**. *Methods Mol Biol* 2007, **381**:59-92.
153. Hucknall A, Rangarajan S, Chilkoti A: **In Pursuit of Zero: Polymer Brushes that**

Resist the Adsorption of Proteins. *Advanced Materials* 2009, **21**:2441-2446.
154. Fare T, Coffey E, Dai H, He Y, Kessler D, Kilian K, Koch J, LeProust E, Marton M, Meyer M, et al.: **Effects of atmospheric ozone on microarray data quality**. *Analytical Chemistry* 2003, **75**:4672-4675.
155. Branham W, Melvin C, Han T, Desai V, Moland C, Scully A, Fuscoe J: **Elimination of laboratory ozone leads to a dramatic improvement in the reproducibility of microarray gene expression measurements**. *Bmc Biotechnology* 2007, **7**:1-8.
156. Rickman D, Herbert C, Aggerbeck L: **Optimizing spotting solutions for increased reproducibility of cDNA microarrays**. *Nucleic Acids Research* 2003, **31**.
157. Carletti E, Guerra E, Alberti S: **The forgotten variables of DNA array hybridization**. *Trends Biotechnol* 2006, **24**:443-448.
158. Han T, Melvin C, Shi L, Branham W, Moland C, Pine P, Thompson K, Fuscoe J: **Improvement in the reproducibility and accuracy of DNA microarray quantification by optimizing hybridization conditions**. *Bmc Bioinformatics* 2006, **7 (Suppl 2)**:S17.
159. Larkin JE, Frank BC, Gavras H, Sultana R, Quackenbush J: **Independence and reproducibility across microarray platforms**. *Nat Methods* 2005, **2**:337-344.
160. Draghici S, Khatri P, Eklund AC, Szallasi Z: **Reliability and reproducibility issues in DNA microarray measurements**. *Trends Genet* 2006, **22**:101-109.
161. Shields R: **MIAME, we have a problem**. *Trends in Genetics* 2006, **22**:65-66.
162. Brewer L, Bianco P: **Laminar flow cells for single-molecule studies of DNA-protein interactions**. *Nature Methods* 2008, **5**:517-525.
163. Hall D, Schasfoort R, Tudos A: **Kinetic models describing biomolecular interactions at surfaces**. *Handbook of Surface Plasmon Resonance* 2008:81-122.
164. de Mol N, Fischer M, Schasfoort R, Tudos A: **Kinetic and thermodynamic analysis of ligand-receptor interactions: SPR applications in drug development**. *Handbook of Surface Plasmon Resonance* 2008:123-172.
165. Eustatia-Rutten C, Smit J, Romijn J, van der Kleij-Corssmit E, Pereira A, Stokkel M, Kievit J: **Diagnostic value of serum thyroglobulin measurements in the follow-up of differentiated thyroid carcinoma, a structured meta-analysis**. *Clinical Endocrinology* 2004, **61**:61-74.
166. Carpi A, Mechanick J, Saussez S, Nicolini A: **Thyroid Tumor Marker Genomics and Proteomics: Diagnostic and Clinical Implications**. *Journal of Cellular Physiology* 2010, **224**:612-619.

167. Iervasi A, Iervasi G, Ferdeghini M, Solimeo C, Bottoni A, Rossi L, Colato C, Zucchelli G: **Clinical relevance of highly sensitive Tg assay in monitoring patients treated for differentiated thyroid cancer**. *Clinical Endocrinology* 2007, **67**:434-441.
168. Giovanella L: **Highly sensitive thyroglobulin measurements in differentiated thyroid carcinoma management**. *Clinical Chemistry and Laboratory Medicine* 2008, **46**:1067-1073.
169. Nistor C, Emneus J, Gorton L: **Immunoassay: potentials and limitations**. *Biosensors and Modern Biospecific Analytical Techniques* 2005, **44**:375-427.
170. Tate J, Ward G: **Interferences in immunoassay**. *Clin Biochem Rev* 2004, **25**:105-120.
171. Lea T, Vartdal F, Nustad K, Funderud S, Berge A, Ellingsen T, Schmid R, Stenstad P, Ugelstad J: **Monosized, magnetic polymer particles: their use in separation of cells and subcellular components, and in the study of lymphocyte function in vitro**. *J Mol Recognit* 1988, **1**:9-18.
172. Burgess R, Thompson N: **Advances in gentle immunoaffinity chromatography**. *Current Opinion in Biotechnology* 2002, **13**:304-308.
173. HEMMILA I: **Fluoroimmunoassays and immunofluorometric assays**. *Clinical Chemistry* 1985, **31**:359-370.
174. Seydack M, ReschGenger U: **Immunoassays: basic concepts, physical chemistry and validation**. In *Standardization and Quality Assurance in Fluorescence Measurements II: Bioanalytical and Biomedical Applications*. 2008:401-428. vol 06.
175. NIEMEYER C, SANO T, SMITH C, CANTOR C: **Oligonuclotide-Directed Self-Assembly of Proteins - Semisynthetic DNA Streptavidin Hybride Molecules as Connectors for the Generation of Macroscopic Arrayes and the Construction of Supermolecular Bioconjugates**. *Nucleic Acids Research* 1994, **22**:5530-5539.
176. Ladd J, Taylor A, Piliarik M, Homola J, Jiang S: **Hybrid surface platform for the simultaneous detection of proteins and DNAs using a surface plasmon resonance imaging sensor**. *Analytical Chemistry* 2008, **80**:4231-4236.
177. CLINE G, HANNA S: **Kinetics and mechanisms of the aminolysis of N-hydroxysuccinimide esters in aqueous buffers**. *Journal of Organic Chemistry* 1988, **53**:3583-3586.
178. Sehgal D, Vijay I: **A method for the high-efficiency of water-soluble carbodimide-mediated amidation**. *Analytical Biochemistry* 1994, **218**:87-91.
179. Diamandis E, Christopoulos T: **The biotin (Strept)avidin system - Principle and applications in biotechnology**. *Clinical Chemistry* 1991, **37**:625-636.

180. Weber P, Ohlendorf D, Wendoloski J, Salemme F: **Structural origins of high-affinity biotin binding to streptavidin**. *Science* 1989, **243**:85-88.
181. Vauquelin G, Charlton S: **Exploring avidity: understanding the potential gains in functional affinity and target residence time of bivalent and heterobivalent ligands**. *British Journal of Pharmacology* 2013, **168**:1771-1785.
182. Mammen M, Choi S, Whitesides G: **Polyvalent interactions in biological systems: Implications for design and use of multivalent ligands and inhibitors**. *Angewandte Chemie-International Edition* 1998, **37**:2755-2794.
183. Fischer M, DeMol N: **Amine Coupling Through EDC/NHS: A Practical Approach**. *Surface Plasmon Resonance: Methods and Protocols* 2010, **627**:55-73.
184. Hermanson G, Hermanson G: **Microparticles and Nanoparticles**. In *Bioconjugate Techniques*. Edited by; 2008:582-626.
185. Kellar K, Kalwar R, Dubois K, Crouse D, Chafin W, Kane B: **Multiplexed fluorescent bead-based immunoassays for quantitation of human cytokines in serum and culture supernatants**. *Cytometry* 2001, **45**:27-36.
186. Cline G, Hanna S: **The aminolysis of N-hydroxysuccinimide esters - Astrucure-reactivity study**. *Journal of of the American Chemical Society* 1987, **109**:3087-3091.
187. Boozer C, Ladd J, Chen S, Yu Q, Homola J, Jiang S: **DNA directed protein immobilization on mixed ssDNA/oligo(ethylene glycol) self-assembled monolayers for sensitive biosensors**. *Analytical Chemistry* 2004, **76**:6967-6972.
188. Boozer C, Ladd J, Chen S, Jiang S: **DNA-directed protein immobilization for simultaneous detection of multiple analytes by surface plasmon resonance biosensor**. *Analytical Chemistry* 2006, **78**:1515-1519.
189. Han K, Ahn D, Yang E: **An Approach to Multiplexing an Immunosorbent Assay with Antibody-Oligonucleotide Conjugates**. *Bioconjugate Chemistry* 2010, **21**:2190-2196.
190. Faulds K, Fruk L, Robson D, Thompson D, Enright A, Smith W, Graham D: **A new approach for DNA detection by SERRS**. *Faraday Discussions* 2006, **132**:261-268.
191. Schroder H, Hoffmann L, Muller J, Alhorn P, Fleger M, Neyer A, Niemeyer C: **Addressable microfluidic polymer chip for DNA-directed immobilization of oligonucleotide-tagged compounds**. *Small* 2009, **5**:1547-1552.
192. Cleland WW: **Dithiothreitol, a new protective reagent for SH groups**. *Biochemistry* 1964, **3**:480-482.
193. Rijal K, Mutharasan R: **PEMC-based method of measuring DNA hybridization at femtomolar concentration directly in human serum and in the presence of copious**

noncomplementary strands. *Analytical Chemistry* 2007, **79**:7392-7400.
194. Maston GA, Landt SG, Snyder M, Green MR: **Characterization of enhancer function from genome-wide analyses**. *Annu Rev Genomics Hum Genet* 2012, **13**:29-57.
195. Gadgil H, Jurado LA, Jarrett HW: **DNA affinity chromatography of transcription factors**. *Anal Biochem* 2001, **290**:147-178.
196. Nagore LI, Nadeau RJ, Guo Q, Jadhav YL, Jarrett HW, Haskins WE: **Purification and characterization of transcription factors**. *Mass Spectrom Rev* 2013, **32**:386-398.
197. Jolma A, Taipale J: **Methods for Analysis of Transcription Factor DNA-Binding Specificity In Vitro**. *Subcell Biochem* 2011, **52**:155-173.
198. Jiang D, Jarrett HW, Haskins WE: **Methods for proteomic analysis of transcription factors**. *J Chromatogr A* 2009, **1216**:6881-6889.
199. Forde CE, McCutchen-Maloney SL: **Characterization of transcription factors by mass spectrometry and the role of SELDI-MS**. *Mass Spectrom Rev* 2002, **21**:419-439.
200. Bane T, LeBlanc J, Lee T, Riggs A: **DNA affinity capture and protein profiling by SELDI-TOF mass spectrometry: effect of DNA methylation**. *Nucleic Acids Research* 2002, **30**:e69.
201. Forde CE, Gonzales AD, Smessaert JM, Murphy GA, Shields SJ, Fitch JP, McCutchen-Maloney SL: **A rapid method to capture and screen for transcription factors by SELDI mass spectrometry**. *Biochem Biophys Res Commun* 2002, **290**:1328-1335.
202. Nordhoff E, Krogsdam A, Jorgensen H, Kallipolitis B, Clark B, Roepstorff P, Kristiansen K: **Rapid identification of DNA-binding proteins by mass spectrometry**. *Nature Biotechnology* 1999, **17**:884-888.
203. Bouffartigues E, Leh H, Anger-Leroy M, Rimsky S, Buckle M: **Rapid coupling of Surface Plasmon Resonance (SPR and SPRi) and ProteinChip based mass spectrometry for the identification of proteins in nucleoprotein interactions**. *Nucleic Acids Res* 2007, **35**:e39.
204. Smith LM, Shortreed MR, Olivier M: **To understand the whole, you must know the parts: unraveling the roles of protein-DNA interactions in genome regulation**. *Analyst* 2011, **136**:3060-3065.
205. Collas P: **The state-of-the-art of chromatin immunoprecipitation**. *Methods Mol Biol* 2009, **567**:1-25.
206. Blecher-Gonen R, Barnett-Itzhaki Z, Jaitin D, Amann-Zalcenstein D, Lara-Astiaso D, Amit I: **High-throughput chromatin immunoprecipitation for genome-wide mapping of in vivo protein-DNA interactions and epigenomic states**. *Nat Protoc* 2013, **8**:539-554.

207. Lefrançois P, Zheng W, Snyder M: **ChIP-Seq: using high-throughput DNA sequencing for genome-wide identification of transcription factor binding sites**. *Methods in Enzymology* 2010, **470**:77-104.
208. Yant L: **Genome-wide mapping of transcription factor binding reveals developmental process integration and a fresh look at evolutionary dynamics**. *Am J Bot* 2012, **99**:277-290.
209. Chen J: **Serial analysis of binding elements for human transcription factors**. *Nat Protoc* 2006, **1**:1481-1493.
210. Rhee HS, Pugh BF: **Comprehensive genome-wide protein-DNA interactions detected at single-nucleotide resolution**. *Cell* 2011, **147**:1408-1419.
211. Ho SW, Jona G, Chen CT, Johnston M, Snyder M: **Linking DNA-binding proteins to their recognition sequences by using protein microarrays**. *Proc Natl Acad Sci U S A* 2006, **103**:9940-9945.
212. Maerkl SJ, Quake SR: **A systems approach to measuring the binding energy landscapes of transcription factors**. *Science* 2007, **315**:233-237.
213. Geertz M, Shore D, Maerkl S: **Massively parallel measurements of molecular interaction kinetics on a microfluidic platform**. *Proceedings of the National Academy of Sciences of the United States of America* 2012, **109**:16540-16545.
214. Odom DT: **Identification of Transcription Factor-DNA Interactions In Vivo**. *Subcell Biochem* 2011, **52**:175-191.
215. Hardison RC, Taylor J: **Genomic approaches towards finding cis-regulatory modules in animals**. *Nat Rev Genet* 2012, **13**:469-483.
216. Ladunga I: **An overview of the computational analyses and discovery of transcription factor binding sites**. *Methods Mol Biol* 2010, **674**:1-22.
217. Bulyk ML: **DNA microarray technologies for measuring protein-DNA interactions**. *Curr Opin Biotechnol* 2006, **17**:422-430.
218. Panda M, Jiang D, Jarrett HW: **Trapping of transcription factors with symmetrical DNA using thiol-disulfide exchange chemistry**. *J Chromatogr A* 2008, **1202**:75-82.
219. Min C, Verdine G: **Immobilized metal affinity chromatography of DNA**. *Nucleic Acids Research* 1996, **24**:3806-3810.
220. Hegarat N, Cardoso GM, Rusconi F, Francois JC, Praseuth D: **Analytical biochemistry of DNA--protein assemblies from crude cell extracts**. *Nucleic Acids Res* 2007, **35**:e92.
221. Wang Z, Gidwani V, Zhang DD, Wong PK: **Separation-free detection of nuclear factor kappa B with double-stranded molecular probes**. *Analyst* 2008, **133**:998-1000.

222. Heyduk T, Heyduk E: **Molecular beacons for detecting DNA binding proteins**. *Nature Biotechnology* 2002, **20**:171-176.
223. Dummitt B, Chang Y: **Molecular beacons for DNA binding proteins: An emerging technology for detection of DNA binding proteins and their ligands**. *Assay and Drug Development Technologies* 2006, **4**:343-349.
224. Arbab M, Mahony S, Cho H, Chick J, Rolfe P, van Hoff J, Morris V, Gygi S, Maas R, Gifford D, et al.: **A multi-parametric flow cytometric assay to analyze DNA-protein interactions**. *Nucleic Acids Research* 2013, **41**:e38.
225. Bruggink F, Hayes S: **Identification of DNA binding proteins using the NoShift transcription factor assay kit**. *Nature Methods* 2004, **1**:177-179.
226. Mirzaei H, Knijnenburg TA, Kim B, Robinson M, Picotti P, Carter GW, Li S, Dilworth DJ, Eng JK, Aitchison JD, et al.: **Systematic measurement of transcription factor-DNA interactions by targeted mass spectrometry identifies candidate gene regulatory proteins**. *Proc Natl Acad Sci U S A* 2013, **110**:3645-3650.
227. MULLER C, REY F, SODEOKA M, VERDINE G, HARRISON S: **Structure of the NF-kappa B p50 homodimer bound to DNA**. *Nature* 1995, **373**:311-317.
228. Oeckinghaus A, Ghosh S: **The NF-kB family of transcription factors and its regulation**. *Cold Spring Harbor Perspectives in Biology* 2009, **1**:a000034.
229. Phelps CB, Sengchanthalangsy LL, Malek S, Ghosh G: **Mechanism of kappa B DNA binding by Rel/NF-kappa B dimers**. *J Biol Chem* 2000, **275**:24392-24399.
230. Zabel U, Schreck R, Baeuerle PA: **DNA binding of purified transcription factor NF-kB. Affinity, specificity, Zn2+ dependence, and differential half-site recognition**. *Journal of Biological Chemistry* 1991, **266**:252-260.
231. Urban MB, Baeuerle PA: **The 65-kD subunit of NF-kappa B is a receptor for I kappa B and a modulator of DNA-binding specificity**. *Genes & Development* 1990, **4**:1975-1984.
232. Hart D, Speight R, Cooper M, Sutherland J, Blackburn J: **The salt dependence of DNA recognition by NF-kappa B p50: a detailed kinetic analysis of the effects on affinity and specificity**. *Nucleic Acids Research* 1999, **27**:1063-1069.
233. Zeng Y, Harrison D: **Self-assembled colloidal arrays as three-dimensional nanofluidic sieves for separation of biomolecules on microchips**. *Analytical Chemistry* 2007, **79**:2289-2295.
234. Vulto P, Dame G, Maier U, Makohliso S, Podszun S, Zahn P, Urban GA: **A microfluidic approach for high efficiency extraction of low molecular weight RNA**. *Lab Chip* 2010,

10:610-616.

235. Jiang G, Harrison DJ: **mRNA isolation in a microfluidic device for eventual integration of cDNA library construction**. *The Analyst* 2000, **125**:2176-2179.

236. Kong W, Zhao JJ, He L, Cheng JQ: **Strategies for profiling microRNA expression**. *J Cell Physiol* 2009, **218**:22-25.

237. Wark AW, Lee HJ, Corn RM: **Multiplexed detection methods for profiling microRNA expression in biological samples**. *Angew Chem Int Ed Engl* 2008, **47**:644-652.

238. Pritchard CC, Cheng HH, Tewari M: **MicroRNA profiling: approaches and considerations**. *Nat Rev Genet* 2012, **13**:358-369.

239. Weirauch MT, Hughes TR: **A catalogue of eukaryotic transcription factor types, their evolutionary origin, and species distribution**. *Subcell Biochem* 2011, **52**:25-73.

240. Kleparnik K: **Recent advances in the combination of capillary electrophoresis with mass spectrometry: from element to single-cell analysis**. *Electrophoresis* 2013, **34**:70-85.

241. Stalmach A, Albalat A, Mullen W, Mischak H: **Recent advances in capillary electrophoresis coupled to mass spectrometry for clinical proteomic applications**. *Electrophoresis* 2013, **34**:1452-1464.

242. Kitagawa F, Otsuka K: **Recent progress in microchip electrophoresis-mass spectrometry**. *J Pharm Biomed Anal* 2011, **55**:668-678.

243. Schappler J, Veuthey J-L, Rudaz S: **Coupling CE and microchip-based devices with mass spectrometry**. In *Capillary Electrophoresis Methods for Pharmaceutical Analysis*. 2008:477-521. vol 9.

244. Jemere AB, Bezuidenhout LW, Brett MJ, Harrison DJ: **Matrix-free laser desorption/ionization mass spectrometry using silicon glancing angle deposition (GLAD) films**. *Rapid Commun Mass Spectrom* 2010, **24**:2305-2311.